Summer 2007

Ion assisted magnetron sputtering of tantalum thin film deposition and characterization

Hua Ren
New Jersey Institute of Technology

ABSTRACT

ION ASSISTED MAGNETRON SPUTTERING OF TANTALUM THIN FILM DEPOSITION AND CHARACTERIZATION

by
Hua Ren

The purpose of this research was to investigate the effects of ion bombardment on the crystallographic phases of tantalum films during their deposition by magnetron sputtering process, and to gain understanding of the mechanism of the ion-solid interactions during the thin film growth. Tantalum (Ta) exists in two distinct crystallographic phases: a stable α-phase with a body centered cubic (bcc) lattice structure and a metastable β-phase with a tetragonal lattice structure. The tough and ductile α-phase Ta is desired in most industrial applications, such as diffusion barrier layers in integrated circuits, metallic corrosion protective layers, and in biomedical devices. The β-phase Ta is hard and brittle, and its presence may compromise the film performance. Bulk Ta metal has the α-phase structure but the β-phase appears in thin films, unless special means are used to avoid its growth.

In this work a DC magnetron sputtering system was modified for RF operation along with a provision for DC biasing the substrate to accelerate inert gas ions towards the tantalum thin film during its growth process. The experiments demonstrated that the ion bombardment energy, controlled by varying the bias voltages, has a strong effect on the crystallographic phase of tantalum films as well as their surface morphology. High quality bcc (α-phase) tantalum thin films were deposited under -150 V substrate bias at an ion current density of approximately ~0.4 mA/cm^2, both on silicon and aluminum substrates. These ion bombardment conditions for bcc α-phase Ta growth are quite

different from those previous reported, however, it was found that the total energy delivered by ions per deposited atom in this and in previous work is approximately the same.

Ion bombardments by plasma Ar ions accelerated to the biased substrate also sputtered away the deposited Ta during the film growth, resulting in thinner films at higher ion energies, which was measured by Rutherford backscattering spectroscopy. The sputtering yield derived from these data was compared with previously published data and theoretical predictions. This ion assisted deposition process was further studied by molecular dynamic simulations and statistical analysis of ion impacts and atom impingements on the film surface. It was concluded that these two events are independent, and that the film crystallographic structure transformation is induced by ion impacts rearranging the deposited atoms after their arrival on the growing film.

The results for this work have demonstrated that bcc α-phase tantalum thin films can be grown on both silicon and aluminum substrates at room temperature by RF magnetron sputter with ion bombardment conditions very different than those previous reported. The advantage of the new process is that it can be carried out in a standard magnetron deposition system with a provision of substrate biasing to control the ion bombardment. Such a system is easier to scale to industrial operation than those described earlier, which requires a more complex apparatus.

ION ASSISTED MAGNETRON SPUTTERING OF TANTALUM THIN FILM DEPOSITION AND CHARACTERIZATION

by
Hua Ren

A Dissertation
Submitted to the Faculty of
New Jersey Institute of Technology
in Partial Fulfillment of the Requirements for the Degree of
Doctor of Philosophy in Materials Science and Engineering

Interdisciplinary Program in Materials Science and Engineering

August 2007

APPROVAL PAGE

ION ASSISTED MAGNETRON SPUTTERING OF TANTALUM THIN FILM DEPOSITION AND CHARACTERIZATION

Hua Ren

Dr. Marek Sosnowski, Dissertation Advisor — Date
Professor of Electrical and Computer Engineering,
and Materials Science and Engineering, NJIT

Dr. James K. Hirvonen, Committee Member — Date
Army Research Laboratory, Aberdeen, MD

Dr. Nuggehalli M. Ravindra, Committee Member — Date
Professor of Department of Physics,
and Materials Science and Engineering, NJIT

Dr. Trevor A. Tyson, Committee Member — Date
Professor of Department of Physics,
and Materials Science and Engineering, NJIT

Dr. Zafar Iqbal, Committee Member — Date
Research Professor of Chemistry and Environmental Science,
and Materials Science and Engineering, NJIT

BIOGRAPHICAL SKETCH

Author: Hua Ren

Degree: Doctor of Philosophy

Date: August 2007

Undergraduate and Graduate Education:

- Doctor of Philosophy in Materials Science and Engineering,
  New Jersey Institute of Technology, Newark, NJ, 2007

- Master of Science in Chemistry and Chemical Engineering,
  Shanghai Jiao Tong University, Shanghai, P. R. China, 2002

- Bachelor of Science in Applied Chemistry,
  Shanghai Jiao Tong University, Shanghai, P. R. China, 1999

Major: Materials Science and Engineering

Presentations and Publications:

H. Ren and M. Sosnowski,
"Tantalum Thin Films Deposited by Ion Assisted Magnetron Sputtering,"
Thin Solid Films (Submitted).

H. Ren and M. Sosnowski,
"Effect of Ion Irradiation on α- and β-Phase Evolution of Sputtered Tantalum Thin Films,"
In: C. Ambromeit, P. Bellon, J-L. Bocquet, D.N. Seidman (Eds.)
Thermodynamics and Kinetics of Phase Transformations in Inorganic Materials, Boston, U.S.A., November 27-December 1, 2006, Materials Research Society Symposium Proceedings 979 (2007) 0979-HH11-09.

H. Ren and M. Sosnowski,
"The Effect of Ion Bombardment during Sputter-deposition on the Crystallography of Thin Tantalum Films,"
In: General Student Poster Session, Denver, U.S.A., May 7-12, 2006, The 209th Electrochemical Society Meeting Abstract (2006) 1.

To my beloved mom (王琴凤) and dad (任文烛) for their long time supporting and encouraging and also to my husband (程彬) for his loving and caring!

I also want to dedicate this work to another very special person, my grandfather (王敦鹤). He'll live deep in my heart for ever, even though he passed away 6 years ago.

ACKNOWLEDGMENT

I would like to express my deepest appreciation to Dr. Marek Sosnowski, who not only served as my research advisor, providing a lot of valuable and countless instructions, suggestions and intuition to make me more professional in research studies, but also constantly supported and encouraged me in producing independent and creative scientific thinking. Special thanks are given to Dr. James K. Hirvonen, Dr. Zafar Iqbal, Dr. Nuggehalli M. Ravindra, and Dr. Trevor A. Tyson for critical reviewing my dissertation document, actively participating in my committee and providing helpful technical suggestions.

I wish to thank Dr. Leszek Wielunski (Director Tandem Accelerator Laboratory of Physics and Astronomy Department, Rutgers State University of New Jersey) for his assistance on RBS measurement and analysis. Also many of my fellow graduate students in Federated Physics Department and Department of Mathematical Sciences are deserving of recognition for their support.

TABLE OF CONTENTS

TABLE OF CONTENTS
(Continued)

TABLE OF CONTENTS
(Continued)

LIST OF TABLES

LIST OF FIGURES

LIST OF FIGURES
(Continued)

Figure **Page**

LIST OF FIGURES
(Continued)

Figure **Page**

LIST OF FIGURES
(Continued)

Figure **Page**

LIST OF FIGURES
(Continued)

Figure **Page**

CHAPTER 1

INTRODUCTION

The thin film material which is the subject of this study is tantalum (Ta). Tantalum is a gray-blue, metallic element. Its atomic number is 73, and atomic weight is 180.9479 g/mole. Ta has two distinct crystallographic structures, stable α-phase Ta with body centered cubic (bcc) crystallographic structure and the metastable β-phase Ta with tetragonal crystallographic structure [1]. The α-phase Ta is desired in most applications because of its many useful properties, such as high strength and good ductility, while β-phase Ta is hard and brittle [2-8]. Ta has a high melting point (2996°C) and is almost completely immune to chemical attack at temperatures below 150°C [9].

Sputter deposited tantalum thin films usually possess the metastable β-phase crystallographic structure or a two phase mixed structure. Many studies have been focused on developing deposition techniques and finding appropriate deposition conditions for obtaining high quality α-phase tantalum thin films. Earlier research done by Leszek Gladczuk and Anamika Patel et al. at NJIT [10] showed that α-phase Ta could grow on steel substrates by DC magnetron sputtering when the substrate is heated to 400 °C.

For various thin film applications, it's vital to control the thin films' microstructure and morphology, as they control their properties. There are several methods that can be used to improve the quality of deposited thin films. The employment of energetic ion species bombarding growing films is considered a very effective way to control thin film microstructures, hence its properties.

The ion bombardment contributes kinetic energy and momentum to the arriving thin film atoms (adatoms), increases their mobility on the surface of substrates or the growing thin films, and therefore affects thin films' nucleation, coalescence and growth. When the deposited thin film atoms are given a high kinetic energy or when other species with high energy impinge on the growing thin films, the properties of the thin films can be controlled and improved [11]. This increase in the energy of the arriving atoms and in their surface mobility enables deposition at lower substrate temperature with dense film microstructures, selectable stress levels, and in some cases desired crystallographic phases. In addition, ion bombardment can knock off loosely attached impurity atoms reaching the deposited film surface, and thus reducing the films' impurity level which is very important for thin films used in microelectronic circuits' fabrication [12]. In this work, the effect of ion bombardment in the RF sputtering deposition process for Ta films was explored, and it was expected to control thin films' crystallographic phase and quality by introducing the ion bombardment into the deposition process.

This study focused on growing the thin tantalum films by a RF magnetron sputtering system with a provision of substrate biasing. During the deposition process, the energy and flux of argon ions which were attracted towards the substrate and the growing films by negatively biasing the substrate electrode was controlled. The preliminary results showed that energetic ion bombardment allowed the control of the crystallographic phase of Ta thin films. The investigation goal was to find the deposition conditions for growing α-phase Ta instead of β-phase or mixed phase Ta films. The ion bombardment effects on the microstructure and morphology of deposited tantalum thin films were also being investigated.

CHAPTER 2

LITERATURE REVIEW

Tantalum was discovered in 1802 by a Swedish chemist Anders Gustaf Ekeberg in minerals obtained from Ytterby, Sweden, and the first relatively pure ductile tantalum was produced by von Bolton in 1903. The commercial use of tantalum also began in 1903 with the production of tantalum wire [13, 14]. Today, tantalum metal has many applications in electronics, mechanical, chemical and biomedical areas.

Tantalum has a number of unique characteristics and attractive properties that triggered extensive research in this element and its compounds. Tantalum is almost completely immune to chemical attack at temperatures below 150° C, and is attacked only by hydrofluoric acid, acidic solutions containing the fluoride ion, and free sulfur trioxide. Alkalis attack it only slowly. Ta is completely immune to body liquids and it is a nonirritating material. At high temperatures, tantalum becomes much more reactive. For tantalum compounds, the oxide films are stable and have good dielectric properties, and the tantalum nitride has similar attractive properties too. Therefore, tantalum and its compounds are most promising materials for corrosion, heat and wear resistant protective coatings [10, 15-19].

As one of the most corrosion resistant materials, tantalum can be milled into sheet used for chemical equipment such as bayonet heaters, vapor condensers, multi-tube heat exchangers, thermo-wells, rupture diaphragms and orifices. In glass-lined steel equipment, tantalum plugs are selected to be repair perforations. Because of its superior chemical stability in various environments, components made by tantalum are used in sulfuric acid concentrators, in temperature controllers for chromium plating and in

distillation and condensation of acids and acidic chemicals. One of the most important tantalum compounds, tantalum carbide, is mixed with some grades of cemented carbides to make hard carbide cutting tools with a low coefficient of friction and a high resistance to mechanical shock [20-22].

In addition to having desirable properties for protective coatings, the major applications of tantalum thin films are in electronic industry. Tantalum can form very stable anodic oxide films which make excellent capacitors. Tantalum capacitors possess higher volumetric capacitance efficiency than any other material capacitors, and provide better performance both at low and high temperatures [20, 23]. In the past, tantalum and tantalum compounds have been investigated as thin film resistors with a low temperature coefficient of resistivity [24]. Recently in the semiconductor industry with the development of copper interconnection in ultra-large-scale integrated circuits (ULSIs), tantalum and tantalum based thin films with their superior chemical and thermal stability are accepted as the most promising diffusion barrier layer preventing copper from diffusing and reacting with the underlying silicon, silicon dioxide and low-k dielectrics [25-31]. Tantalum is also used in the copper metallization, damascene process, as an adhesion layer and polish stop in chemical mechanical polishing (CMP) [32]. Another application of tantalum is in X-ray optics such as absorbers in x-ray lithography [33].

Biotechnology is another area of application of tantalum and its compounds. The metal possesses excellent histo-compatibility, and it has been used as a biomedical material in orthopedics since 1940s. Many other wide applications of tantalum in making surgical components for surgical implants, for suture wire, cranial repair plates and for wire gauze for abdominal muscle support in hernia repair surgery, etc. also attract a lot of

attention because it is extraordinarily inert to body fluids and tissues. More recently, tantalum nitride has been investigated for surface modification of blood-contacting biomaterials [34].

Several investigations have been conducted on developing techniques for depositing tantalum and its compounds, and connecting the processing parameters with the resulting film properties. In this chapter, a review of different properties of two different crystallographic phases of tantalum thin films is presented. Then the key factors which are considered to affect and control the phase, microstructure and properties of deposited tantalum thin films are reviewed. Previous research done on the ion bombardment effect on the deposited tantalum thin film structures is addressed in particular.

2.1 Properties of α-phase and β-phase Tantalum

Tantalum metal is known in two distinct crystalline phases or structures: the earliest known, a stable α-phase tantalum (Im3m space group, a=3.304 Å) with a body centered cubic crystal lattice structure and the metastable β-phase tantalum (P42/mnm space group, a=5.313 Å, c=10.194 Å) with a tetragonal crystal lattice structure known since 1965 [1, 35, 36].

The physical properties of β-phase Ta are not well known, except that it is hard, brittle and thermally unstable. Common bulk tantalum has the α-phase structure and possesses good chemical, thermal and mechanical properties, including a high melting temperature (2996 °C), high elastic modulus similar to that of steel, good ductility and formability, and resistance to acids and aggressive hot propellant gases [36-38]. It has a relatively low thermal conductivity (57 W/m °C) and a low electrical resistivity of 15-60

μΩ/cm which makes it a good choice for the thin film interconnection and for barrier coatings. The resistivity of β-phase Ta is much higher, 170-210 μΩ/cm [39, 40]. The α-phase Ta has a superconducting transition temperature (T_c) of 3.25 K while the β-phase Ta has a superconducting transition temperature of (T_c) of 0.5 K. Typical Knoop microhardness values for the β-phase Ta are greater than 900, while the values for α-phase Ta are in the 300-400 range. These properties make β-phase Ta more susceptible to crack formation and failure, and hence less desirable for protective coating applications where thermal shock and high shear forces are present [16].

There is only one report on β-phase Ta being grown in the bulk form [41]. The metastable β-phase Ta or mixed phase Ta is usually observed in sputtering deposited thin films [16, 42]. The metastable β-phase Ta transforms into α-phase Ta when heated up to 750-1000 °C [1, 36, 42]. The properties of the α-phase and β-phase Ta are listed in Table 2.1 [1, 41, 43].

Table 2.1 Thermal-mechanical Properties of α-phase and β-phase Ta

Phase	Alpha tantalum	Beta tantalum
Structure	BCC, S.G. Im3m	Tetragonal, S.G. P42/mnm
Lattice parameters	a=b=c=0.33058nm	a=b=1.0194nm c=0.5313 nm
Density (g/cm^3)	16.55	16.9
Hardness	300-400 KHN	900 KHN
Ductility	Ductile	Brittle
Resistivity (μΩ/cm)	15-60	170-210
Temperature coef. of resistivity (ppm/ °C)	+500+1800	-100+100
Superconducting transition temperature (K)	3.25	0.5
Thermal stability	$T_{melting\ point}$ at 2996°C	$T_{beta\text{-}alpha}$ at 750-1000°C

Sources: [1, 41, 43]

2.2 Factors Affecting the Crystallographic Structure of Deposited Tantalum Thin Films

Various techniques have been used for depositing tantalum thin films, such as physical vapor deposition, including electron beam evaporation [44, 45] and different sputtering techniques, such as DC sputtering [46, 47], RF sputtering [47], triode sputtering [38, 48], ion beam assisted sputtering [49], magnetron sputtering [50, 51]. Chemical vapor deposition [52], and electrochemical deposition [36] have also been successfully used. With these deposition processes, α-phase tantalum, β-phase tantalum or mixed phase

tantalum will grow on different substrates depending on specific deposition conditions. Based on the prior research work, a summary of the deposition conditions which contribute to controlling the crystallographic structure of deposited tantalum thin films on different substrates was reviewed and summarized below.

2.2.1 Deposition Conditions

(1) Vacuum Condition and Impurities

The deposition environment is very important for thin film deposition process, especially the residual gas contents (such as nitrogen, water vapor and oxygen) in the vacuum system. These are critical parameters in controlling the structures and properties of the deposited thin films. For tantalum thin film deposition, several investigations have been focused on this aspect, and different groups of researchers claimed that the vacuum conditions and the impurities existing in the vacuum environment would affect the deposited tantalum thin film structure (α-phase structure, β-phase structure or mixed phase structure).

Initially, many researchers questioned whether β-phase Ta was an allotrope of bcc α-phase Ta or an impurity-stabilized Ta phase. Read and Altman's research [1] showed that β-phase Ta films were as pure or even purer than α-phase Ta films, and as the pressure of any reactive residual gas content in the deposition vacuum system increased, the deposited Ta films were always grown in the α-phase structure. Others [2, 7] also reported that increasing the amounts of residual gases in the deposition vacuum system favored the normal α-phase Ta growth. They thought that body-centered cubic lattice structure of α-phase Ta was a more open structure where interstitials (impurities) could

order themselves at extremely low concentrations and thus form a super lattice different from the normal structure. Also the stresses in thin film could govern the choice of specific interstitial sites for impurities in thin films [7].

Similarly, Feinstein and Huttemann et al. [53] concluded that the presence of O or possibly OH on the substrate surface was necessary for the β-phase Ta nucleation at the initial stage, and not for keeping it growing with the same structure during the later growth stage. Moreover, if the impurities incorporated into the Ta films during the growth stage exceeded the solubility limit of β-phase, eventually the α-phase Ta would be formed.

On the other hand, Schauer et al. [54, 55] reported that the β-phase Ta was an impurity stabilized phase with a certain relatively small amount of foreign atoms built into the films. Unlike the observation which Feinstein and Huttemann et al. made, they found that impurity atoms were necessary not only for the nucleation but also for the growth of β-phase Ta. They even concluded that the formation of β-phase Ta was caused either by impurity atoms adsorbed at the substrate surface or by reactive gases added into the sputtering argon atmosphere. They also noted that clean substrates and clean conditions with regard to the reactive gases maintained in the deposition environment during sputtering produced the α-phase Ta.

Gersteng [24], Krikorian [56] and Baker [57] observed that increasing of the oxygen or nitrogen concentration in the discharge atmosphere always produced α-phase Ta for a defined sputtering condition which normally produced the β-phase form. Westwood [58] claimed that an increase of oxygen partial pressure in the discharge was associated with the formation of β-phase and he interpreted the β-phase structure as an

impurity-stabilized phase which is formed to accommodate impurities in the coatings at levels higher than the solubility limit for the bcc α-phase tantalum.

The question of whether the incorporation of impurities is a necessary condition for the formation of α-phase Ta or β-phase Ta still can not be answered from these contradictory results.

(2) Sputtering Gas

One obvious phenomenon is that the sputtering yield of tantalum (atomic mass 181) will increase when bombarded by inert gas ions of increasing atomic number [59]. However, another question is whether the different inert sputtering gas species will affect the crystallographic structures of the deposited Ta thin films, and how? Matson et al. [16, 42] evaluated the effect of different sputtering gas species (Ar^{18}, Kr^{36} and Xe^{54}) on the microstructure of deposited tantalum coatings. They observed that heavier sputtering gases promoted the formation of bcc α-phase Ta, which agreed with the work of Ino et al. [60]. They also reported that high energy ion bombardment promoted growth of the β-phase but noted that the ion bombardment energy and momentum required for the bcc to β-phase transition was shifted to higher values when xenon was used instead of argon as the sputtering gas. They attributed the change in crystallographic phase of films grown using different sputtering gases to differences in the abilities of the gases to induce forward recoil-implanted Ta atom defects into the growing film structures.

(3) Substrate Temperature

Heating the substrates during the deposition process can help grow thin films with the desired stable crystalline structure and also improve their properties. For tantalum thin film deposition, it was reported that high substrate temperature favored the growth of α-phase tantalum, but different researchers reported different temperature ranges for growing α-phase or β-phase tantalum.

Matson et al. [37, 42] reported that typically substrate temperatures above 300 °C and as high as 600 °C were necessary to produce a completely bcc phase coating using argon, and substrate temperatures in excess of 200 °C were required to produce 100% bcc α-phase Ta when using krypton as the sputtering gas.

Fischer et al. [61] and research previously done in our NJIT lab by Leszek Gladczuk and Anamika Patel et al. [10] showed that heating the substrate to a moderate temperature of 400 °C resulted in the growth of pure bcc α-phase Ta by DC magnetron sputtering using Ar gas.

Schwartz et al. [62] demonstrated that mixtures of α- and β-phases could be deposited by sputtering at substrate temperatures of 400~465 °C. Mattox et al. [63] observed the formation of a mixture of α-phase and β-phase Ta on heated substrates during deposition too. Schauer et al. [64] deposited tantalum films on Corning 7059 glass and Ta_2O_5-coated substrates at a temperature above 300 °C. It was observed that most of the films deposited onto the substrates at a temperature higher than 300 °C produced pure α-phase while a few of the films showed mixtures of α-phase and β-phase. Heiber et al. [65] used Corning 7059 glass and sapphire as substrates for tantalum deposition.

Mixtures of α-phase and β-phases were formed when the substrates were heated to temperatures above 300 °C during sputtering.

Mills [8] studied the structure as a function of temperature of deposition, and he showed that the tetragonal β-phase was only formed below 300 °C; above 600 °C the structure was independent of substrate and was always bcc α-phase Ta. At intermediate temperatures, the structure was a mixture of two phases, the dominant phase depending on whether the deposition temperature was closer to 300 °C or 600 °C. The effect of higher substrate temperatures on the promotion of bcc α-phase Ta over the β-phase in sputtered coatings has generally been attributed to the increased mobility of Ta atoms in the growing films at the higher temperatures.

2.2.2 The Effect of Substrate and Underlayers

(1) Substrate Materials

Several authors found that the nature of the substrate has a large effect on the nucleation of either tetragonal β-phase Ta or bcc α-phase Ta. Previous research results of deposited tantalum on about twenty different substrate materials, which included single crystal, polycrystalline, and amorphous materials, fell into three groups based on their influence on the structure of tantalum thin films [8, 29, 38, 50, 53]. These include: (I) the substrates that were readily oxidized or formed surface oxides in air at room temperature (SiO_2, copper, nickel, amorphous glass) nucleated the β-phase tantalum; (II) substrates that did not form surface oxides even in oxidizing atmospheres (Au, Rh, Pt and W) always nucleated α-phase tantalum; and (III) substrates which did not form surface oxides in air at room temperature but which could be oxidized at elevated temperatures always

nucleated bcc α-phase tantalum when deposited directly on the freshly prepared substrate, and β-phase Ta when they were fully oxidized, while mixtures of both phases were formed when the substrates were partially oxidized, e.g., Ta_2N.

(2) Underlayers

Epitaxy is a thin film growth technology in which a thin film with approximately the same lattice structure parameter as the substrate material will grow successfully and orderly the substrate. The principle behind this is that the substrate lattice will promote the growth of a thin film with the same size and geometry of its lattice. Similarly, a thin layer of material different from the substrate and different from the final top thin film if deposited as the interlayer between the substrate and the top thin film can play a similar role. This interlayer, sometimes also called an under-layer, will promote the growth of the top thin film with the same lattice structure.

Investigations of depositing tantalum thin films on different types of substrates and under-layers have been done previously. Westwood [66] studied depositing tantalum films on a thin layer of gold and also on a carbon layer on glass. It was observed that these under-layers which cover the whole substrate and are electrically connected to the anode in the sputtering system encouraged the formation of the bcc α-phase tantalum rather than the tetragonal β-phase tantalum. The percentage of the α-phase of tantalum was higher in films deposited on substrates covered by these under-layers than in films deposited at the same time on adjacent substrates without under-layers.

Hoogeveen et al. [31] observed that β-phase tantalum always formed on SiO_2 and (111) textured copper, whereas α-phase tantalum formed on a (111) textured aluminum under layer. They claimed that some atoms in the (111) planes of fcc Al, which consisted of regular triangles with side length 0.28635 nm, were close in spacing to the atoms of the (110) planes of bcc α-phase Ta, consisting of isosceles triangles with one side length 0.28629 nm. Indeed, in this one direction, the Ta and the Al atom rows fitted extremely well, differing only by 0.02%, even though in the perpendicular direction there was no matching at all, as was usually necessary for epitaxial growth.

Sajovec [49] and Face [39] et al. showed that α-phase tantalum was always formed when deposited on an under-layer of niobium. This study also revealed that the niobium under-layer thickness was very critical to the initial nucleation step of tantalum thin films, and a minimum Nb under-layer thickness of 0.25 μ was required for the α-phase tantalum nucleation. The presence of water vapor and its possible reaction with the Nb surface caused the Ta film to grow in the β-phase structure rather than the intended bcc α-phase structure [19, 38].

Heiber and Lautenbacher [65] found that β-phase tantalum could be stabilized by a tantalum silicide interlayer. A titanium adhesion layer on SiO_2 dielectric or Si easily altered the phase formation behavior of tantalum and tantalum based thin films by promoting the formation of α-phase Ta [67]. The lattice parameter of titanium layers with hexagonal and highly (0001) preferred orientation was very close to α-phase Ta with bcc and (110) preferred orientation. The (0001) closest packed planes of the underlying titanium had a regular hexagonal mesh with a side length of 2.890 Å, and the (110)

planes of the bcc α-phase Ta consisted of an irregular hexagonal mesh with a side length 2.876 Å and thus two-dimensionally matched to the underlying titanium.

Colgan et al. [68] demonstrated that a reactively sputtered Ta(N) seed layer could promote the growth of α-phase tantalum thin films at room temperature. Earlier experiments by Leszek Gladczuk and Anamika Patel et al. [69] in our NJIT laboratory further indicated that the nitride layer which promoted the growth of α-phase Ta consisted of stoichiometric TaN.

Shimada et al. [70] also found out that TaN_x could work as a seed layer which helped self-growth of α-phase tantalum films by hetero-epitaxy. Tanaka et al. [71] found that the phase of sputtered Ta formed on a molybdenum under-layer depended on its thickness. As the thickness of molybdenum was increased, the percentage of the α-phase formed was found to be higher.

2.2.3 Post Deposition Treatment-Annealing Temperature

When the tantalum films of β-phase were heated in a vacuum of 10^{-6}~10^{-5} Torr, the β-phase to α-phase Ta transformation was reported at 700-750 °C, while the transformation temperature was lowered to 600-650 °C if in the presence of residual gases [2, 40]. Lee et al. [41] reported that upon annealing, β-phase tantalum became unstable at 300 °C, and complete β-phase to α-phase transformation occurred at ~750 °C.

2.3 Substrate Biasing

Energetic ion bombardment of the substrate and the growing film can strongly influence the film structure and properties [72]. For tantalum thin film deposition, it is still not clear from previous work whether energetic species bombardment promotes α-phase or β-phase Ta growth. The results of these different researchers are also quite contradictory and the reason for a preferential creation of one or the other phase is still not known.

In the paper of Das [7], he mentioned that RF and DC sputtered Ta films deposited without bias possessed b.c.c. α-phase structures, however, DC sputtered Ta films (at around -100 V negative substrate bias) had the structure which was interpreted as a tetragonal distorted b.c.c. superlattice. He provided an explanation by combining the effect of applying a negative potential to the substrate on the relative interstitial residual gas content and then the formation of tantalum film phase. He said that various chemically reactive and non-reactive impurities, such as sputtering gas (usually inert gas, Ar) and some residual gases (nitrogen and oxygen) in the high vacuum systems could be trapped in the thin films during the sputtering process. However, by applying a negative substrate bias, the loosely bonded impurities were re-sputtered by bringing more energetic bombardment carried by those attracted ions, and the vacuum conditions were improved dramatically. According to Knewstubb et al. [73], among the different ionization species in plasma discharges, such as N_2^+, N^+, and NO^+ ions, NO^+ will be less bonded to tantalum thin films and easily knocked off in a way described by Maissel and Schaible [74]. So the final results are an increase in the N/O ratio. He summarized that the improvements of vacuum conditions by applying substrate bias led to an over-all reduction in residual gas content in the system, so the N/O ratio, and thus the specific

interstitial nitrogen and not oxygen promote the formation of a tetragonal distorted b.c.c. superlattice, some people thought as β-tantalum phase.

The experiment done by Maissel et al. [74] further showed that high resistivity β-phase Ta formed at low bias because the positively charged impurity ions were attracted to the substrate at voltages too low for ion bombardment cleaning to be effective. While increasing the bias voltage, the low resistivity α-phase Ta formed because the ion clean-up was in effective operation.

In contrast, an IBM research group, Catania et al. [75, 76] reported more recently that β-phase tantalum was deposited by hollow cathode enhanced magnetron sputtering technique under -100 V bias, or even lower, with no significant change in film impurity levels. The results suggested that the formation of the β-phase Ta was not controlled by impurity effects but by Ta forward scattering and related stress changes. In another paper [77], these authors pointed out that the substrate bias voltage during the later stages of thin film growth was more important than that during nucleation on the substrate, and even offset initial conditions to favor the formation of the opposite phase. They also concluded that the momentum transfer effects were the central factor controlling the phase formation.

However, Cook [59, 78] indicated that the formation of α-phase tantalum was favored by enhanced ion bombardment (i.e. flux and energy) of the substrate/growing film. He claimed that a certain bombarding energy was necessary to be supplied for the formation of the low resistivity α-phase Ta, and a -100 V bias was required at 6 kV cathode voltage whilst -200 V was needed at 4 kV.

Matson et al. [16, 37] also evaluated the effect of sputtering gas species and substrate bias during deposition on the phase and microstructure of sputtered Ta coatings. They stated dense b.c.c. α-phase tantalum was the primary structure in Ta thin films deposited by Kr or Xe sputtering gases at 200°C substrate temperature, −1500 V target bias, and a higher substrate bias voltage (−100 V) during the deposit, while the β-phase Ta with distinctive columnar microstructure was formed by Ar under similar conditions. Ino et al. [60] reported that the b.c.c. α-phase Ta could be grown on SiO_2 when the ratio of ion flux to Ta flux was higher than 13 and impinging ion energy was lower than 20 eV for an Ar plasma. For different inert gas ion irradiations, the ion flux to atom flux ratio and ion energy conditions for growing the b.c.c. α-phase Ta were different. They reported that when the normalized ion to atom flux ratio is 26, the b.c.c. α-phase Ta can be grown on silicon at ion energies lower than 30 eV for Ar ions and at ion energies ranging from 30 to 90 eV for Xe ions. They claimed that there are two effects in biased sputtering that cause the phase transition from bcc α-phase to β-phase Ta. One is defect generation by the recoil implantation of Ta atoms under high ion bombardment conditions. The other is insufficient total energy input to a growing Ta film surface at low ion irradiation and resulting poor quality.

Others have stated that the β- to α-phase transformation that occurrs at high temperature is accompanied by stress relief, and they believe that the main stress relief mechanism for tantalum films with intrinsic compressive stresses to completely relax their stress is the phase transformation [79]. Impurity incorporation was another reason given for the phase transformation [38].

A major goal of this work was to find the range of conditions for growing α-phase Ta film in a RF magnetron sputtering system with substrate biasing. Table 2.2 lists the ion bombardment conditions for promoting α-phase Ta growth reported recently by researchers from the IBM group [75, 76] and the Japanese group[60]. These are the only detailed and extensive data related to this work that have been published. Both groups, however, used rather special equipment, operating at unusually low pressure (IBM group) or with a complex dual RF and dual DC power supply system (Japanese group). Their results are also quite different. To establish the conditions for α-phase Ta growth in a more standard and simpler system suitable for scaling to industrial applications is the final goal.

Table 2.2 Ion Bombardment Conditions for Growing α-phase Ta

	IBM group[75, 76]	Japanese group[60]
Deposition system	Hollow cathode enhanced magnetron sputtering system	Dual RF sputtering process
Bombarding Energy (eV)	~150, 22*	10 - 30
Energetic particles per deposited Ta atom	0.5, 1*	>13
Energy per deposited Ta atom (eV/atom)	~100	>130

* Refers to energetic Ta atoms

2.4 Tantalum Nitride Thin Film

Tantalum nitride is also a very interesting material with various excellent properties, such as chemical inertness, high hardness, corrosion resistance, high thermal stability, and a low temperature coefficient of resistance (TCR) [80] which is desired in microelectronics, especially in portable terminal and telecommunication devices for the purpose of high reliability. Tantalum nitride thin films are the most promising candidate for copper metallization diffusion barrier layers for sub-quarter-micron devices since the copper interconnects for deep submicron multilevel integrated circuit (ICs) become widely used in the electric industry [81]. Besides being widely used in the electronic industry as a barrier layer and in precise and stable thin film resistors [82-84], tantalum nitride can be deposited as a hard, wear and corrosion resistance protective coating for metals [85]. A new application of tantalum nitride is in high-speed thermal printing heads [86, 87]. One of its most promising applications is as a diffusion barrier layer in $[FeN/TaN]_n$ multilayer structures for the application as write-head materials in high-density magnetic recording systems [88].

Since the 1940s, tantalum and its compounds have been used as biomedical materials because of its excellent corrosion resistance, chemical stability and histo-compatibity. Tantalum nitride as a surface modification material, which possesses good blood compatibility and mechanical durability, has attracted considerable attention recently [34].

Tantalum nitride thin films have been successfully deposited using different types of techniques such as reactive sputtering [89-95], metalorganic chemical vapor deposition (MOCVD) [96], ion-beam-assisted deposition (IBAD) [97, 98], and electron-beam evaporation [99]. The phases sequentially formed by sputtering tantalum under increasing amounts of nitrogen partial flows include nitrogen-incorporated cubic Ta [α-Ta(N)], hexagonal Ta_2N and NaCl-type TaN [67, 83, 100, 101] based on the literatures accounts.

CHAPTER 3

EXPERIMENTAL

In this work, tantalum thin films were deposited by a RF magnetron sputtering system together with DC substrate biasing apparatus as shown in Figure 3.1. In order to have a significant fraction of Ar ions to bombard the growing Ta thin films during growth, the original DC magnetron sputtering system was modified into a RF magnetron sputtering system with the consideration of simplicity and no necessity of installing an external ion source. The modifications involved assembling a RF power supply with matching net work and tuning controlling unit with the Ta target electrode, and attaching a RF filter and the external DC power supply for providing bias on the substrate electrode. Electrical meters were hooked into the circuit for measuring the ion current. Detailed information about the apparatus used is described below followed by a description of the preparation procedures for substrates and the characterization techniques which were used to characterize the deposited tantalum thin films.

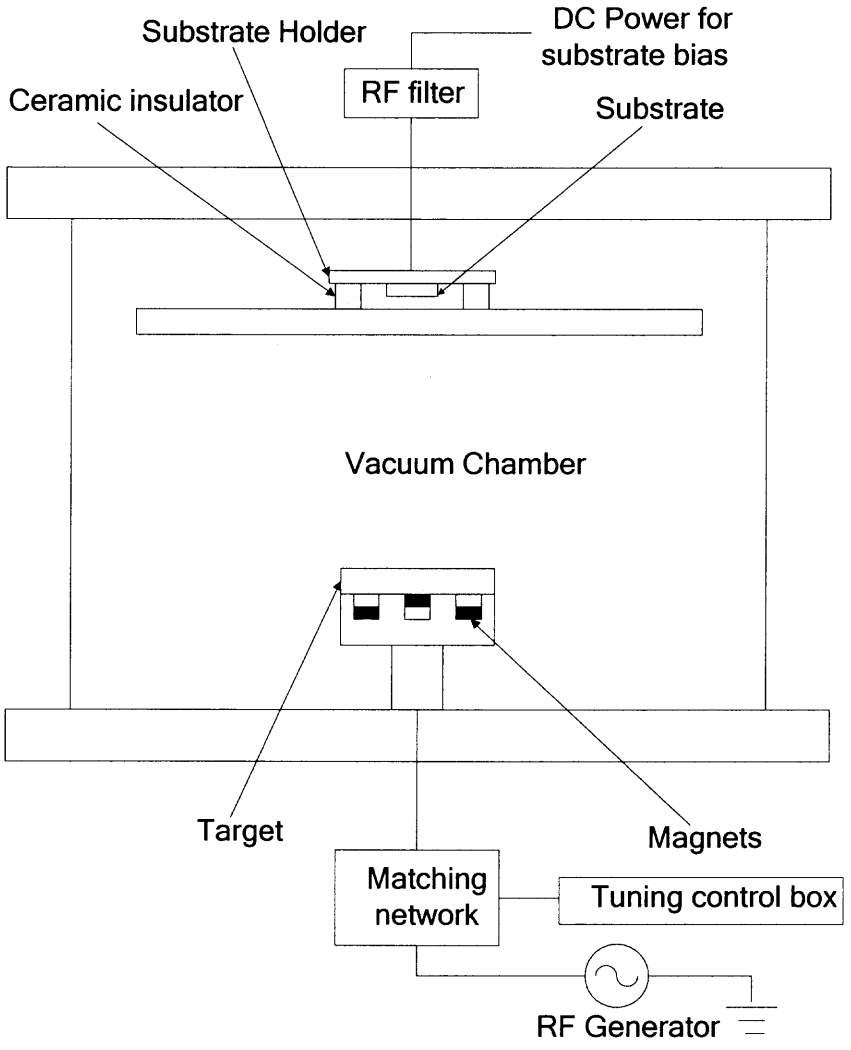

Figure 3.1 Schematic of biased RF magnetron sputtering system.

3.1 Biased RF Magnetron Sputtering

The idea of biased sputtering was to increase the electric field surrounding the substrate by applying a negative potential to the substrate beyond the field normally created by the plasma potential and thus to increase the energy and flux of positive plasma ions that could be used to bombard the growing thin films. The initial experiment with DC magnetron sputtering was simply putting a negative DC voltage on the substrate, and this only resulted in a relatively low ion current and very limited ion bombardment of the growing thin films, thus had no effect on the crystallographic structure of the deposited

tantalum thin films at all. The measured ion current and its effects on thin film growth increased significantly when the same magnetron sputtering source was powered by RF at the frequency of 13.56 MHz. The relationship between ion current and the negative substrate bias voltage is illustrated in Figure 3.2. The Ta sputtering source was operated in a 5 mTorr pressure argon environment.

In the DC mode, the target voltage was -300 V and target current 0.5 A corresponding to a power of 150 W. While in the RF mode, the RF input power was150 W and the reflected power was about 1W with the best tuning. The net input power was 149W which was close to the DC mode. However, the obtained ion current under different substrate bias voltages was relatively higher when the magnetron sputtering system was operated in the RF mode versus the DC mode as illustrated in Figure 3.2. The ion current was measured by an isolated meter attached through the substrate. One thing that needs to be kept in mind is that the secondary electrons that were ejected from the target also contribute to the measured current. Generally the secondary electron emission rate per bombardment ion was about 0.1 for metal targets in the energy range of typically observed in dc glows 100 to 1000 eV, and this depends on energy and the ion species and surface material condition as well [102]. Also, it was hard to set up the proper device and connection for measuring the ejected Ar ion current only, so here the measured current could be all counted to the attracted Ar ions with the ignorance of secondary electrons' contribution.

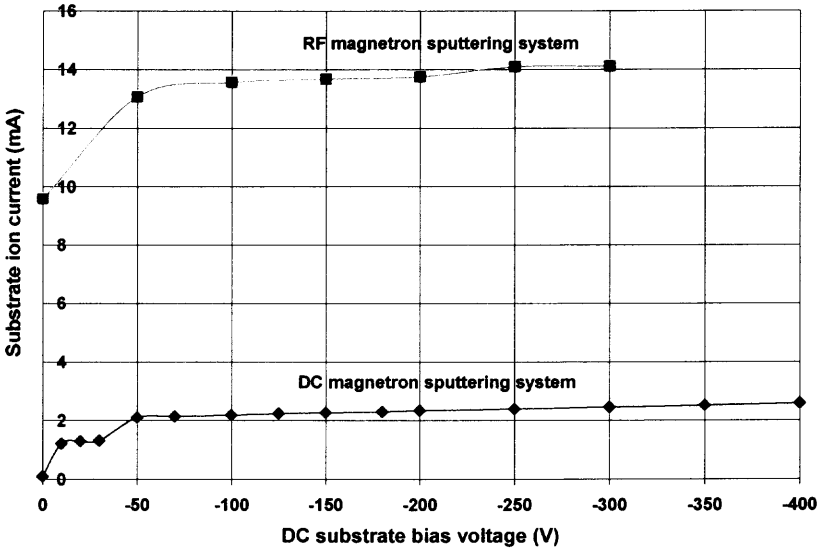

Figure 3.2 The relationship between ion current and negative DC bias voltage in DC and RF magnetron sputtering system.

The reason for this difference could be attributed to the ion density difference for magnetron system operated in the DC and RF mode. The ion density in the DC mode was only very high in the magnetic field near the target electrode where electrons were trapped, and very few ions could escape and move toward the substrate. On the other hand, the ionization efficiency of the RF electric field was much higher compared with DC electric field, and ions were effectively generated farther away from the target electrode from where they could be more easily attracted to the substrate.

The RF magnetron sputtering system for biased substrate deposition was shown schematically in Figure 3.1. The proper installation of the RF power generator and matching network was critical to the proper operation of the system. Operation of the system required proper tuning of the RF power supply with the magnetron sputtering source to maximize the transferred power for initiating and maintaining the plasma too. This function was performed by a matching network and tuning control box. Proper tuning was accomplished by maximizing the output power and minimizing the reflected

power as shown by the meters on the RF power supply. The RF filter was a type of device that allowed the passing or rejecting of signals by their frequency. Here it is connected between the substrate holder and the DC power supply to prevent AC or RF signals form entering the DC power supply, which may interfere with its operation and also with the measurement of DC voltage by the volt meter, specifically disturbing DC power operation for biasing. The detailed electric modification work was described in the Master Thesis of Savita Raina [103].

3.2 Sample Preparations

3.2.1 Substrate Clean Procedure

Two types of substrates were used to deposit tantalum thin films on, one was (100) oriented silicon wafer and the other was an aluminum disk substrate (1.0 mm thick, 15 mm diameter, 99.0% purity produced by Goodfellow Cambridge Limited). The 0.5×0.5 inch silicon substrates were first immersed into a 10% diluted hydrofluoric acid for about 2 mins. This step was used to remove the silicon native oxide top layers and also surface contaminants. The second step was to rinse the substrates several times in the de-ionized water. Then the substrates were rapidly mounted on the substrate holder and loaded into the vacuum chamber in order to avoid the fresh cleaned silicon substrate getting oxidized and contaminated again.

For the aluminum substrates, general ultrasonic cleaning steps were performed in two types of chemical solutions in the sequence of ethanol, acetone and ethanol, and each for 10 mins. The freshly cleaned substrates needed to be mounted and loaded into the vacuum chamber quickly after ultrasonic cleaning. After loading the substrates, pumping

the sputtering vacuum chamber was done as soon as possible, to keep the substrates in a relatively clean environment.

3.2.2 Vacuum

The chamber baking step was performed after the base pressure of sputtering vacuum chamber reached the 10^{-7} Torr level indicated by a vacuum sensor. This step was mainly used to remove the water vapor which was absorbed on the internal chamber wall. The baking temperature was monitored by a thermal couple at a temperature around 150 °C for 24 hrs. The pressures of various residual gases were listed in Table 3.1, monitored by an INFICON - QUADREX 200 Residual Gas Analyzer before baking and after the baking (when system cooling about 12 hrs).

The concentration (partial pressures) of various gases in the vacuum, especially water vapor and carbon dioxide, decreased dramatically after performing chamber baking as indicated by the Residual Gas Analyzer. It was found that this step was necessary for depositing thin films with lower contamination and consistent structure and quality. Considering a partial pressure of 10^{-6} Torr, it corresponds to approximately 0.42 monolayers of air impurity atoms striking the surface during deposition per sec. Then the 0.42 monolayers impurity atoms were comparable to 0.07 nm per sec of deposited Ta. If the impurity arrival rate (partial pressure) was a high fraction of the deposition rate, then significant contamination could be expected for deposited Ta thin films, such as reactive elements O and OH. However, in the case of the experiment done here, the Ta thin films were deposited under the argon inert gas working pressure of 5 mTorr, and the impurity arrival rate was only a very small fraction of deposition rate.

Table 3.1 The Pressure of Residual Gas in the Sputtering System Vacuum Chamber before and after Baking

Residual gas	Gas pressure before baking (Torr)	Gas pressure after baking (Torr)
Total base pressure	1.5×10^{-6}	3.5×10^{-7}
Hydrogen	5.4×10^{-8}	5.1×10^{-8}
Water	7.7×10^{-6}	5.8×10^{-7}
N_2/CO	3.7×10^{-7}	3.7×10^{-7}
Oxygen	3.6×10^{-8}	7.8×10^{-8}
CO_2	1.9×10^{-7}	3.2×10^{-8}

3.2.3 Thin Film Deposition

The base pressure of the sputtering system was about 5.0×10^{-8} Torr with pumping by the turbo-pump and crypo-pump after chamber baking, and readied for thin film deposition. Substrate sputter etching cleaning prior the deposition was proven to be another important step for depositing thin films with consistent quality in this investigation. By doing this, the 99.999% pure Ar gas was first introduced into the sputtering chamber, at a gas flow of 18 sccm which could be regulated and controlled by a gas flow control meter. The substrate holder was turned to the position directly in front of the observation window, and an electrical connection made between the substrate holder and the power supply for conducting sputter etching cleaning to the substrates attached to it. The sputter etching step was processed at 400 V DC power with the substrate ion current in the range of 1~10 mA (0.03~0.3 mA/cm^2), and the Ar gas pressure of 250~350 mTorr for 20 min.

According to the sputtering yield (S, the number of atoms sputtered by one incident ion) data for different materials summarized in ref. [104] Table 3-4 of page 113, S = 1.05 for Al and S = 0.5 for Si at 0.5 keV Ar, this leads to 10^{15} Al or 5×10^{14} Si atoms per square cm per sec. sputter removed from the substrate by sputtering etching based on the average ion current density 0.16 mA/cm^2 per sec. i.e., ~10^{15} ions/cm^2 per sec. So for the 20 min sputter etching exposure time, about 1.2×10^{18}/cm^2 (~200 nm) Al and 6×10^{17}/cm^2 (~120 nm) Si atoms were removed during these process at the extreme conditions.

After the substrates finish sputter etching, it was moved directly to the position right above the magnetron sputtering source for deposition. The sputtering source was running approximately half an hour prior the deposition for removing the accumulated contaminations of the Ta target, such as oxidized surface layer, as well as for stabilizing the target operation, and the substrates were properly shielded during this cleaning step. The Ar gas work pressure during thin film deposition was 5 mTorr. The pre-determined substrate bias voltage was then applied, and the substrates shield was removed to deposit Ta film on substrate. The deposited Ta film thickness was controlled by deposition time, and later was measured based on the Rutherford Backscattered measurement.

3.3 Characterization Techniques

3.3.1 X-Ray Diffraction

For deposited tantalum thin films, learning the crystallographic structures of deposited tantalum films was the priority task, and X-ray diffraction (XRD) methodology was used here for this purpose. XRD could be used to identify the structure of single crystalline, polycrystalline and amorphous material for both powder and thin film samples. It also could be used to determine the internal stress of different samples by knowing the peak position shift relative to stress-free samples and the crystal size by analyzing the full width at half maximum intensity (FWHM) of the peak. Here a Philips PW3040 X-Ray diffractometer was used to perform a continuous scan under the conventional 2theta scan and the generator settings of 45 kV and 40 mA. The X-ray was provided by copper (Cu) with the Kα-1 wave length of 1.540598 nm.

For tantalum, the typical XRD spectra of sputter deposited tantalum thin film is shown in Figure 3.3. As the figure shows, the first primary peak for the sputtered α-phase Ta is the (110) peak at a (2θ) angle of 38.438° and for the β-phase is a (002) peak at a (2θ) angle of 33.555° [105, 106]. These peaks appearing between 30 to 40 degrees turned out to be the major peaks used for identifying the sputtered Ta films crystallographic phase structures.

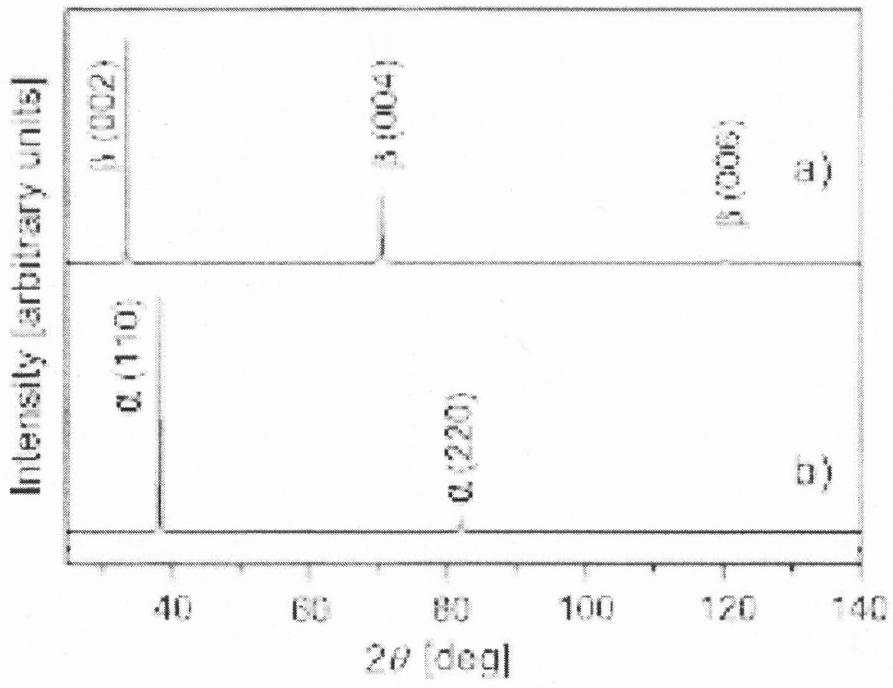

Figure 3.3 Typical XRD spectra of sputter deposited α-phase and β-phase tantalum thin films.

Based on Bragg's Equation, the spacing, d, between the crystals planes with the specific orientation (hkl) which shared the same normal direction respective to the sample surface could be expressed as Equation 3.1:

$$\text{Bragg's equation: } 2A = 2d_{(hkl)} \sin\theta = n\lambda \tag{3.1}$$

The lattice strain could be calculated by using the lattice spacing d as an internal gauge, expressed by Equation 3.2.

$$\varepsilon = \frac{d - d_0}{d_0} \tag{3.2}$$

Where ε is the lattice strain, d is the plane spacing of the sample and d_0 is the plane spacing of a strain free reference sample. In the majority of cases of thin films only a biaxial stress was formed so that the measurement in the Bragg-Brentano geometry was possible. If the strain was homogeneous and isotropic in the thin film substrate interface,

the lattice stress could be determined from the shift of a diffraction line or peak by using Equation 3.3 below.

$$\sigma_1 + \sigma_2 = -\frac{E}{\mu} * \varepsilon \tag{3.3}$$

Where σ represents the stress, E is Young's modulus and μ is Poisson's ratio of the material investigated [107].

By using the Scherrer Equation 3.4, the crystal size of deposited tantalum thin films could be estimated. It describes peak broadening in terms of incident beam divergence which made it possible to satisfy the Bragg condition for non-adjacent diffraction planes. Once instrument effects had been excluded, the crystallite size could be easily calculated as a function of peak width (specified as the full width at half maximum peak intensity, FWHM), peak position and wavelength [28, 108].

$$t = \frac{0.9\lambda}{B\cos\theta_B} \tag{3.4}$$

$$B^2 = B_M^2 - B_S^2 \tag{3.5}$$

Here λ is the wavelength of the X-ray source, θ_B is the Bragg angle, and B is the full width at half maximum height at $2\theta_B$ referred to a standard sample.

3.3.2 Rutherford Backscattering

Rutherford backscattering (RBS) is a material analytical technique based on scattering of high energetic ions, generally MeV, from atoms at the surface and in the near-surface area of tested material. A 2~4 MeV high energy and low mass He^{2+} was directed toward the sample, and a small fraction of particles (~10^5) backscattered from the sample after colliding with the sample atom nuclei were detected by an energy-sensitive detector

placed at an angle close to 180° with respective to the sample surface normal. The backscattered energy of these energetic particles is related by momentum and energy conservation laws of the incident energy to the mass of the sample elements from which the particle backscattered. RBS is an absolute analytical technique since the relative number of particles backscattered from a sample atom for a given number of incident particles is related to the probability of incident high energy ions backscattered from a given material. The scattering cross section determined by the Coulomb potential was used to express this probability, and it was proportional to the square of the atomic number of the target atom. On the other hand, those ions which backscattered from an element at some depth in the sample would have less energy than those backscattered from the sample surface, and the energy loss of the ions was due to interaction with electrons and collision with nucleus when penetrating to some depth in the sample. The amount of energy loss for each ions distance traversed in the sample depends on the element in the sample, and most importantly, the element density. This can provide the information of the sample composition versus different depth as well as sample thickness for thin films.

As for billiard ball scattering, particles such as helium 4 ions used here (m=4) backscattered from a heavy element nucleus like Ta retains a higher fraction of its energy therefore produced a higher energy signal in the spectrum than lighter elements (Si) in the substrate. Thin films could were analyzed by RBS for composition, thickness and uniformity with depth. The RBS operation conditions listed in the Table 3.2.

Table 3.2 RBS Operating Conditions

Incident ion	Incident ion	^{4}He
	Incident ion energy (keV)	2000.00
Geometry	α Incident angle (Deg.)	0.00
	β Exit angle (Deg.)	26.00
	θ Scattering angle (Deg.)	154.00
Calibration	Calibration offset (keV)	53
	Energy per channel (keV/ch)	5.7150
Energy resolution	Detector resolution (keV)	19.0

Generally, the values obtained for element concentrations from RBS were absolute values needing no further calibration, while the depth and thickness numbers (in nm) were not absolute unless the density of the material was correctly known. Usually, a model based on the actual scattering cross section and the stopping power was used to generate a theoretical spectrum which was then adjusted until a fit was obtained to the experimental data. Here the software "SIMNRA 5.02" was used to simulate the RBS energy spectrum by adjusting element concentration, and film thickness as identified by number of atoms per square cm. By knowing the tantalum thin film density and assuming the density uniformity though the film thickness, the actual film thickness could be determined by the following Equation 3.6.

$$T = \frac{n \times W_{atomic}}{\rho \times N_A} \tag{3.6}$$

Where n (number/cm^2) was the Ta film thickness (aerial density) obtained by RBS simulation, W_{atomic} (g/mole) was the element atomic weight (180.92 for Ta), ρ (g/cm^3) was density and N_A (6.02×10^{23}/mole) was Avogadro's number.

3.3.3 Scanning Electron Microscope (SEM)

Unlike conventional optical microscopes which use a series of glass lenses to bend light waves and create a magnified image, SEM is a microscope that uses electrons to form a detailed 3-dimension image with much higher magnifications. For example, with the beam angular width of 0.3° (5 mrad) and under the same magnification of 30, the depth of field for SEM was 670 μm while 4 μm for optical microscope. This allows people a view of the substance with much smaller features.

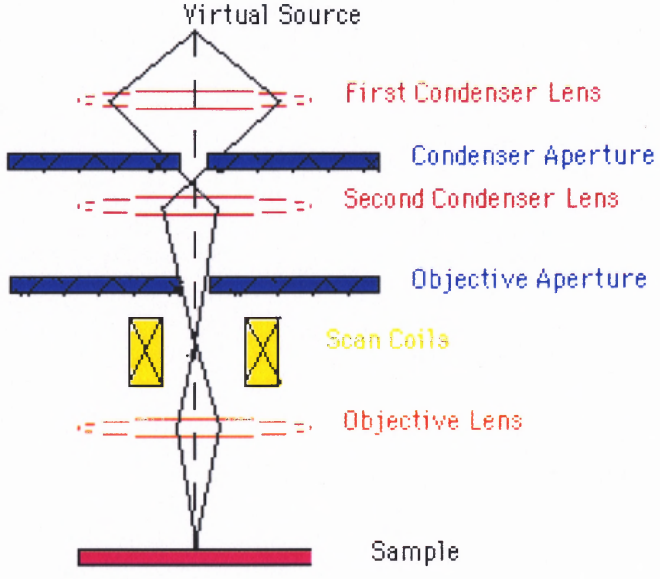

Figure 3.4 Schematic of SEM [109].

The electron beam came from a fine filament, typically a tungsten hairpin gun, and then was accelerated toward the anode. Some electrons were accelerated right by the anode and on down the column, to the sample, as shown in Figure 3.4. The Cylindrical Magnetic Lens played a role of focus and directed the electrons to the sample. When the electron beam struck the sample, both photon and electron signals were emitted. But not all of them were detected and recorded, commonly only secondary electrons, the backscattered electron and X-rays were caught and used for information.

Here the field emission scanning electron microscopy (LEO 130 FE_SEM) was used under "inlens" detection mode to obtain the surface morphology information of deposited tantalum thin films, in which the secondary electron detector produced a clear and focused topographical image of the samples. Samples for SEM require electrically conductive adhesive. For the metallic conductive samples, the sample was directly placed on the sample holder by adhesion conductive carbon glue tape. The SEM images were taken to see the top morphology of the tantalum thin film.

3.3.4 Atomic Force Microscopy (AFM)

The atomic force microscopy (AFM), one kind of scanning probe microscopy (SPM), was invented in 1986 by Binnig, Quate and Gerber. By utilizing a sharp probe moving over the surface of a sample in a raster scan, the tip of the AFM which was on the end of a cantilever bent in response to the interaction between the tip and the sample, therefore the topography features of the surfaces could be imaged and recorded.

Normally there were two different modes, contact mode and tapping mode. Tapping mode was used for soft, adhesive or fragile samples since the forces imposed on samples using the tapping mode was much weaker than using contact mode. The contact mode was the most common method of operation of the AFM, in which the tip and sample remained in close contact as the scanning proceeded (in the repulsive regime of the inter-molecular force curve). One of the drawbacks of the contact mode was that there existed large lateral forces on the sample as the tip was "dragged" over the specimen. In this work, the contact mode was chosen to image the surface topography of deposited different Ta thin films. A Nano-Scope IIIa manufactured by Digital Instruments was

used. The AFM images were shown and discussed further in the following chapter. It had 2~10 nm lateral resolution and 0.1 nm vertical resolution.

CHAPTER 4

EXPERIMENTAL RESULTS

For this investigation, different thickness tantalum thin films on silicon and aluminum substrates have been prepared by the modified biased RF magnetron sputtering system under different substrate bias voltages. Below are the experimental results of film thickness and foreign atom incorporation measured by RBS, crystallographic structure, lattice strain and crystal size of Ta thin films obtained by XRD spectra analysis, and the top surface film morphology observed by SEM and AFM.

4.1 RBS Measurement

RBS measurements were performed on tantalum thin films deposited for 10 min under different bias voltages. Two representative RBS spectra of Ta thin films deposited on Si-100 substrates for 10 min with substrate bias voltages of 0 V and -300 V are shown in Figure 4.1. The thin film thicknesses shown in Figure 4.2 was obtained (in terms of the number of atoms per unit area) from fitting the measured spectra with simulated curves by using SIMNRA 5.02, and the film thickness was derived based on the formula described in Section 3.3.2 with the assumption that tantalum thin films have the same density as bulk Ta (16.8 g/cm^3).

(a)

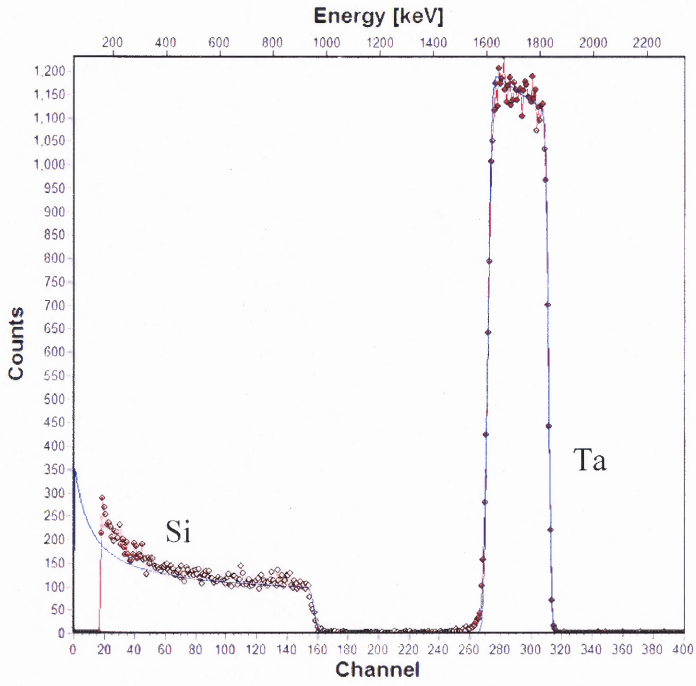

(b)

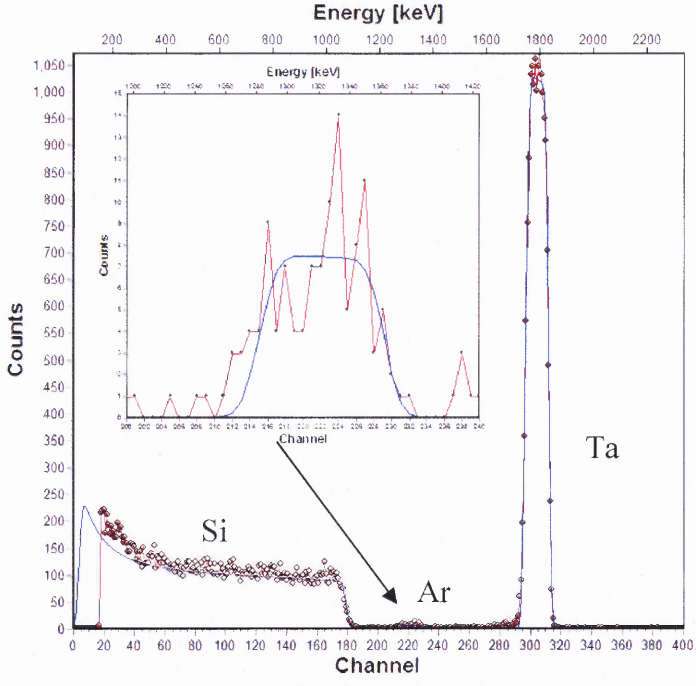

Figure 4.1 RBS spectra of tantalum thin films deposited under (a) 0 V and (b) -300 V for 10 min. (—•— Experimental points — Fitting line)

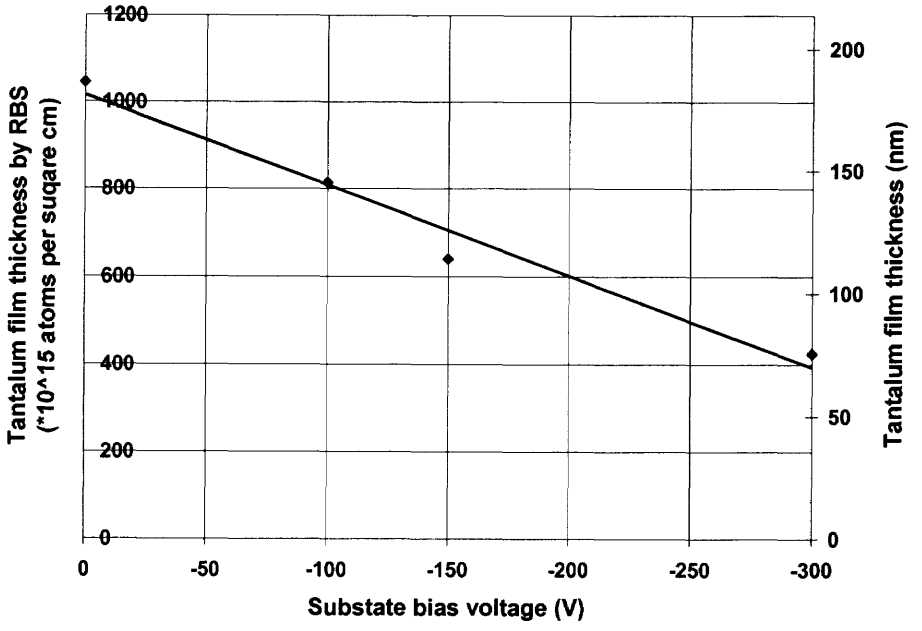

Figure 4.2 The film thickness of tantalum thin films deposited for 10 min under different substrate bias voltages.

The tantalum thin film thickness are expressed in units of 10^{15} atoms per square cm, which corresponds to about one monolayer of Ta, since one monolayer of material roughly contained 10^{15} atoms per cm^2. It was seen that the tantalum thin film thickness decreased with increasing negative substrate bias voltage. The Ta film thickness deposited with the bias voltage of the -300 V was only a half of that deposited at 0 V and this indicated that the tantalum thin film got re-sputtered by Ar ions accelerated by -300 V substrate bias voltages. It was also found that the film thickness of tantalum deposited under the same bias voltage of 0 V for 10 min was 186 nm and 260 nm by using two different Ta sputtering targets. One of these targets was used for many hours and showed deep erosion, and one was a new target. This was reasonable, because people could expect the difference in the sputtering angular distribution between the brand new target and the used target.

The RBS spectrum of tantalum thin film deposited under -300 V for 10min is shown in Figure 4.1 (b), and the simulation result also indicated that there was about 10% Argon (Ar) implanted into the tantalum thin film under -300 V bias, while there was undetectable Ar incorporation indicated by RBS for tantalum thin films deposited under the lower bias voltages (0 ~ -200 V).

From the RBS measurements of tantalum films deposited for 10 min and the measured in-situ ion current, a ratio of Ar ions to arriving Ta atoms at the substrate and the growing Ta thin film sputtering yield by different substrate bias voltages attracted Ar ions were derived and listed in the Table 4.1 below.

Table 4.1 Substrate Ion Bombardment Parameters

Bias voltage (V)	0	-100	-150	-300
Substrate Ar ion current (mA)	9.60	13.58	13.69	14.13
Film thickness ($\times 10^{15}$Atoms/cm^2)	1046	815	640	425
Ratio of Ar Ions/incoming Ta atoms	0.90	1.27	1.28	1.32
Sputtering Yield of growing Ta films	-	0.17	0.30	0.45

During the biased sputtering deposition, Ar ions transfer their energy and momentum to Ta atoms of the film, and the number of Ar ions needed to sputter away each Ta atom from the growing films decreased as the ion energy increased. The sputter yield is defined as the number of atoms or molecules ejected from a target surface per incident ion. It is a fundamental parameter for measuring the efficiency of sputtering. In this case, the sputtering yield of the growing Ta thin films was defined as the number of Ta atoms removed from the growing thin film surface per incident Ar ion.

The Ta sputtering yield under different bias voltages was then derived under the assumption that the flux of incoming Ta atoms under different bias voltages never changed and was the same as it was under 0 V bias. Also it was assumed that there was no sputtering of the growing Ta thin films under 0 V bias. The Ta thin film sputtering yield of 0.45 at 0.3 keV Ar was close to that extrapolates to the previously reported experimental value of 0.57 at 500 eV [104]. Detailed sputtering yield comparisons of semi-empirical formula calculation results, experimental data would be introduced along with MD simulation results in Section 5.4. When the substrate bias voltage increased to -300 V, approximately 10% atomic Ar was incorporated into the Ta thin film as found by RBS measurement. These incorporated Ar atoms are about 3% of the total impinging Ar ions (derived by ion current).

4.2 XRD Measurements of Tantalum Thin Films

In order to understand the crystallographic phases, XRD measurements were performed for the bias sputtering deposited tantalum thin films. The analysis methods described in Section 3.3.1 for XRD spectra were used to further determine the internal lattice strain and crystal size of those tantalum thin films too. The detailed results are shown as below.

4.2.1 The Crystallographic Structure Identification of Tantalum Thin Films

Thin tantalum films were first deposited under different substrate bias voltages ranging from 0 V to -300 V for 10 min, on both silicon and aluminum substrates subjected to a approximately 20 min sputter etching prior to deposition. The XRD spectra of these thin tantalum films are illustrated in Figures 4.3 and 4.4. Scans over a wide 2θ range (20^{o}-

160°) have not revealed other significant reflections, and convinced us that these two prominent peaks represent the films crystallographic texture and are a reliable measure of the presence of the two phases.

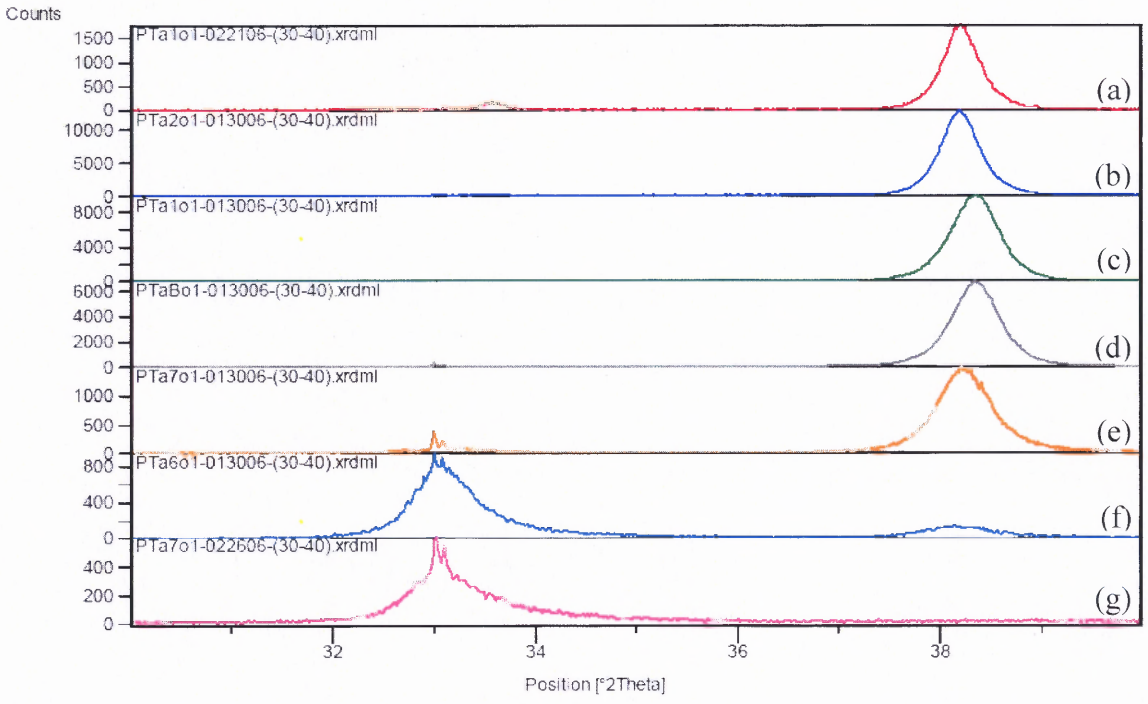

Figure 4.3 XRD spectra of tantalum thin films deposited on silicon substrates with sputter etch (S.E.) for 10 min under different substrate bias voltages (a) 0 V, (b) -50 V, (c) -100 V, (d) -150 V, (e) -200 V, (f) -250 V, and (g) -300 V.

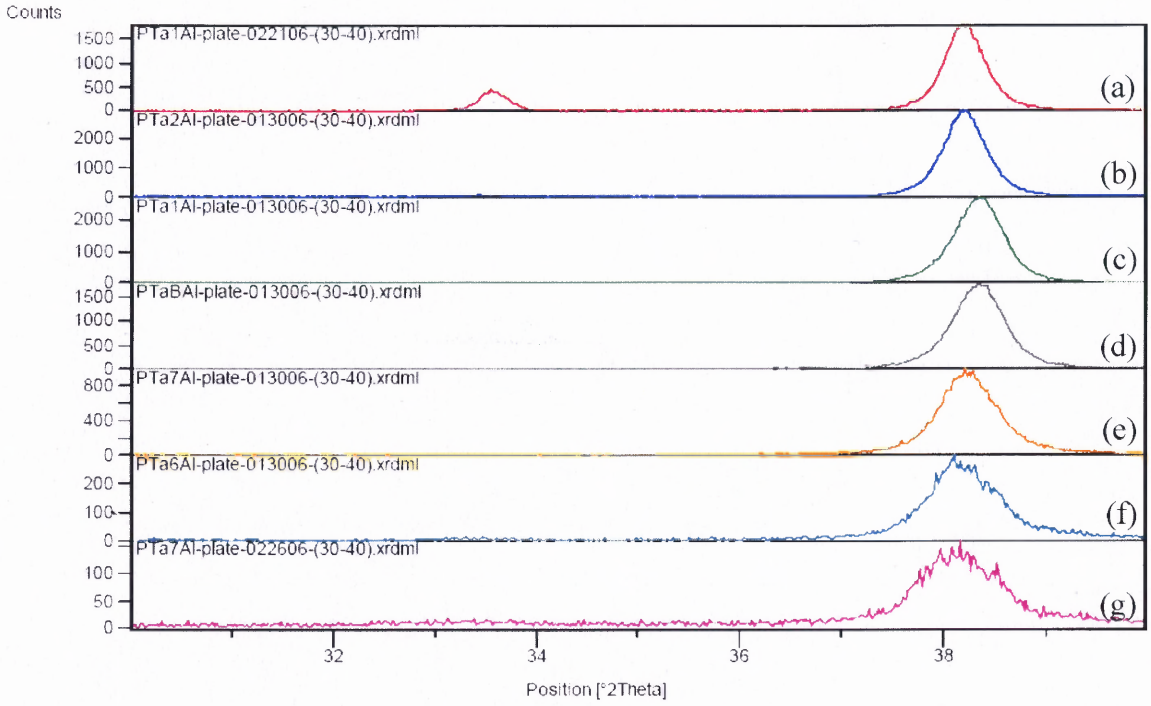

Figure 4.4 XRD spectra of tantalum thin films deposited on aluminum substrates with S.E. for 10 min under different substrate bias voltages (a) 0 V, (b) -50 V, (c) -100 V, (d) -150 V, (e) -200 V, (f) -250 V, and (g) -300 V.

Figures 4.3 (a) and 4.4 (a) clearly show that tantalum thin films with mixed phases, identified by the α-phase Ta (110) peak at 38.438 and the β-phase (002) peak at 33.555, grew with 0 V substrate bias on both silicon and aluminum substrates. The intensity of the α-phase Ta peak was higher than the β-phase Ta peak in these figures, but it was also observed that sometimes the intensity of the β-phase Ta peak was higher than that of the α-phase Ta peak for 0 V bias deposited Ta thin films as shown in Figure 4.5. This indicates that the tantalum thin film phase formation is quite sensitive to over all deposition conditions.

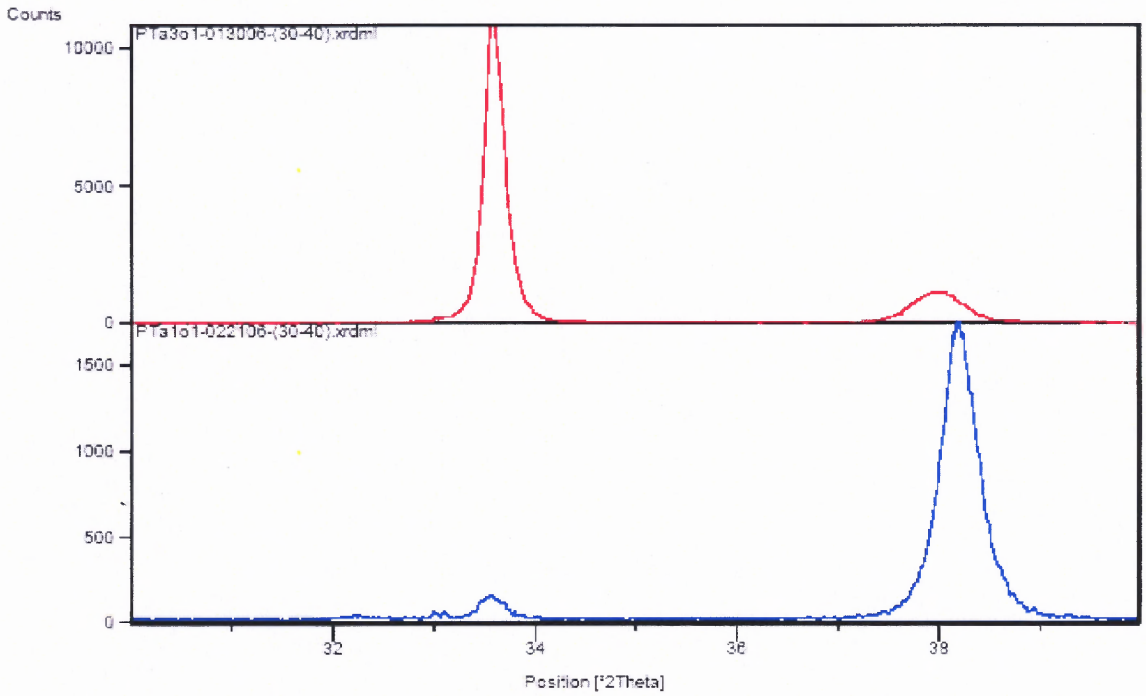

Figure 4.5 XRD spectra of tantalum thin film deposited under the same nominal conditions, 0 V bias for 10 min deposition, under different runs.

At a negative substrate bias voltage of -50 V (Figures 4.3 (b) and 4.4 (b)), α-phase Ta became the dominant crystallographic structure of the thin films, and 100% pure α-phase Ta grew for substrate bias voltage of -100 V, -150 V and even -200 V (Figures 4.3 (c)~(e) and 4.4 (c)~(e)) on both silicon and aluminum substrates. However, upon further increasing the substrate bias voltage up to -250 V and -300 V, tantalum thin films grown on silicon substrates returned back to the β-phase, while tantalum thin films grown on aluminum substrate were still α-phase as shown in Figures 4.3 (f), (g) and 4.4 (f), (g) .

As mentioned in Section 3.2.2, the substrate sputter etching prior the deposition was a very important step for depositing consistently high quality thin films. The XRD spectra in Figures 4.6 and 4.7 were obtained for the thin tantalum films deposited on both silicon and aluminum substrates without performing a sputter etching cleansing step.

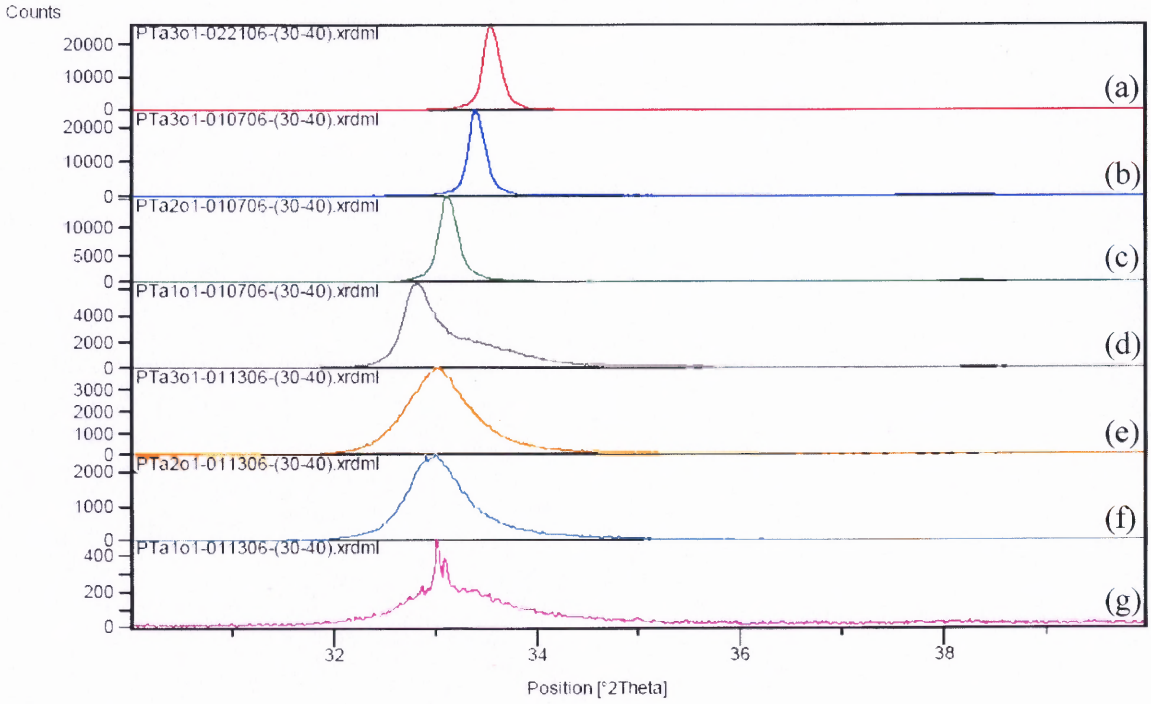

Figure 4.6 XRD spectra of tantalum thin films deposited on silicon substrates without S.E. for 10 min under different substrate bias voltages (a) 0 V, (b) -50 V, (c) -100 V, (d) -150 V, (e) -200 V, (f) -250 V, and (g) -300 V.

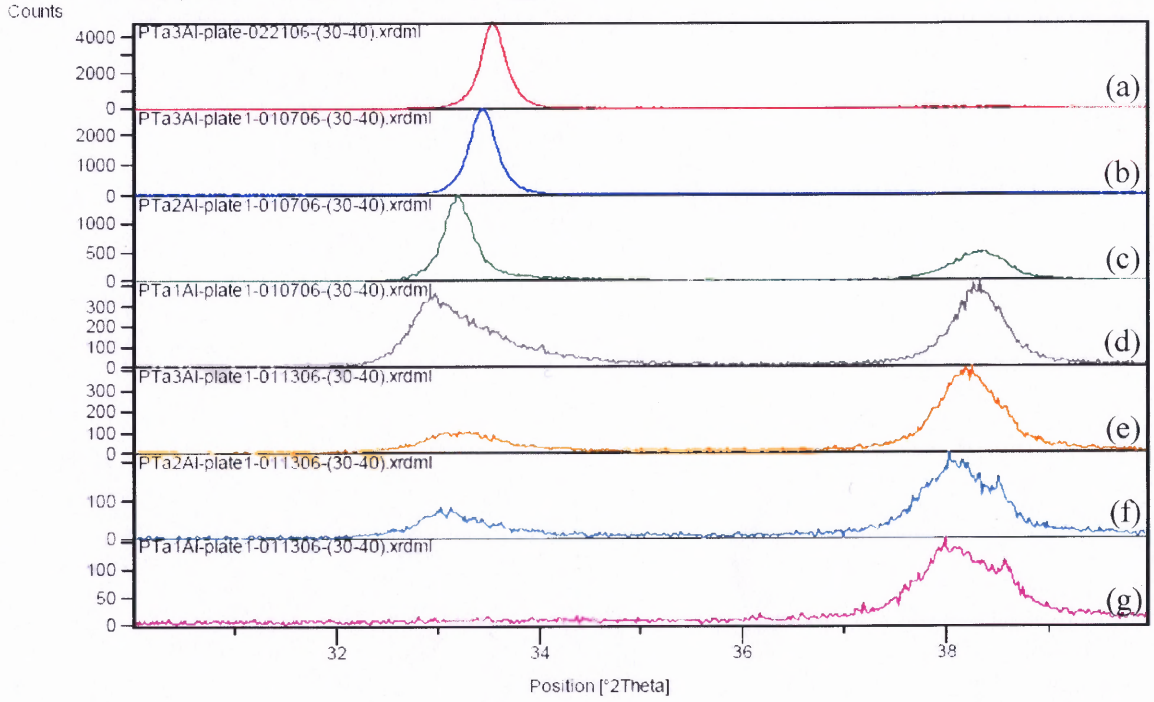

Figure 4.7 XRD spectra of tantalum thin films deposited on aluminum substrates without S.E. for 10 min under different substrate bias voltages (a) 0 V, (b) -50 V, (c) -100 V, (d) -150 V, (e) -200 V, (f) -250 V, and (g) -300 V.

By comparing the spectra of Figures 4.3, 4.4 with Figures 4.6, 4.7, it was clear that the β-peak Ta dominated the structure of Ta films which were deposited without performing the pre-deposition sputter etching under different substrate bias voltages on both silicon and aluminum substrates. The sputter etching effect appeared to be dramatically stronger even for films deposited on silicon substrates since there was only a strong β-phase Ta peak and no detectable α-phase Ta peak regardless of the bias voltage for those Ta films deposited without a sputter etching (S.E.) step.

Figures 4.8 and 4.9 showed XRD spectra were for tantalum thin films deposited with different thicknesses by controlling the deposition times under 0 V bias conditions. These figures showed that tantalum thin films grew initially with strong α-phase component, and which even dominated the structure of the 15 min deposition films.

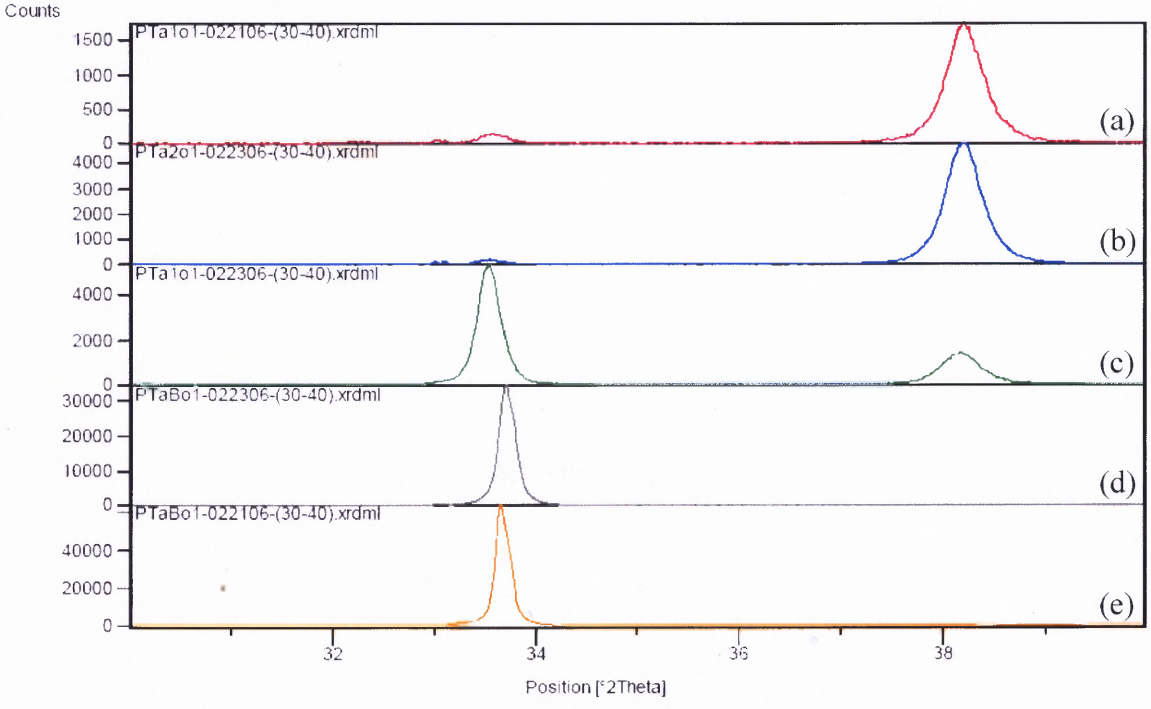

Figure 4.8 Tantalum thin films deposited on silicon substrates with S.E. under 0 V bias for (a) 10 min, (b) 15 min, (c) 20 min, (d) 30 min, and (e) 40 min.

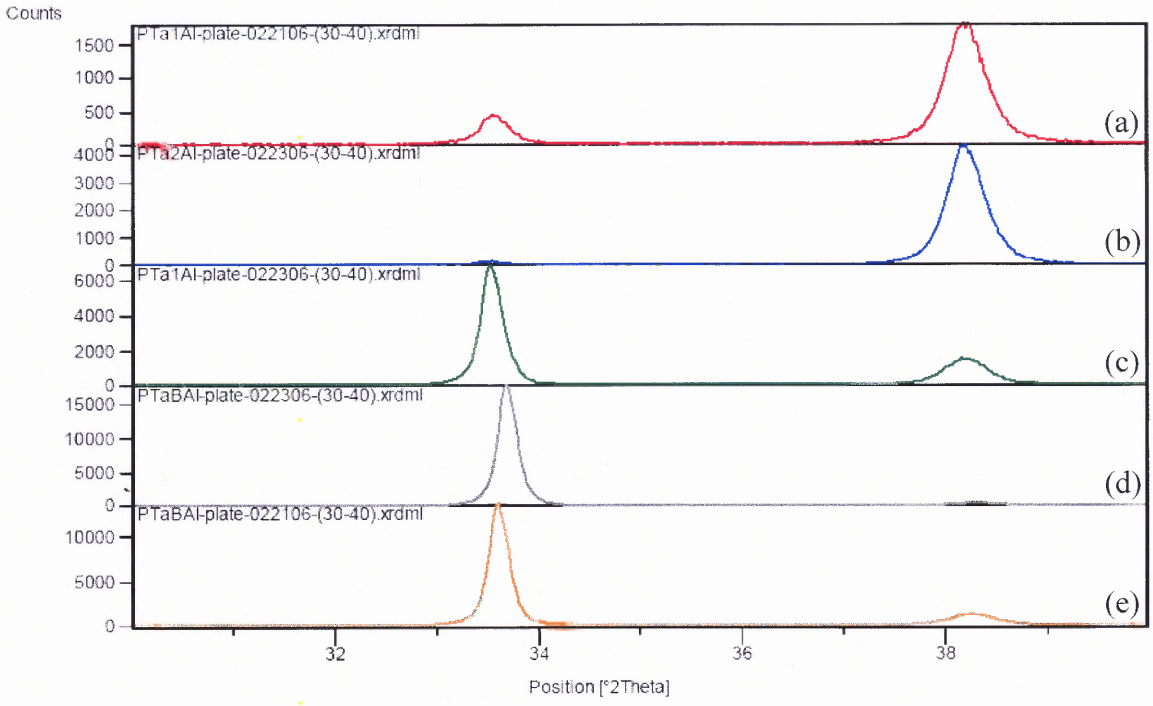

Figure 4.9 Tantalum thin films deposited on aluminum substrates with S.E. under 0 V bias for (a) 10 min, (b) 15 min, (c) 20 min, (d) 30 min, and (e) 40 min.

But for thicker tantalum films (20 min deposition films), the β-phase was dominant structure and there was only very small amount α-phase component detected. This phase transformation happened for thicker tantalum films deposited on both silicon and aluminum substrates. Different thickness tantalum thin films deposited under other substrate bias voltages ranged from -50 V to -150 V were also deposited, and the XRD spectra of those films were illustrated in Figures 4.10~4.15.

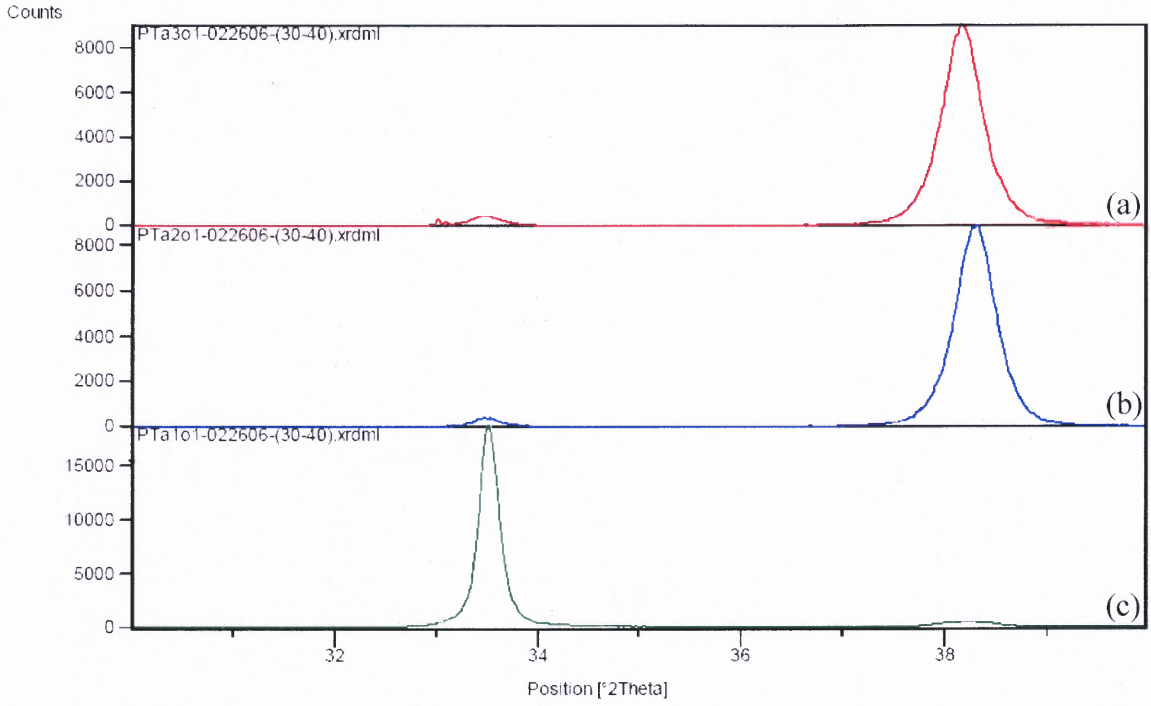

Figure 4.10 Tantalum thin films deposited on silicon substrates with S.E. under -50 V bias for (a) 10 min, (b) 20 min, and (c) 30 min.

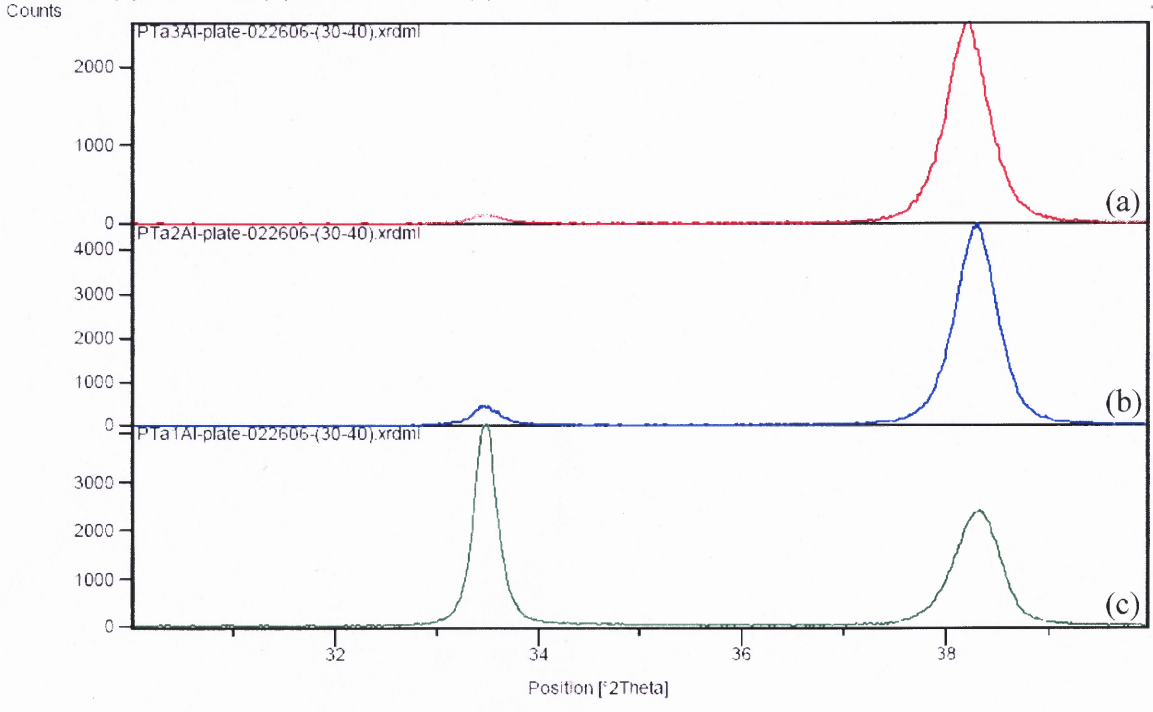

Figure 4.11 Tantalum thin films deposited on aluminum substrates with S.E. under 50 V bias for (a) 10 min, (b) 20 min, and (c) 30 min.

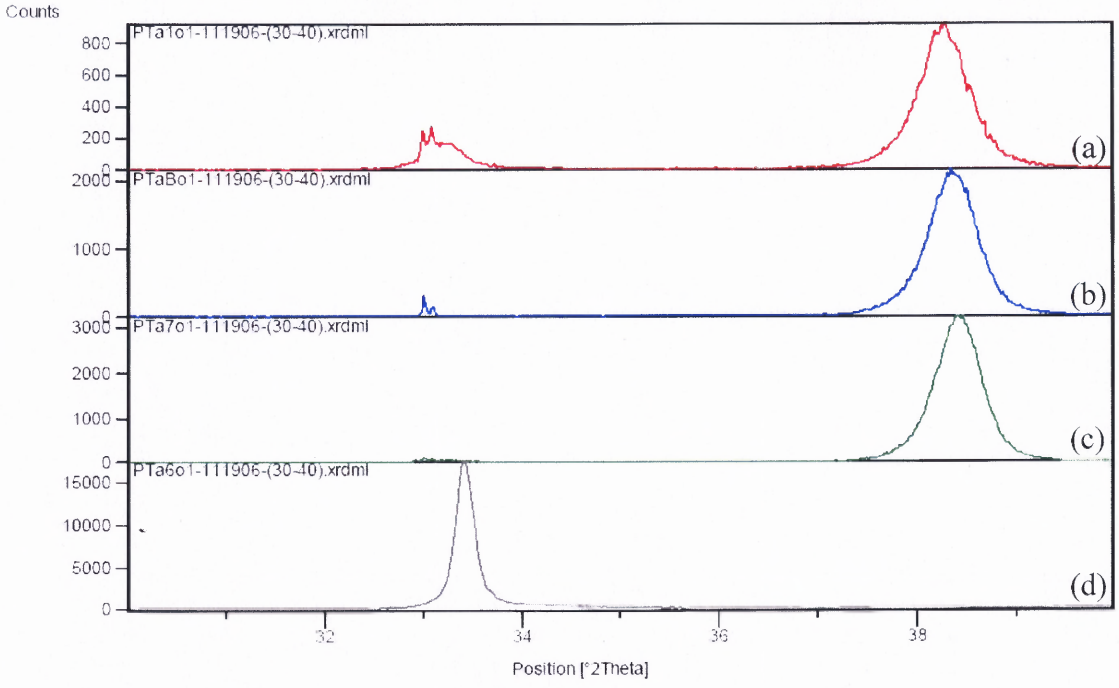

Figure 4.12 Tantalum thin films deposited on silicon substrates with S.E. under -100 V bias for (a) 5 min, (b) 10 min, (c) 15 min, and (d) 20 min.

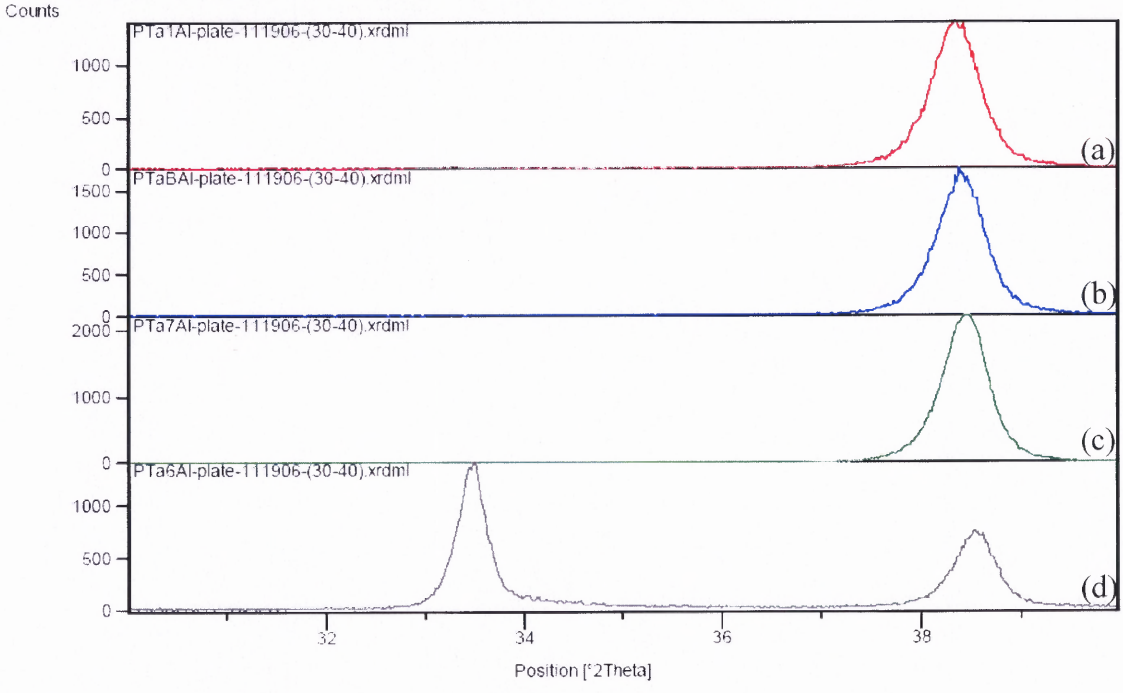

Figure 4.13 Tantalum thin films deposited on aluminum substrates with S.E. under -100 V bias for (a) 5 min, (b) 10 min, (c) 15 min, and (d) 20 min.

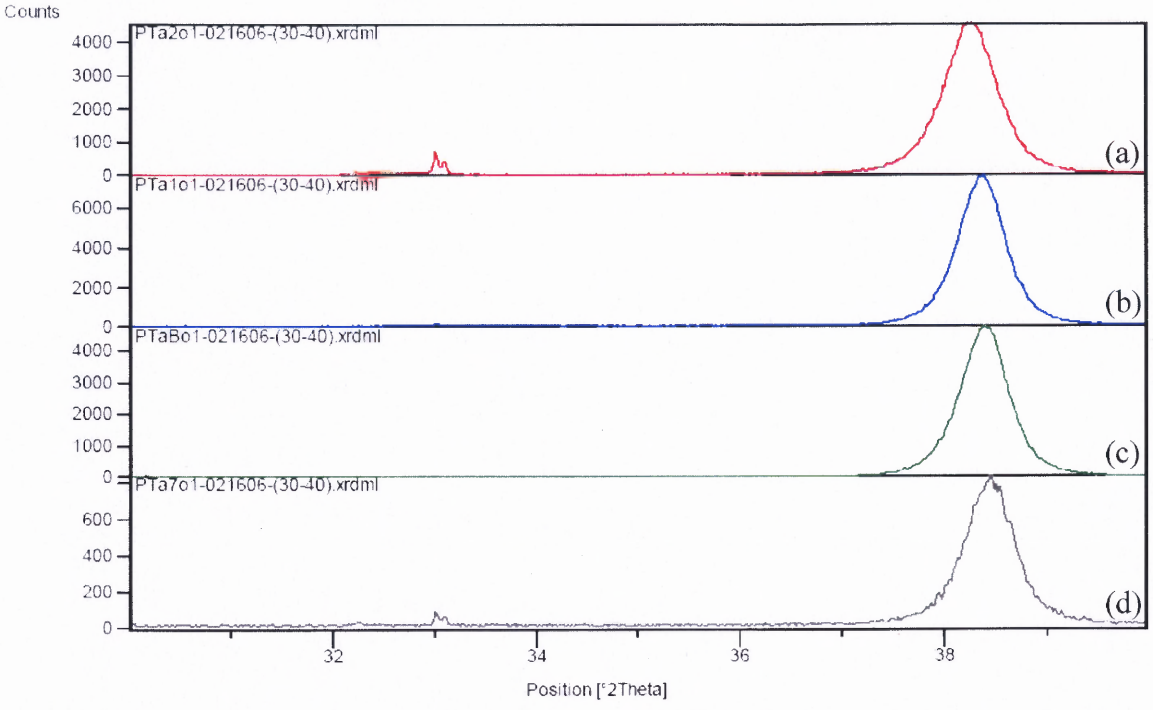

Figure 4.14 Tantalum thin films deposited on silicon substrates with S.E. under -150 V bias for (a) 5 min, (b) 10 min, (c) 20 min, and (d) 40 min.

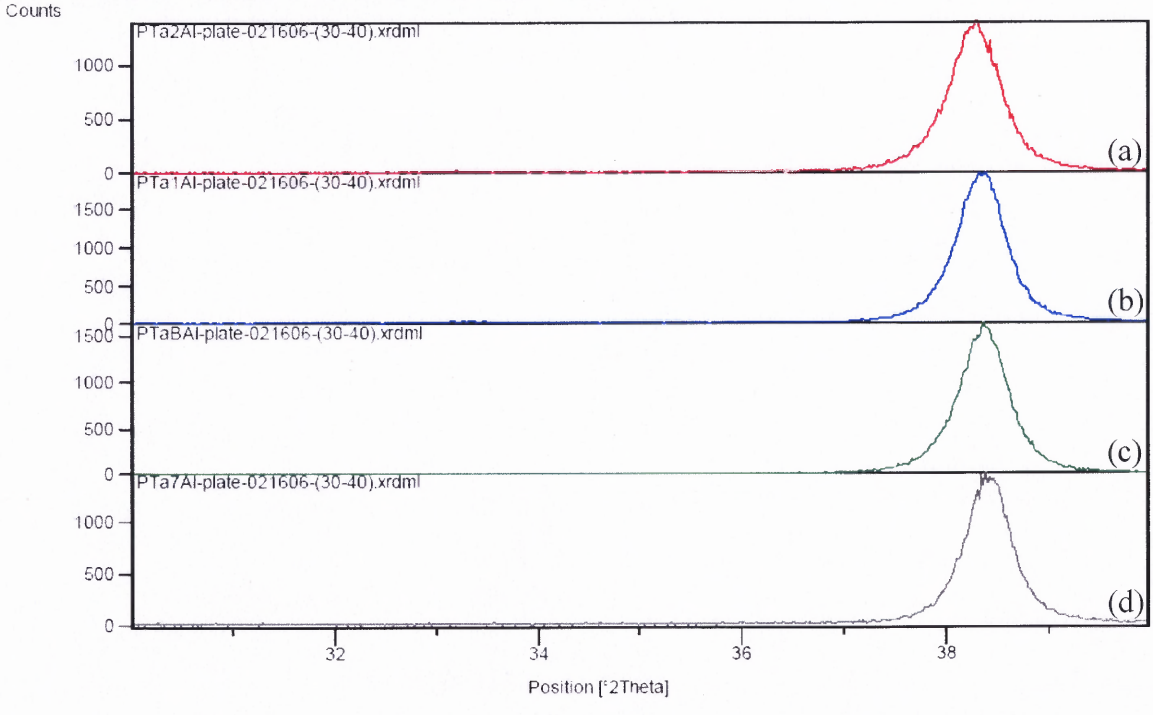

Figure 4.15 Tantalum thin films deposited on aluminum substrates with S.E. under -150 V bias for (a) 5 min, (b) 10 min, (c) 20 min, and (d) 40 min.

The intensity (peak height) of the β-phase peak relative to the α-phase peak increased when the film became thicker (longer times deposition than 10 min) for bias voltages -50 V and -100 V. While on the other hand for tantalum thin films deposited under -150 V bias, the β-phase structure never appeared, and the α-phase structure always remained to be the only type even for Ta thin films deposited for longer times as shown in Figures 4.14 and 4.15.

For 20 min deposition, tantalum thin films deposited under higher bias voltages such as -300 V, the β-phase structure dominated in the film deposited on silicon substrates, but the film deposited on aluminum substrates at the same time still had α-phase as shown in Figures 4.16 and 4.17.

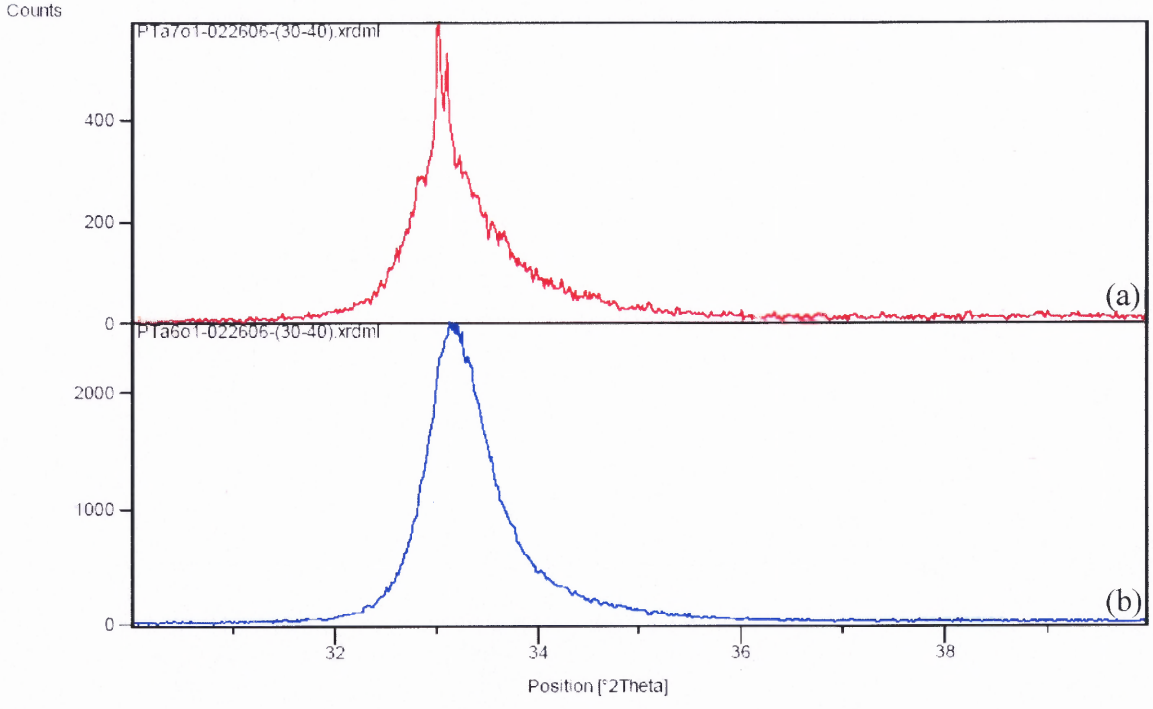

Figure 4.16 Tantalum thin films deposited on silicon substrates with S.E. under -300 V bias for (a) 10 min, and (b) 20 min.

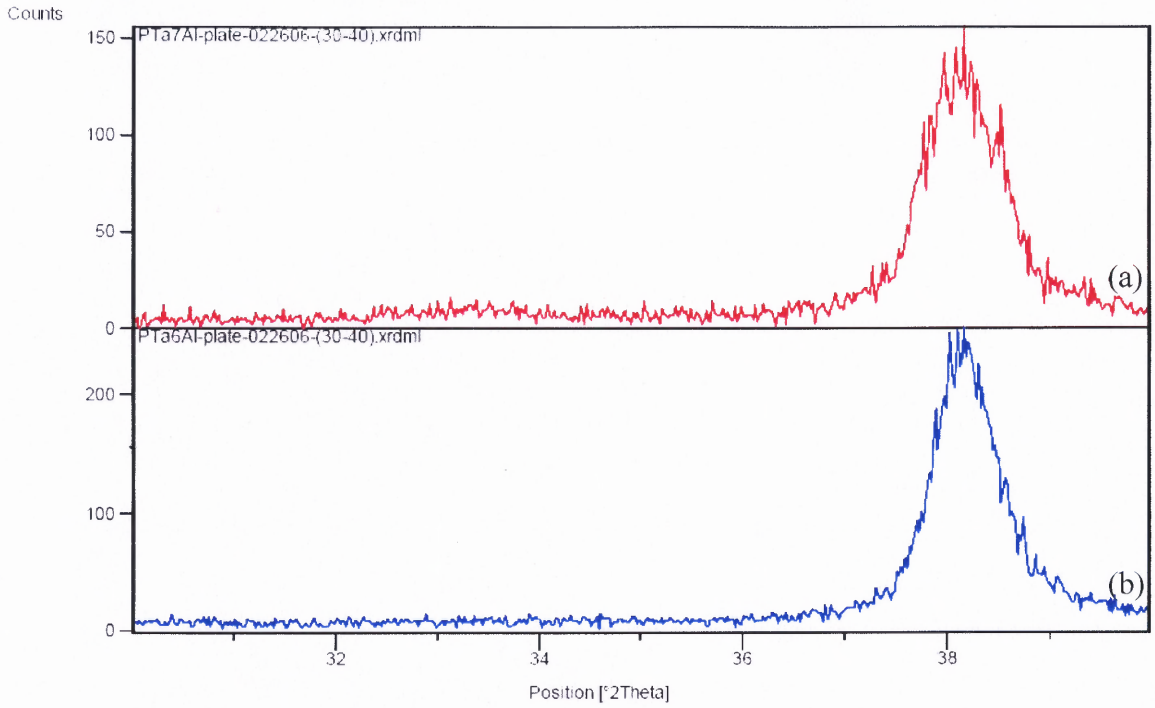

Figure 4.17 Tantalum thin films deposited on aluminum substrates with S.E. under -300 V bias for (a) 10 min, and (b) 20 min.

After the observation of the tantalum thin films phase changing with applying different substrate bias voltages (0 ~ -300 V) and different thickness, there were still questions left like whether the substrate negative bias condition was only needed for the initial nucleation stage or even later for the growth stage of the thin film deposition process.

In order to answer this, tantalum thin films were deposited in two steps. First by providing -150 V bias voltage (the conditions at which the crystallographic structure of tantalum thin film deposited on silicon substrate was identified to be α-phase Ta) for 10 min, and then the bias voltage was changed to -300 V (the conditions at which the crystallographic structure of tantalum thin film deposited on silicon substrate was identified to be β-phase Ta) to continue the deposition for another 10 min. The XRD

spectrum of this thin film sample is shown in Figure 4.18 (d). It was clear that once the α-phase Ta grew under -150 V bias voltages, it would keep growing with the same structure even when the bias voltage was increased to -300 V.

A further confirmation experiment was performed by depositing tantalum thin film under -300 V for 10 min on the α-phase Ta thin films deposited earlier (under -150 V for 10 min) and had been removed from the deposition chamber for XRD analysis. The XRD spectrum of the Ta thin film deposited earlier under -150 V is shown in Figure 4.18 (a), while the film also consisting of additional later deposited tantalum thin film layer under -300 V is shown in Figure 4.18(c). Only the α-phase Ta peak appeared too. As a reference, another bare silicon substrate was placed on the same substrate holder next to the one already with earlier deposited Ta thin film, and a tantalum film was deposited only under the -300 V for 10 min at the same time. This reference sample showed only β-phase peak, as expected (Figure 4.18 (b)). This experiment even provided a convincing proof that the substrate bias condition for getting the α-phase Ta at the initial thin film nucleation stage was most important and necessary.

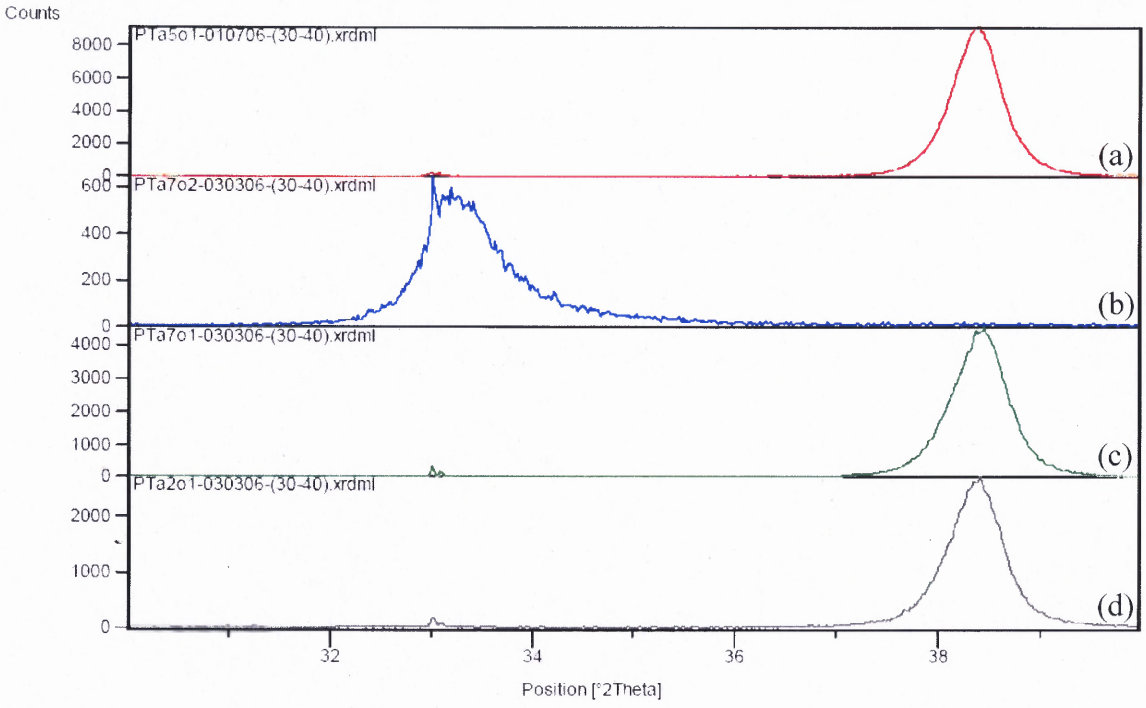

Figure 4.18 XRD spectra of tantalum thin films deposited on silicon substrates: (a) under -150 V for 10 min, (b) under -300 V for 10 min, (c) under -300 V for 10 min on earlier deposited film (a), and (d) initially under -150 V for 10 min then continuing deposition under -300 V for 10 min.

By reversing the order of applied substrate bias conditions, the tantalum thin films were initially deposited under -300 V bias for only 1 min, and then changed the bias voltage to -150 V for the rest 9 min deposition. Figure 4.19 shows the XRD spectra of the crystallographic structure of the films on silicon and aluminum substrates.

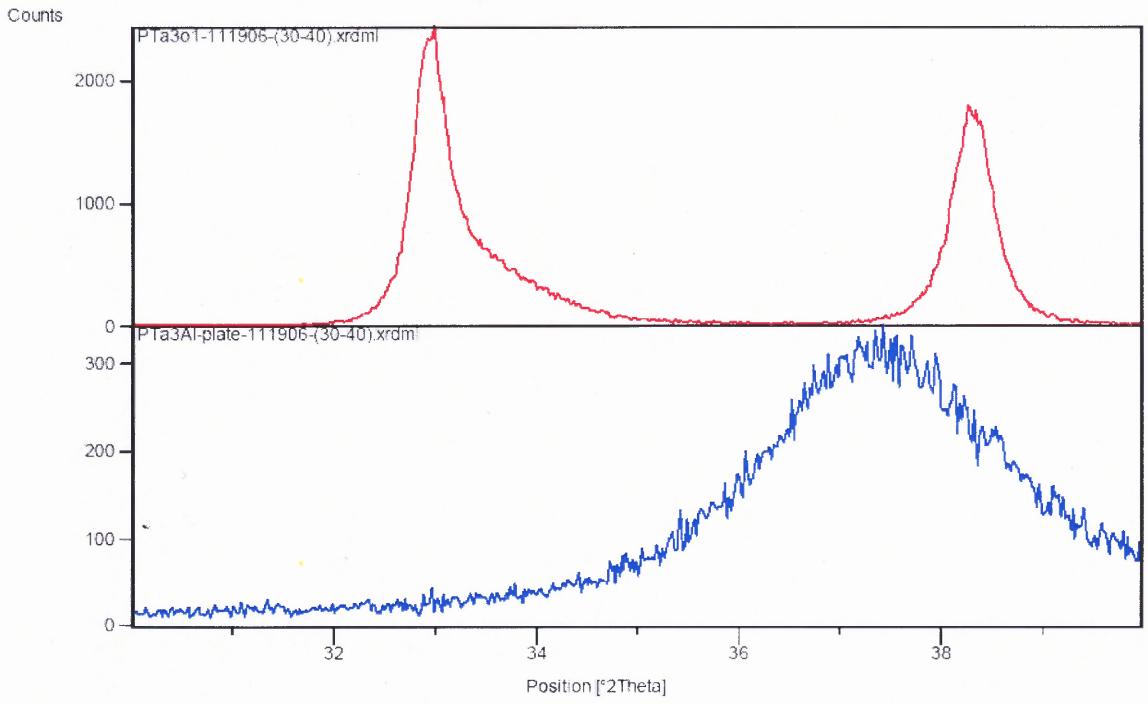

Figure 4.19 XRD spectra of tantalum thin films deposited with mixed bias conditions: -300 V for 1 min then changes to -150 V for 9 min on (a) silicon, and (b) aluminum substrate.

It appeared to be a mixed phase growing on the silicon substrate, while still only α-phase Ta on aluminum substrate but a very broad peak. This indicated that the tantalum thin films initial nucleation stage was most important for defining the final film crystallographic structures.

4.2.2 Internal Lattice Strain and Crystal Size of Tantalum Thin Films

Internal lattice strain and the crystal size are other important issues for thin films deposited by different technologies, and it is believed that these are correlated with the thin film phase structure changes too. Using the formula introduced in Section 3.3.1, the internal lattice strain of thin tantalum films could be determined by comparing the XRD peak position shift with respect to the peak position of strain-free films. According to the

unit cell lattice constant of tetragonal β-phase reported by Moseley et al. [110], a=10.194 Å and c=5.313 Å, the spacing of the (002) crystal planes was 2.6565 Å, and the spacing between the (110) crystal planes of bcc α-phase Ta was 2.3376 Å, based on the lattice constant of 3.3058 Å [41].The crystal size also could be calculated by Scherrer Equation 3.4 from the full width at half maximum of the designated XRD peak.

The results derived from the width of the (110) α-phase peak show that this phase grows in small crystals (8 – 24 nm) as seen in Table 4.2 and Figure 4.20. The grain size does not change appreciably with the film thickness (Figure 4.21). The grain size of β-phase were found to be much larger, and in contrast to the α-phase significantly decreasing with increasing bias voltages (Table 4.2).

Table 4.2 Grain Size in Ta Thin Films

Bias Voltage (V)	Deposition Time (minutes)	Film Thickness* (nm)	α-phase (nm)	β-phase (nm)
0	10	186.4	24	32
	20	(369)	25	32
	30	(554)	-	86
	40	(738)	-	128
100	10	145	18	-
	20	(290)	-	62
150	10	114	19	-
	20	(228)	19	-
	40	(456)	18	-
250	10	(89)	9	12
300	10	76	7**	10
	20	(152)	11**	12

* Determined from RBS using bulk Ta density (16.8 g/cm^3)
Numbers in parentheses interpolated form deposition time

** Films on Al substrate, all other on Si

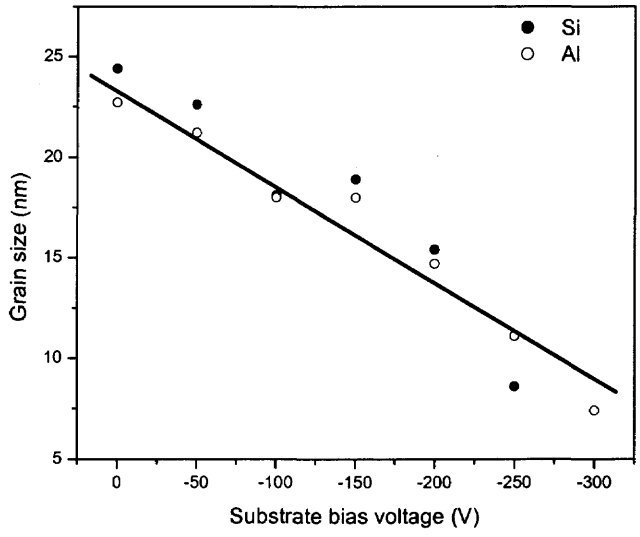

Figure 4.20 The grain size of the α-phase crystals in Ta thin films deposited for 10 min. with different substrate bias voltages based on Sherrer formula.

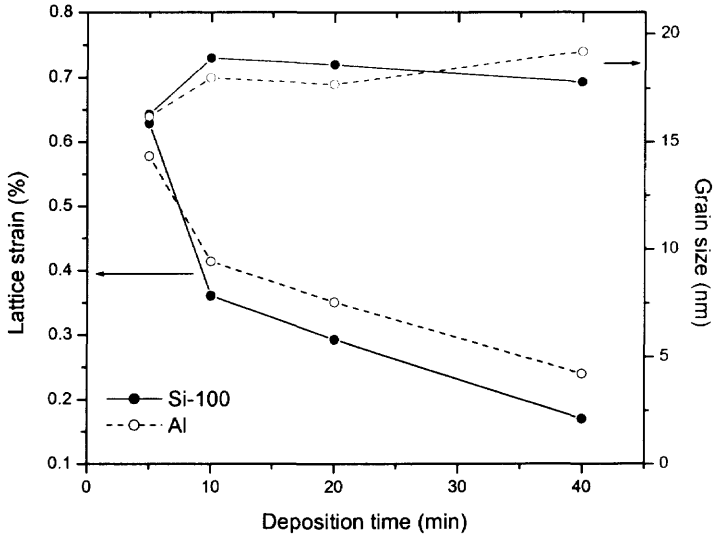

Figure 4.21 Lattice strain and grain size in α-phase Ta thin films deposited for different times at a substrate bias voltage of -150 V.

The internal bcc lattice strain for films on Si substrates deposited for 10 min under different bias voltage is shown in Figure 4.22. There is a significant drop in compressive strain at -100 V and -150 V bias, where the α-phase dominates the film structure. Further increases in bias increases the compressive strain. The dependence of strain on thickness of the films deposited with -150 V bias, consisting of the α-phase, is shown in Figure 4.21.

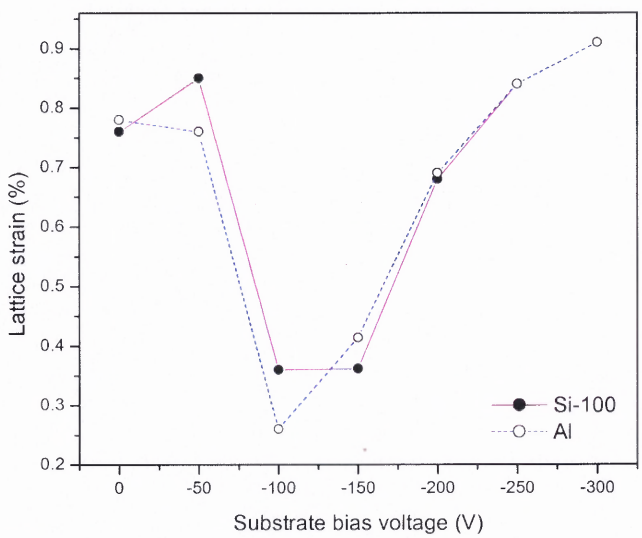

Figure 4.22 Lattice stain in α--phase crystals Ta thin films deposited for 10 min. with different substrate bias voltage for 10 min.

The crystallite size of tantalum thin films decreased with increasing substrate bias, and this decrease partially reflects their smaller thickness, due to re-sputtering, as shown by RBS measurements. The minimum internal lattice strain was observed in the thin film deposited under -100 V and -150 V bias. By observing the XRD spectra, it was also seen that a large β-phase Ta (002) peak position shift for films deposited on silicon substrates, seeing Figures 4.3 (a) and (g), 2θ angle of 33.548° (with 0 V substrate bias) changed to 33.07° (under -300 V substrate bias). Usually the strain free β-phase (002) oriented peak

position was at a 2θ angle of 33.555 degrees. So the strains of β-phase Ta in the films deposited on silicon substrates with 0 V substrate bias and -300 V substrate bias voltages were 0.5% and 1.9% respectively. This meant that the β-phase Ta crystal was highly expanded in the direction normal to the film surface while highly compressed in the direction parallel to film surface.

It had also been noticed for the XRD spectra (Figure 4.6) of tantalum thin films deposited under different substrate bias voltages on silicon substrates, without pre-deposition sputter etching cleaning that only the β-phase (002) Ta peak appeared, and the peak shifted significantly toward lower angles when the bias voltage increased. This indicated that the compressed stress accumulated in the lattice plane which was parallel to the thin film surface too.

In addition, the crystallographic phase of thicker (deposition time longer than 10 min) tantalum thin films on silicon substrates would change from mainly α-phase (undetectable β-phase) to β-phase dominant mixed phases when the applied substrate bias voltage was -100 V, and would not change, for pure α-phase, when the applied substrate bias voltage was -150 V, even thought the internal lattice strain of α-phase for both 10 min deposition tantalum thin films under -100 V and -150 V bias possessed the similar minimum value. The concern was that how the internal lattice strain developed for both phases with the film thickness increases when the applied substrate bias voltages were -100 V, and how this was related with the phases changing. In order to answer these questions, the internal lattice strain and crystal size for both phases in the different thickness tantalum thin films deposited under -100 V bias were evaluated, and listed in the Table 4.3. The relative amount of β-phase Ta listed in the table was determined by

peak intensity in XRD spectra, i.e., the percentage of β-phase (002) peak intensity relative to the peak intensity of α-phase (110) peak and β-phase (002) peak.

Table 4.3 The Relative amount of β-phases Tantalum with Different Thickness Deposited under -100 V Bias and Their Lattice Strain and Grain Size

Substrate	Deposition time (min)	Film thickness* (nm)	Relative amount of β-phase Ta (%)	β-phase (002) peak		α-phase (110) peak	
				Lattice strain (%)	Grain size (nm)	Lattice strain (%)	Grain size (nm)
Si	5	(73)	0.16	1.55	21	0.59	17
	10	145	~0			0.36	18
	15	(218)	0.02	1.59	20	0.22	20
	20	(290)	1	0.95	62		
Al	5		0			0.4	18
	10		0			0.26	18
	15		0			0.16	20
	20		0.65	0.76	29	-0.08	20

* Determined from RBS using bulk Ta density (16.8 g/cm^3)

Similarly, the internal lattice strain and grain size for only α-phase Ta in the different thickness tantalum thin films deposited under -150 V bias were also evaluated, and listed in the Table 4.4.

Table 4.4 The Lattice Strain and Grain Size of α-phases for Different Thickness Tantalum Thin Films Deposited under -150 V Bias

Substrate	Deposition time (min)	α-phase (110) peak	
		Lattice strain (%)	Grain size (nm)
Si	5	0.63	16
	10	0.36	19
	20	0.29	19
	40	0.17	18
Al	5	0.58	16
	10	0.41	18
	20	0.35	18
	40	0.24	19

It was concluded that tantalum thin films deposited under -150 V bias possessed only the stable α-phase structure, and the crystal size did not change much with the film thickness, while the lattice strain decreased when the film thickness increased. For tantalum thin films deposited under -100 V bias on silicon, it grew initially with the mixed phases structures with small amount of highly stressed β-phase (about two times higher than α-phase in the same film) at the 5 min deposition. It then became almost pure α-phase at 10 min deposition, but this bias condition could not stabilize the film crystal structures as it finally turned to be only the β-phase with a lower level stress and very large size crystals when the deposition time was 20 min. During increasing Ta film thickness at -100 V bias, the lattice strain and crystal size of α-phase component for the same group of films changed in the same manner as observed in those films deposited under -150 V bias. For tantalum thin film deposited under -100 V bias on aluminum substrates, the β-phase structure was also observed in the film deposited for 20 min with low level stress and comparable large size crystals, and even the α-phase component became expanded in the direction parallel to the film surface.

4.3 SEM Images of Tantalum Thin Films

SEM images of different magnification were taken for tantalum thin films deposited on silicon substrate under 0 V, -100 V, -150 V and -300 V bias for 10 min. These images presented in Figures 4.23 ~4.25 showed the surface morphology of these thin films.

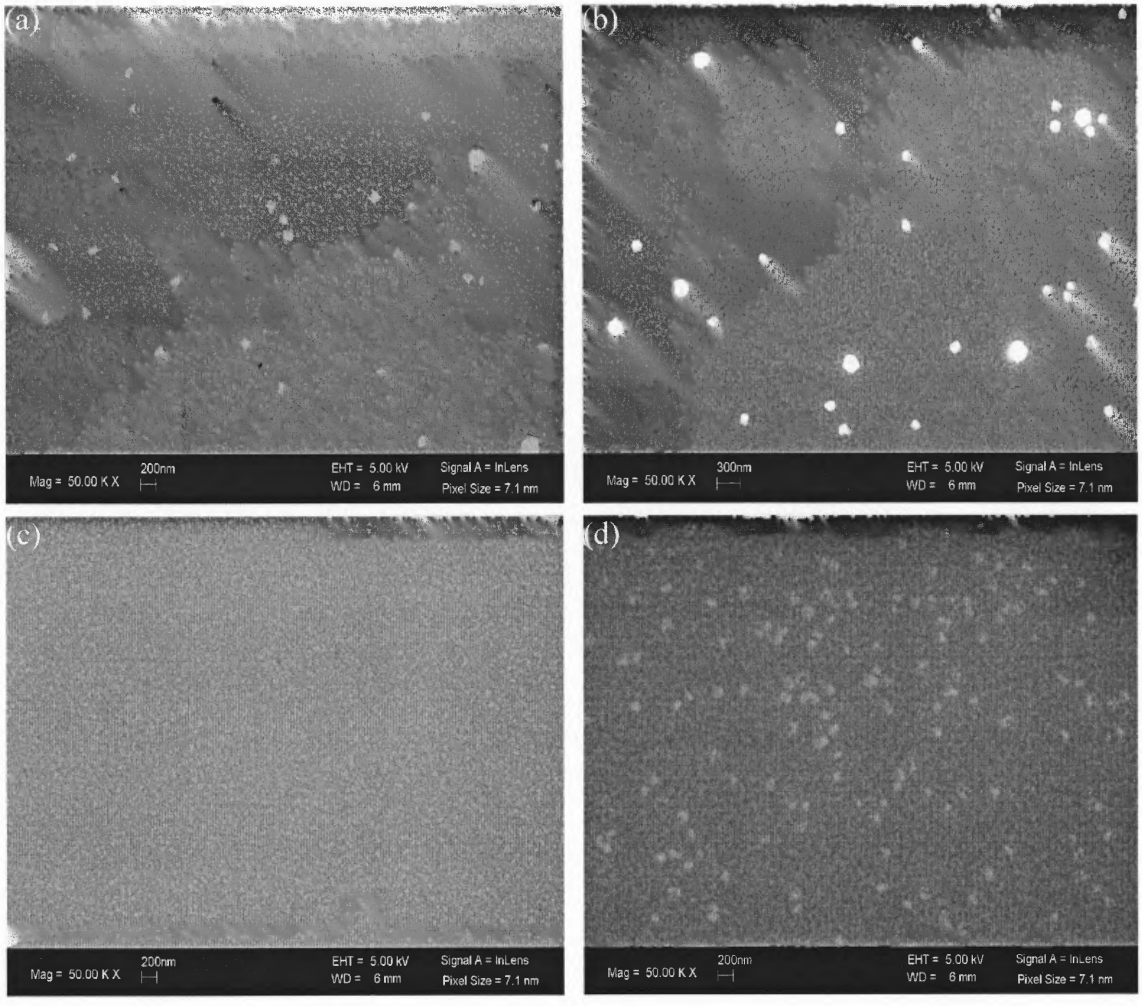

Figure 4.23 SEM image of Ta thin films deposited on silicon substrates under (a) 0 V, (b) -100 V, (c) -150 V, and (d) -300 V for 10 min at magnification of 50K.

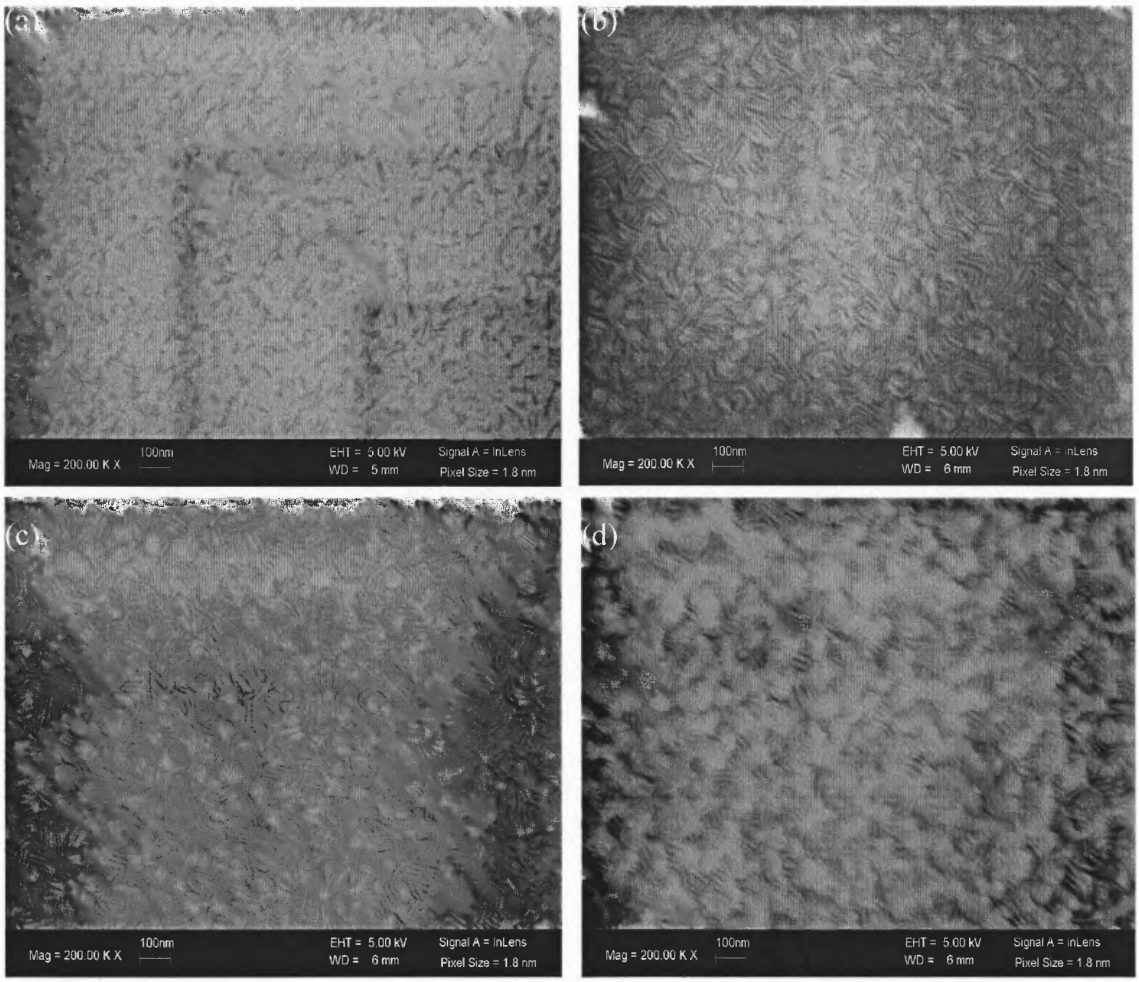

Figure 4.24 SEM image of Ta thin films deposited on silicon substrates under (a) 0 V, (b) -100 V, (c) -150 V, and (d) -300 V for 10 min at magnification of 200K.

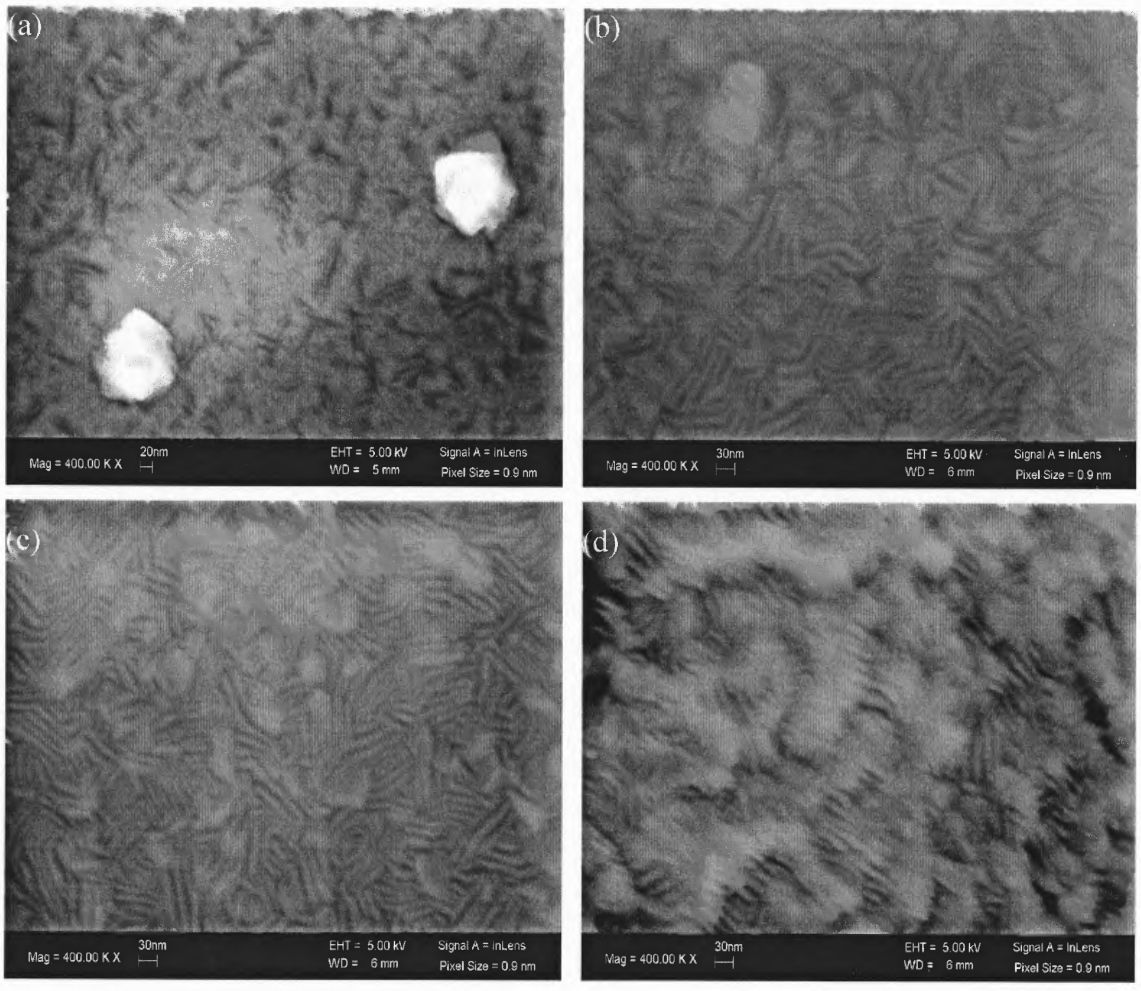

Figure 4.25 SEM image of Ta thin films deposited on silicon substrates under (a) 0 V, (b) -100 V, (c) -150 V, and (d) -300 V for 10 min at magnification of 400K.

In Figure 4.23 (a), the SEM images of tantalum thin film deposited under 0 V taken under 50K magnification showed a lot of small bright white spots, which represented protrusions from the film surface. The size of these bright white protrusion spots increased when the bias voltage was changed from 0 V to -100 V, as was seen in the image of Figure 4.23 (b). There was no obvious white protrusion spots in the image (Figure 4.23 (c)) of tantalum thin film deposited under -150 V, which consisted of only α-

phase structure. For tantalum thin film deposited under -300 V, the white spots appeared again but they were very dense and not so bright (shown in Figure 4.23 (d)).

By increasing the magnification to 200K, more details in the top morphology of the tantalum thin films could be clearly revealed. The images for different films looked similar except for the film deposited under -300 V, which appeared to be more textured with rising rounded and elongated grains and deeper grain boundaries. This could be seen even more clearly from the images taken at the 400K magnification. In order to see the feature of those white spots, an image of one of those white spots for tantalum thin film deposited under -150 V which could not be seen under low 50K magnification was taken as shown in Figure 4.26. This white spot had the same feature as surrounding crystal grains.

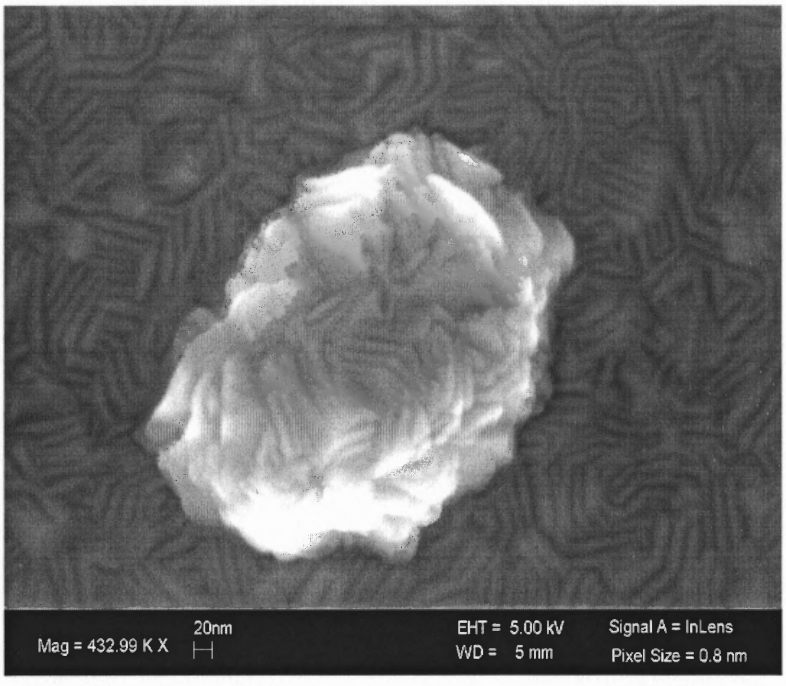

Figure 4.26 SEM image of a protrusion on the surface of Ta thin film deposited under -150 V for 10 min.

SEM images also had been taken for thicker tantalum thin films (i.e. deposited for longer time) to show their surface morphology. Figure 4.27~4.230 showed the SEM images of tantalum thin films deposited for 20 min under 0V, -100 V, -150 V and -300 V bias on silicon substrates.

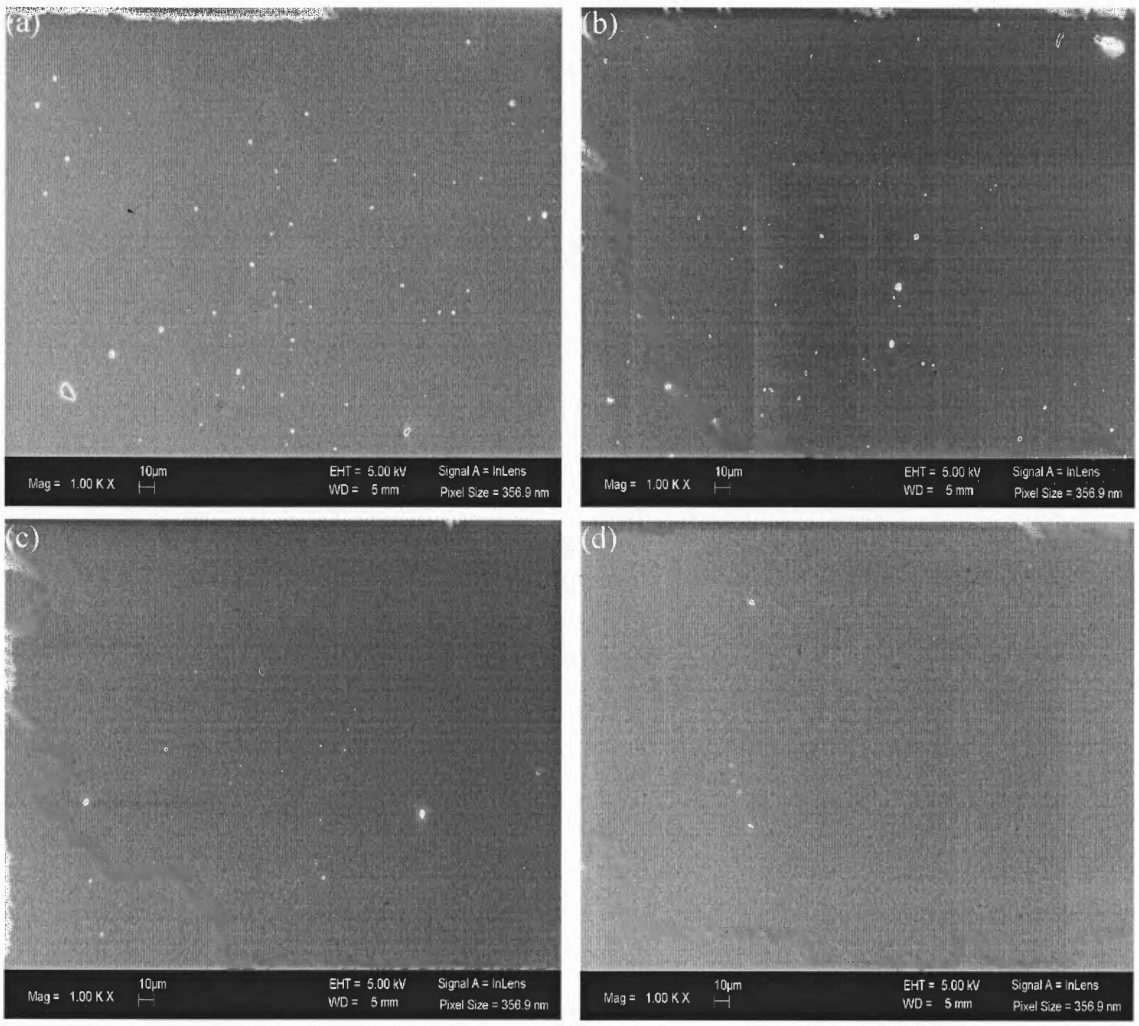

Figure 4.27 SEM images of Ta thin films deposited on silicon substrates under (a) 0 V, (b) -100 V, (c) -150 V, and (d) -300 V for 20 min at magnification of 1K.

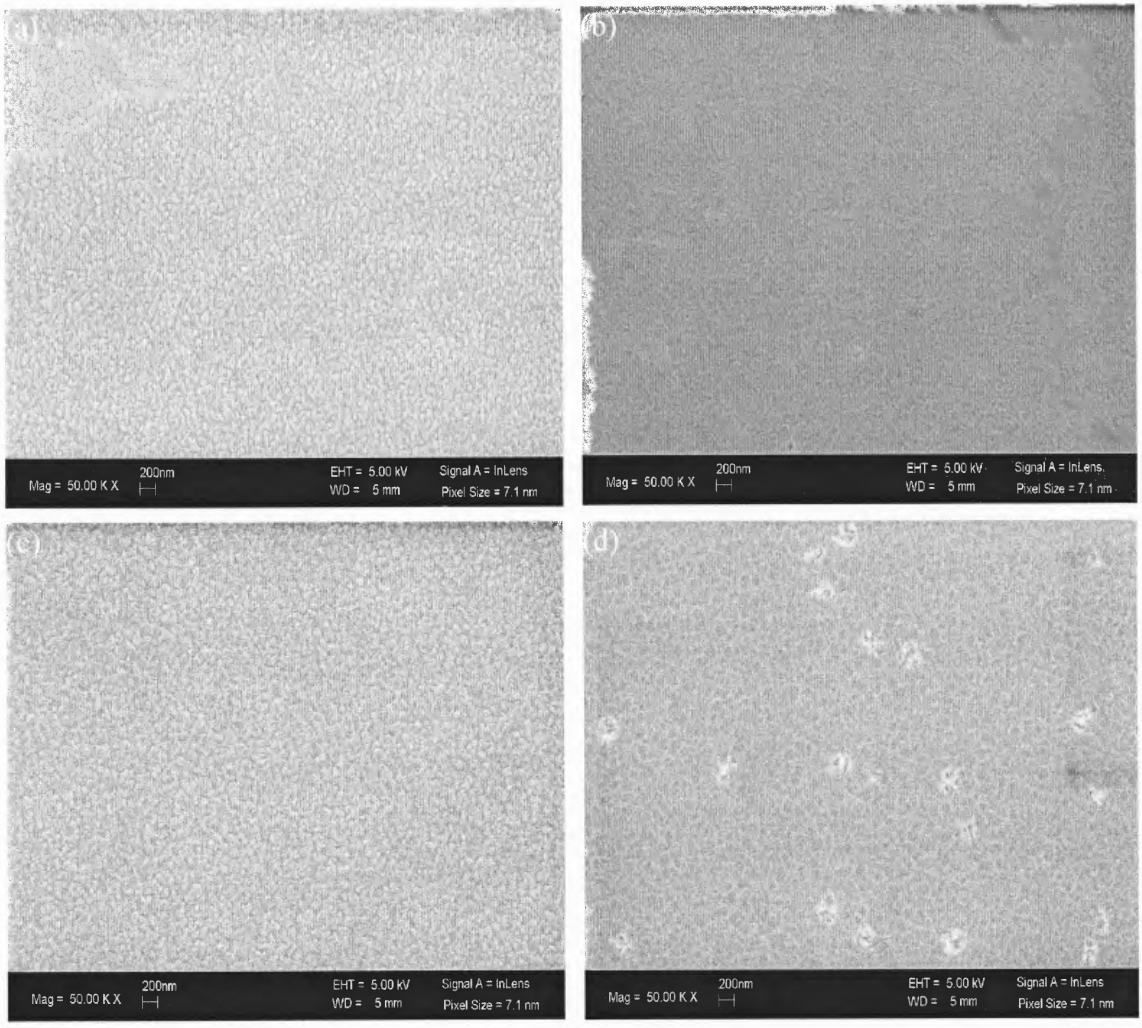

Figure 4.28 SEM images of Ta thin films deposited on silicon substrates under (a) 0 V, (b) -100 V, (c) -150 V, and (d) -300 V for 20 min at magnification of 50K.

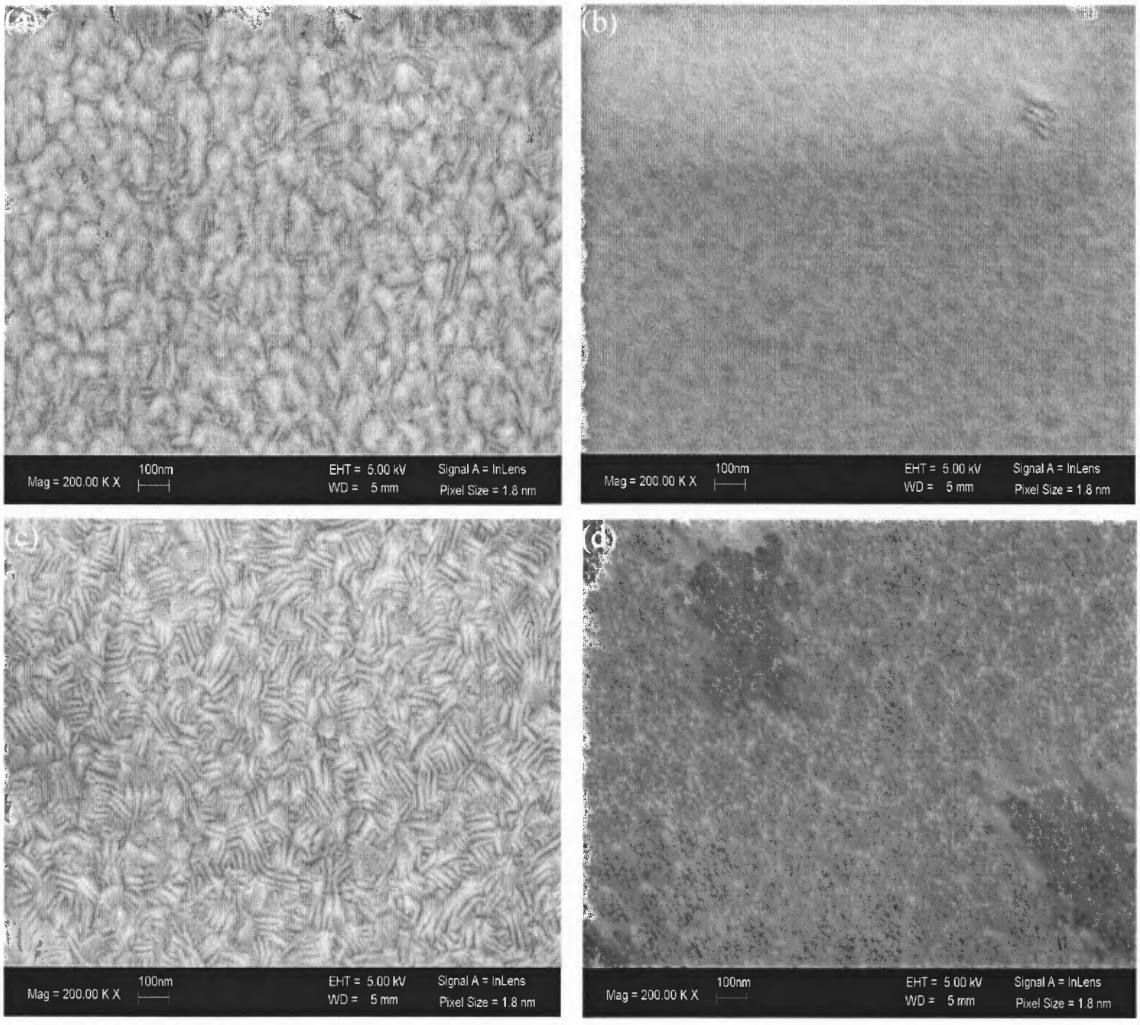

Figure 4.29 SEM images of Ta thin films deposited on silicon substrates under (a) 0 V, (b) -100 V, (c) -150 V, and (d) -300 V for 20 min at magnification of 200K.

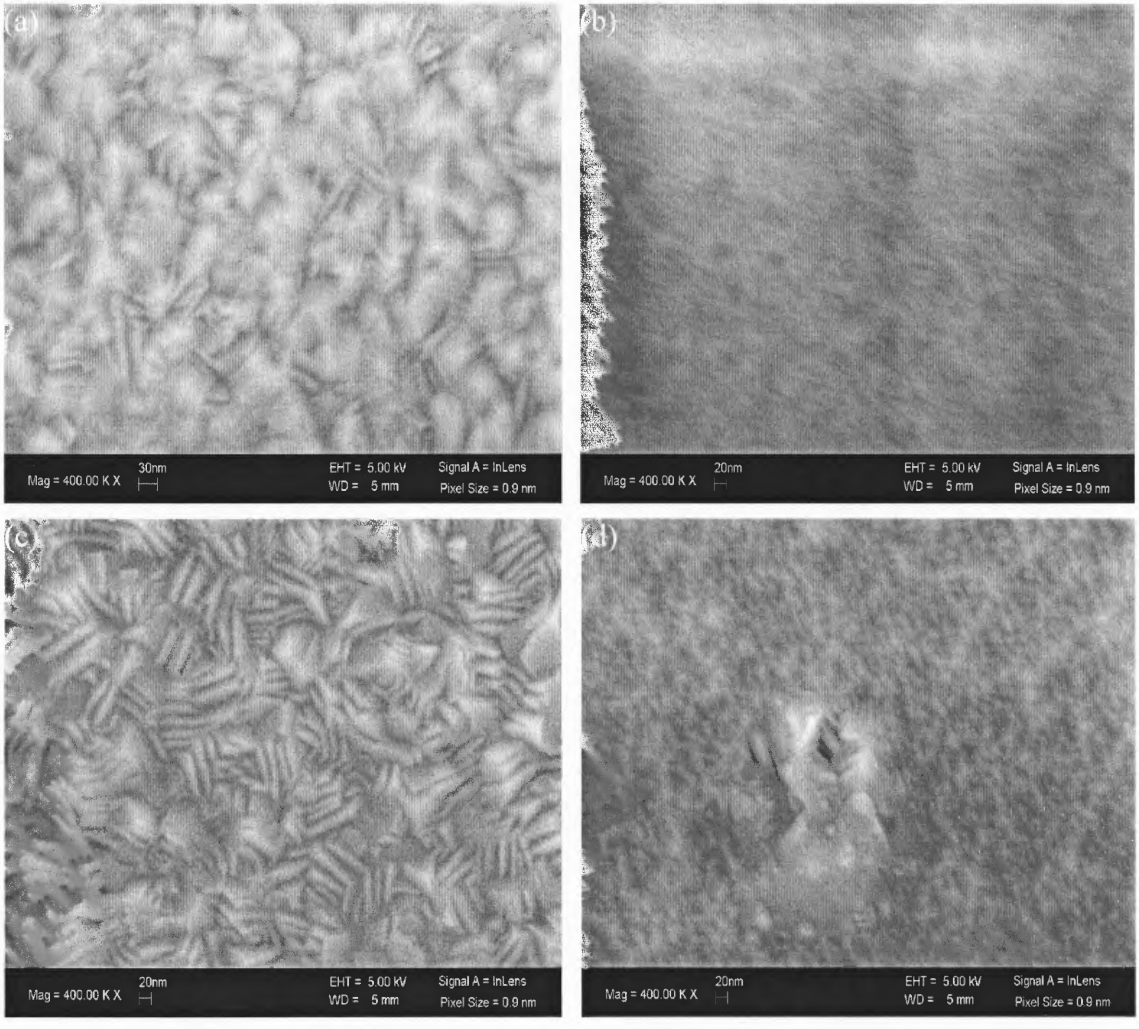

Figure 4.30 SEM images of Ta thin films deposited on silicon substrates under (a) 0 V, (b) -100 V, (c) -150 V, and (d) -300 V for 20 min at magnification of 400K.

In Figure 4.27, the SEM images taken under 1K magnification of tantalum thin films deposited under different bias voltages showed a lot of small bright white protrusions on the film surface except for the tantalum thin films deposited under -300 V. One (Figure 4.27 (d)) showed relatively less protrusions. The size of those protrusions and the density were also quite non-uniform for all the thin films.

Tantalum thin films deposited under -100 V and -300 V showed relatively smooth surface morphology under different magnifications as seen in Figure 4.28~ 4.30 (b) and (d). For tantalum thin films deposited under -300 V bias voltage, the SEM image taken under 50K (Figure 4.28 (d)) showed a lot of small area with some grain features, however, the rest area showed just smooth background without any clear features.

Tantalum thin films deposited under -150 V showed similar grain structures as thinner films (10 min deposition one as shown in Figure 4.24 (c) and 4.25 (c)) as shown in Figure 4.29 (c) and 4.30 (c). For tantalum thin films deposited under 0 V bias, SEM images showed similar but incomplete grain structure as the thin tantalum film deposited under -150 V in Figure 4.29 (d) and 4.30 (d).

The features of those white protrusions on these different 20 min deposition tantalum thin films had been imaged and shown in Figure 4.31 below. As shown here, the white protrusions area always showed similar features as the surface morphology of tantalum thin film deposited under -150 V.

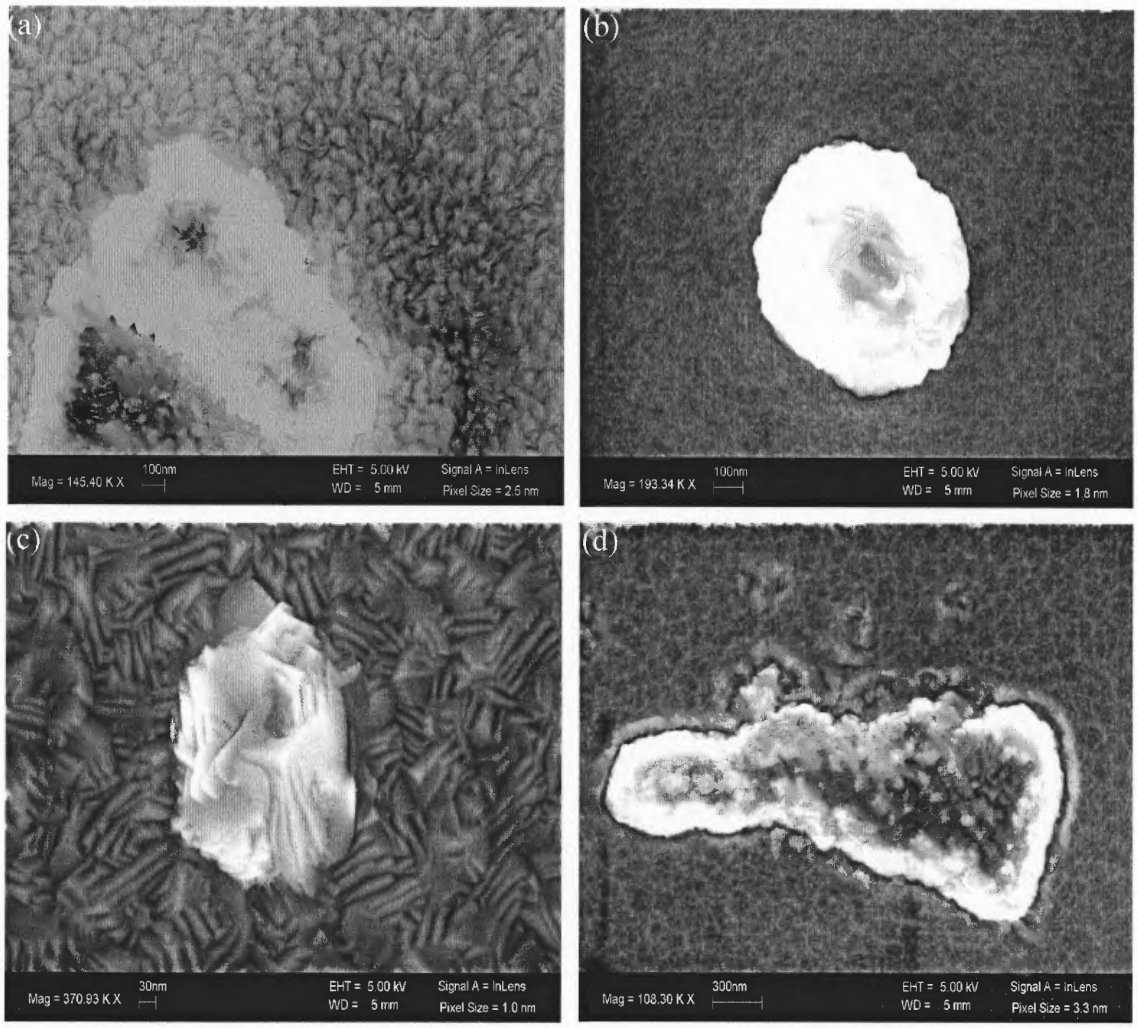

Figure 4.31 SEM images of white protrusions on the surface of Ta thin films deposited on silicon substrates under (a) 0 V, (b) -100 V, (c) -150 V, and (d) -300 V for 20 min.

By observing these SEM images of Ta thin films, we found that the Ta thin film surface appearance correlates with the crystallographic phase content of the films. The α-phase film surface is characterized by dense regularly spaced grain facets while the small grained β films show finer features within a network of ridges. Occasionally, protrusions with the α-phase features were observed on the surface of the films which consisted mostly of the β-phase. Mixed phase films show less regular surface with local α-phase facets interspersed with larger areas of less distinct features.

4.4 AFM Images of Tantalum Thin Films

Tantalum thin films deposited on silicon substrates for 10 min under different substrate bias voltages were also observed by AFM using the contact mode. AFM images in Figure 4.32 and Figure 4.33 below showed the surface morphology of these different thin films.

(a)

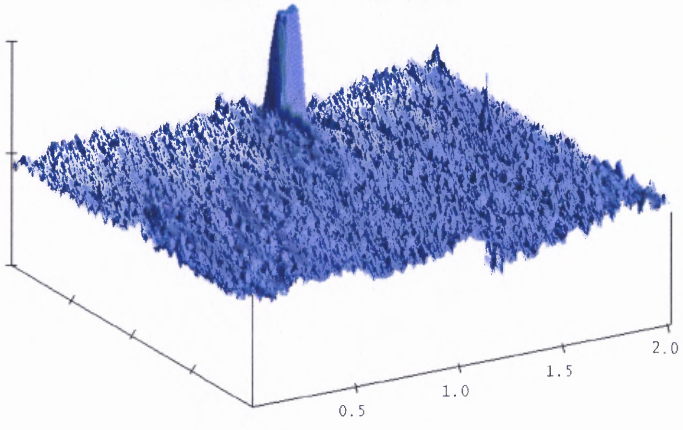

(b)

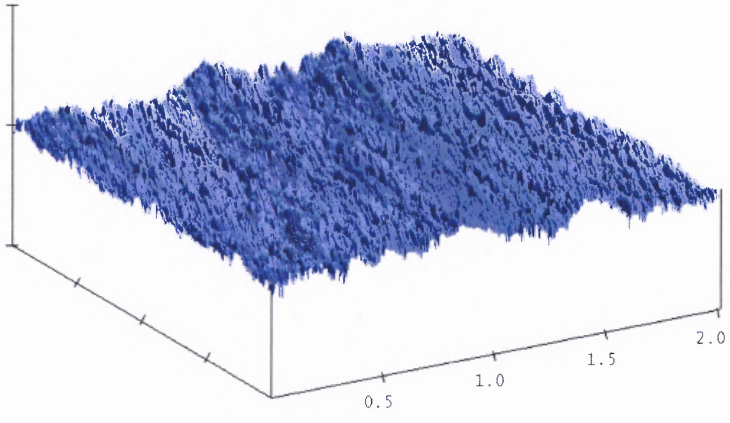

Figure 4.32 AFM images of 2 μm × 2 μm area (z=50nm/div) of tantalum thin films deposited on silicon substrates for 10 min under substrate bias voltages: (a) 0 V, and (b) -100 V.

(a)

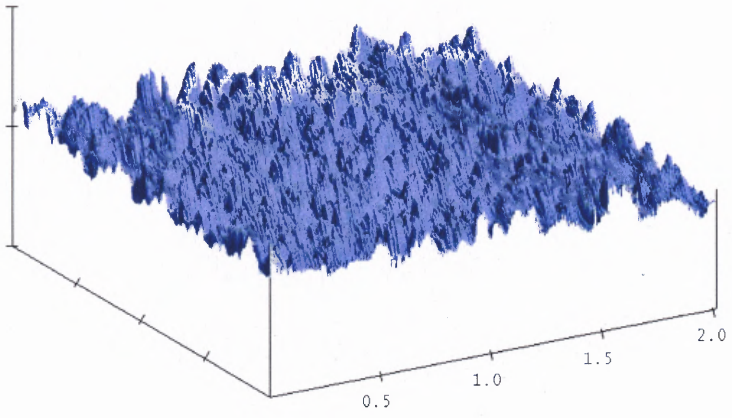

(b)

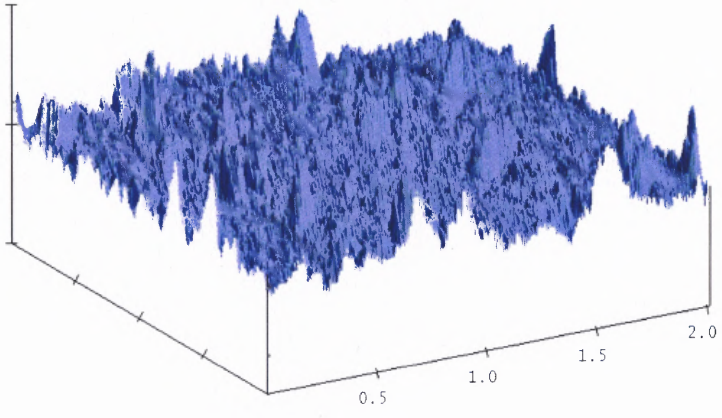

Figure 4.33 AFM images of 2 μm × 2 μm area (z=50nm/div) of tantalum thin films deposited on silicon substrates for 10 min under substrate bias voltages: (a) -150 V, and (b) -300 V.

The surface roughness of tantalum thin films surface roughness increased with increasing substrate bias voltages, i.e., ion bombardment energy. However, there were more large protrusions on the surface of tantalum thin films deposited under 0 V bias as shown in Figure 4.34 (a) than the others observed by the large area AFM image below.

(a)

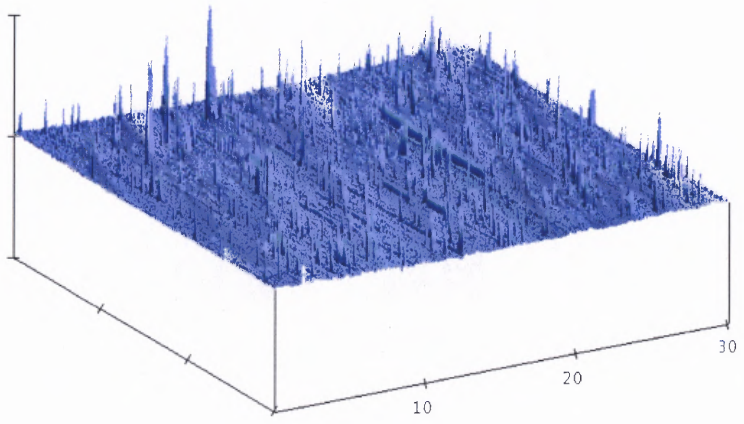

(b)

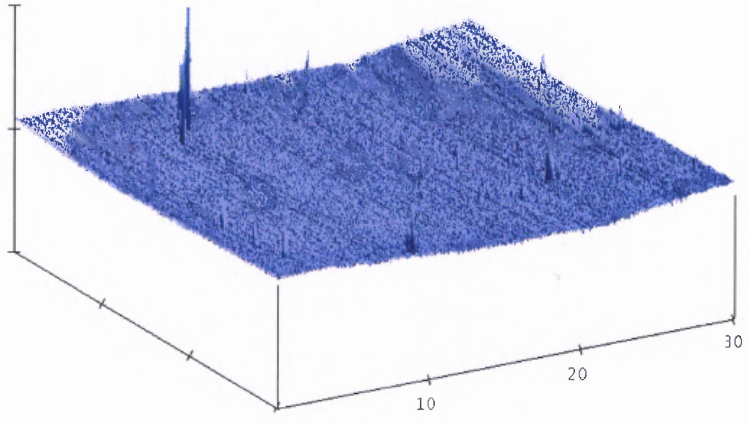

Figure 4.34 AFM images of 30 μm × 30 μm area (z=250nm/ div) of tantalum thin films deposited on silicon substrates for 10 min under substrate bias voltages: (a) 0 V, and (b) -100 V.

(a)

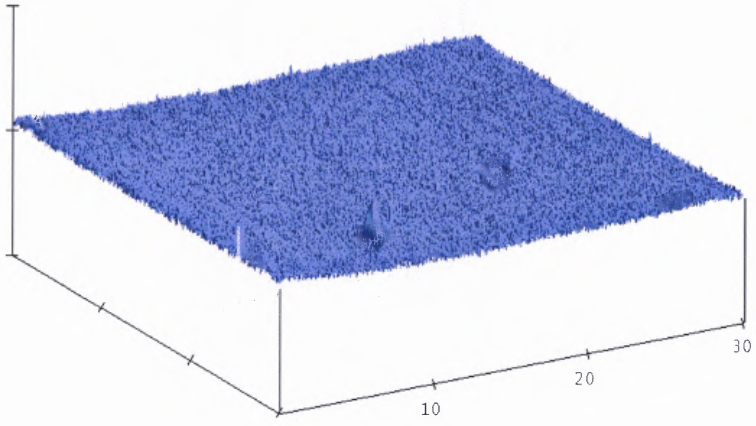

(b)

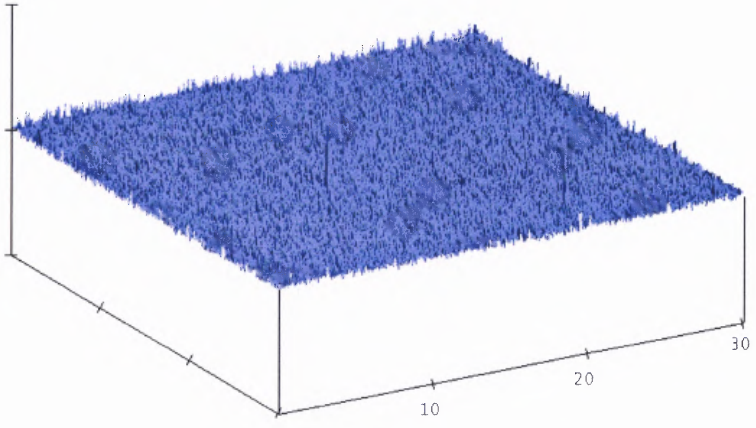

Figure 4.35 AFM images of 30 μm × 30 μm area (z=250nm/ div) of tantalum thin films deposited on silicon substrates for 10 min under substrate bias voltages: (a) -150 V, and (b) -300 V.

The mean roughness (R_a) of tantalum thin films based on large area and small area AFM image analysis were shown in Table 4.5.

Table 4.5 The Roughness of Tantalum Thin Films Deposited using Different Bias Voltages

Bias voltage (V)	R_a (nm) over 2 μm × 2 μm area	R_a (nm) 30 μm × 30 μm area
0	3.618	3.760
-100	2.980	9.598
-150	3.495	5.288
-300	3.920	4.629

In order to further characterize the shape and density of the protrusions on the surface of tantalum thin films according to their AFM images, the section analysis was also performed on the 30 μm × 30 μm area AFM images. Figure 4.36 showed the section analysis of a tantalum thin film deposited on a silicon substrate under 0 V bias for 10 min as an example. The section analysis of top view AFM image could provide the information of protrusion height, width and density. Table 4.6 summarizes the protrusion size and density on the surface of tantalum thin films deposited on silicon substrate under different bias voltages based on the section analysis of their 30 μm × 30 μm area AFM images.

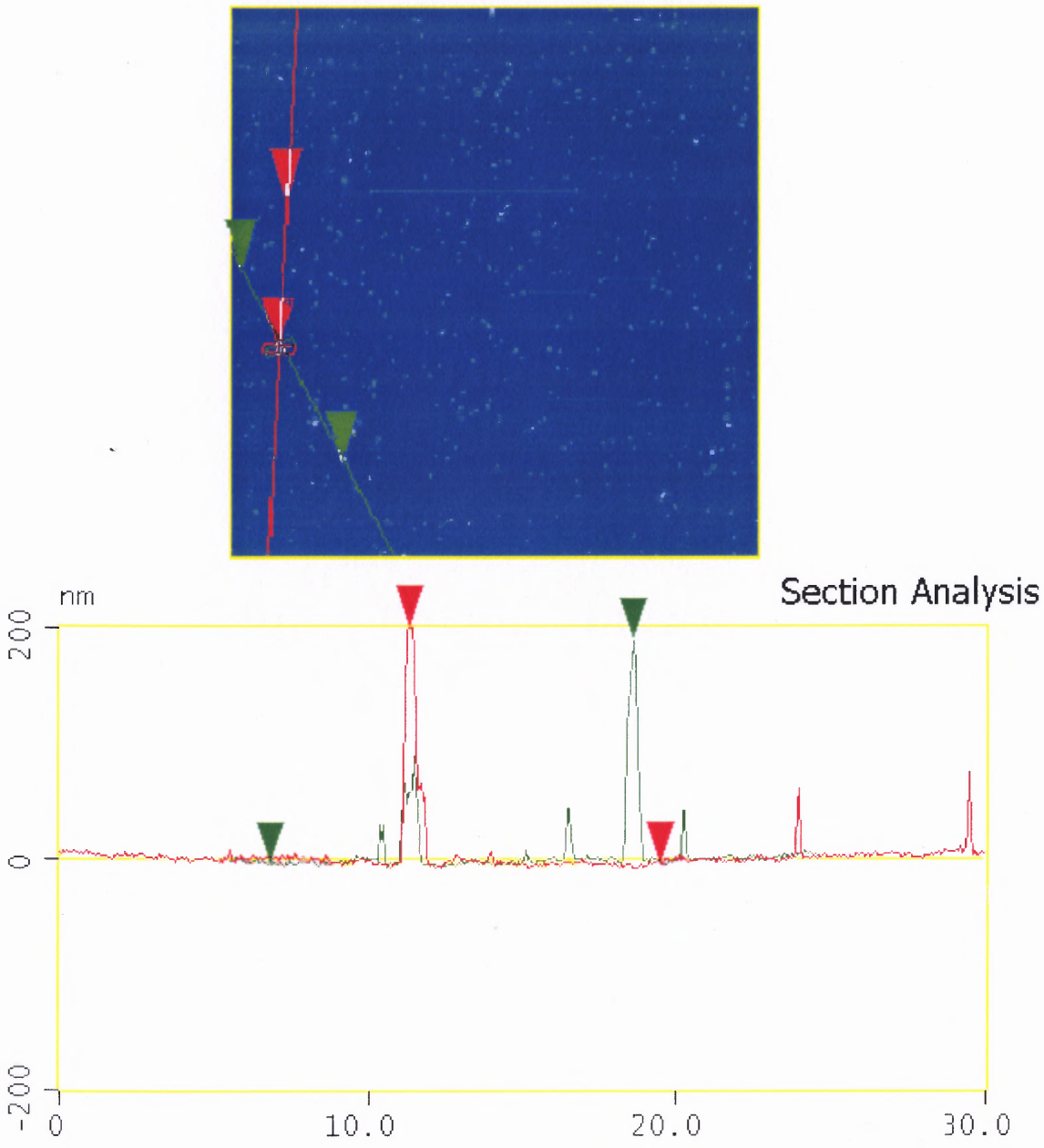

Figure 4.36 Section analysis of a 30 μm × 30 μm area AFM image of tantalum thin film deposited on silicon substrate for 10 min under 0 V bias.

Table 4.6 The Protrusion Size and Density on the Surface of Tantalum Thin Films Deposited on a Silicon Substrate under Different Bias Voltages Based on the Section Analysis of their 30 μm × 30 μm Area AFM Images

Bias voltage (V)	Protrusion height (nm)	Protrusion width (nm)	Height/width ratio	Protrusion density (/μm^2)
0	<225.16	<879	0.26	0.6
-100	<86.453	<644	0.13	0.02
-150	<72.547	<1026	0.07	~0
-300	<125.28	<762	0.17	~3

The section analysis result revealed that large protrusions appeared on the tantalum thin films deposited under 0 V and -300 V bias voltages, and the protrusion density increased dramatically when increasing the bias voltage. Tantalum thin films deposited under -150 V bias surfaces were relatively smooth with relatively low density, spread base and short protrusions. This thin film was also shown by XRD to be pure α-phase tantalum.

CHAPTER 5

THEORETICAL ANALYSIS

In order to better understand the ion assisted Ta film deposition process as well as the effects of ion bombardment on the film growth, molecular dynamic (MD) simulations were performed in this study. In MD simulations, the positions, velocities, kinetic energies and potential energies of each atom or molecule in the system are determined by solving the equations of motion based on the assumed intermolecular potentials. They can reveal the molecular system changes during certain process, such as deposition of atoms, ion impact, etc. Here the Ta film was represented by a finite number of atoms arranged in a perfect single crystal lattice, and the energy of the bombarding Ar ions was varied in the range corresponding to the substrate bias voltage in the deposition experiments. Motion of the Ta atoms and the Ar projectile during the impact was followed and the probabilities of the Ar projectile reflection and of sputtering Ta film atoms was derived.

By doing the MD simulation, the sputtering yields of Ta thin films by Ar ions at different bias voltages was obtained and compared with the results calculated using the semi-empirical formula of Yamamura [111] as well as to the values extracted from RBS measurements. Moreover, the MD simulation provides us the information of time, volume and the surface area of the ion impact event evolution on the Ta thin films, which will help to understand the mechanism of ion assisted deposition.

5.1 MD Simulation Introduction

First introduced by Alder and Wainwright in the late 1950's, the molecular dynamic method was used to explore the interactions of hard spheres. In 1964, a major milestone in the history of the MD simulation development, Rahman did the first simulation for liquid argon by using a realistic potential. In 1974, Rahman and Stillinger performed a MD simulation for liquid water [112]. MD simulation has been developed for carrying out many different types of theoretical research since then. A number of phenomena can be studied for understanding the interaction between the energetic projectile atoms and solid by performing MD simulations, including cluster deposition, melting, and sputtering. In this work, the method is used to explain the physical phenomena occurring during ion bombardment of the growing tantalum thin films.

A MD program "Kalypso", written by M. A. Karolewski [113-115] for personal computers running under Windows operating system, was used here. The program is designed to analyze several surface atomic bombardment phenomena, such as ion scattering spectroscopy, secondary ion mass spectrometry and ion-induced Auger electron emission, etc. The "Kalypso" program package is based on classical dynamics to model the atomic interactions between projectile atoms and the solid (also called "Target"). A composite screened-Coulomb, many-body, tight-binding (TB) potential is used to model interactions between the atoms of the target [113]. Classical dynamics describes the motion of the atoms by Newton's second law, F=ma, where "F" is the force exerted on the atom, "m" is its mass and "a" is its acceleration. Providing the energy and direction of the projectile atoms and the positions of the target atoms, it is possible to determine the acceleration of each atom in the target system. Integration of the motion

equations then yields the information of the positions and velocities for the atoms as they vary with time [112]. Thus a picture of the target system can be derived at any time state during the interaction.

The atomic interactions in the target modeled in the program are described by a repulsive screened-Coulombic potential (V_c) at short inter-nuclear distances and an attractive many-body tight-binding (TB) potential (V_a) at inter-nuclear distances which are comparable to chemical bond lengths. At intermediate distances, the repulsive and attractive potentials are joined smoothly at short distances by means of a switching (i.e. interpolation) function, a so called core switching function, and the attractive TB potential is also terminated smoothly at the cut-off distance by means of another switching function, a so called cut-off switching function. The classical equations of motion are integrated using the finite difference "velocity Verlet" integration algorithm [116].

In order to process the simulation, the first step is to set up the molecular system which includes the target atomic mass, target geometry and size, its crystallographic structures and the projectile with the atomic mass and bombarding energy as close as possible to the real system using the "Spider" program within this Kalypso program packages.

By using this simulation program, a growing tantalum thin film with the ion bombardment process was simulated. The time sequence of images of the tantalum film surface after the ion impact was obtained, the sputtering yield of the growing tantalum thin films by energetic ions attracted under different negative substrate bias voltages was calculated, and the net energy transferred into the growing tantalum thin film by the ion

bombardment was analyzed. The detailed simulation results are described and shown below.

5.2 Evolution of BCC α-Phase Tantalum Film after Ion Bombardment

First, the MD simulations were conducted for the purpose of revealing the lattice changes of growing tantalum film after the ion impact. Initially, the MD simulations were carried out on the Ta target which consisted of 13500 atoms (15×30 rows in x-y plane and 30 layers in z depth). This program was run with varying termination times: 50 fs, 100 fs, 150 fs, 200 fs, 250 fs, 300 fs and 400 fs, then the sequence images of bcc α-phase Ta (110) surface bombarded by 150 eV ion at the end of each time sequences were stored and viewed through the "visualiser" function of the kalypso MD simulation program. Corresponding to the Ar ion impact position as shown in Figure 5.1, two representative sequences of images of ion bombardment development on tantalum thin film targets in the x-z and x-y planes are shown in Figure 5.2~5.7.

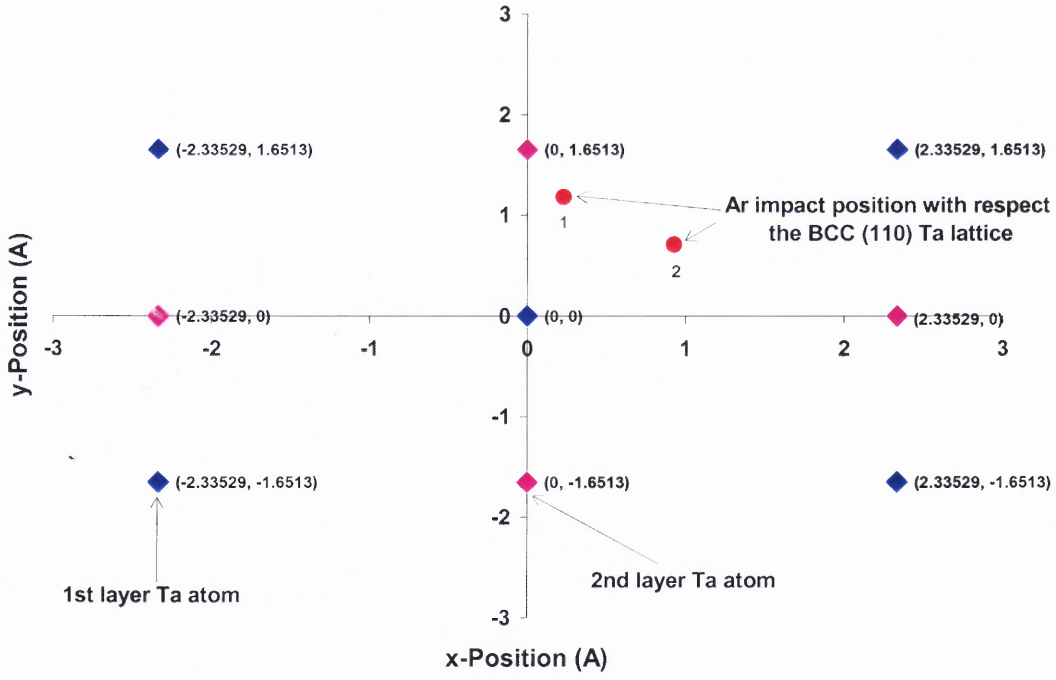

Figure 5.1 Schematic of the Ar ion impact coordinate position with respect to the BCC Ta (110) lattice (Ar ion 1 and 2 refers to the impact position of Figure 5.2~5.4 and 5.5~5.7, respectively).

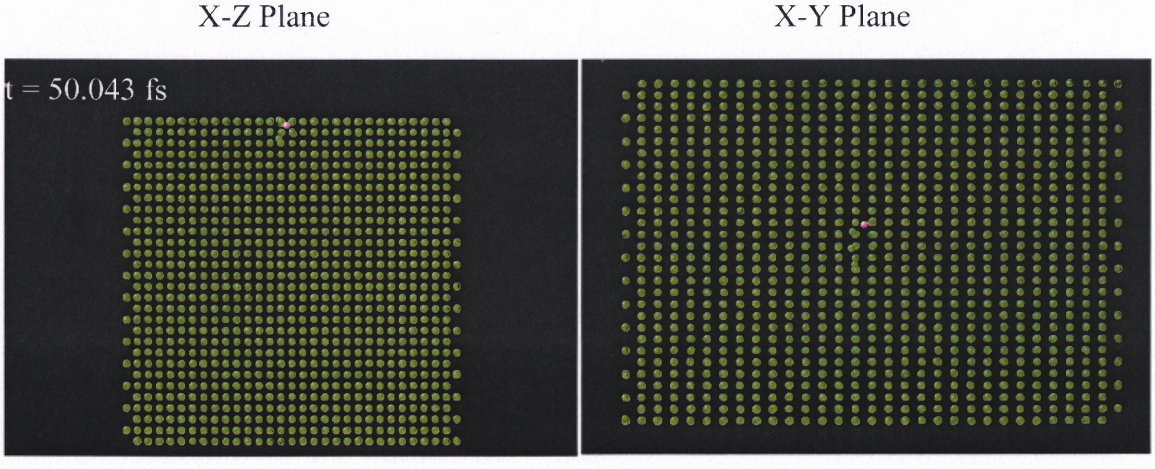

Figure 5.2 Ion impact event development (for the time shown) in cross section (X-Z plane) and on the surface (X-Y plane). Consecutive frames show the system x, y, z at 50 fs after the ion collision with the surface. Ion energy is 150 eV, impact point 1 (see Figure 5.1).

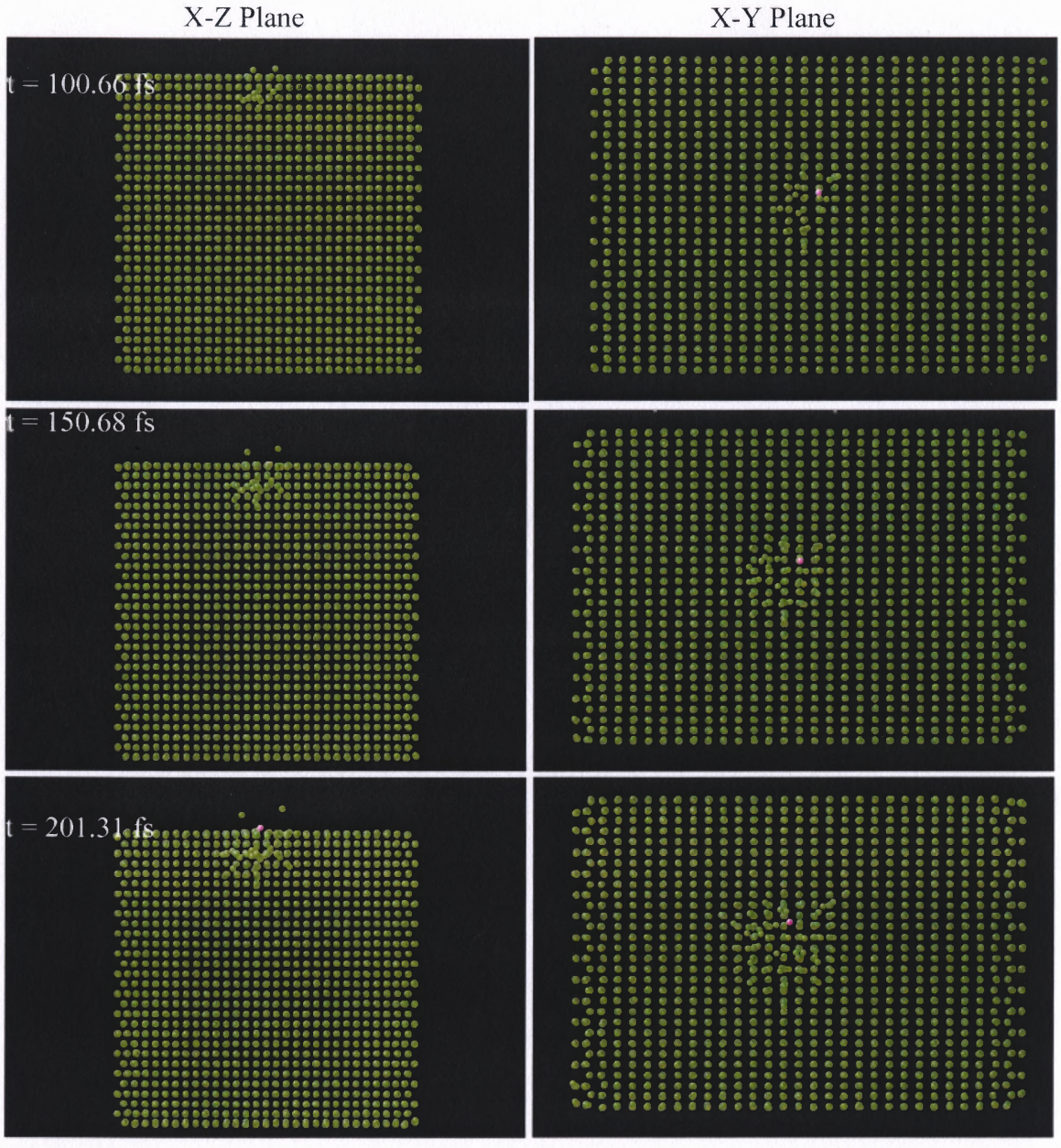

Figure 5.3 Ion impact event development (for the times shown) in cross section (X-Z plane) and on the surface (X-Y plane). Consecutive frames show the system x, y, z at 100~200 fs after the ion collision with the surface. Ion energy is 150 eV, impact point 1 (see Figure 5.1).

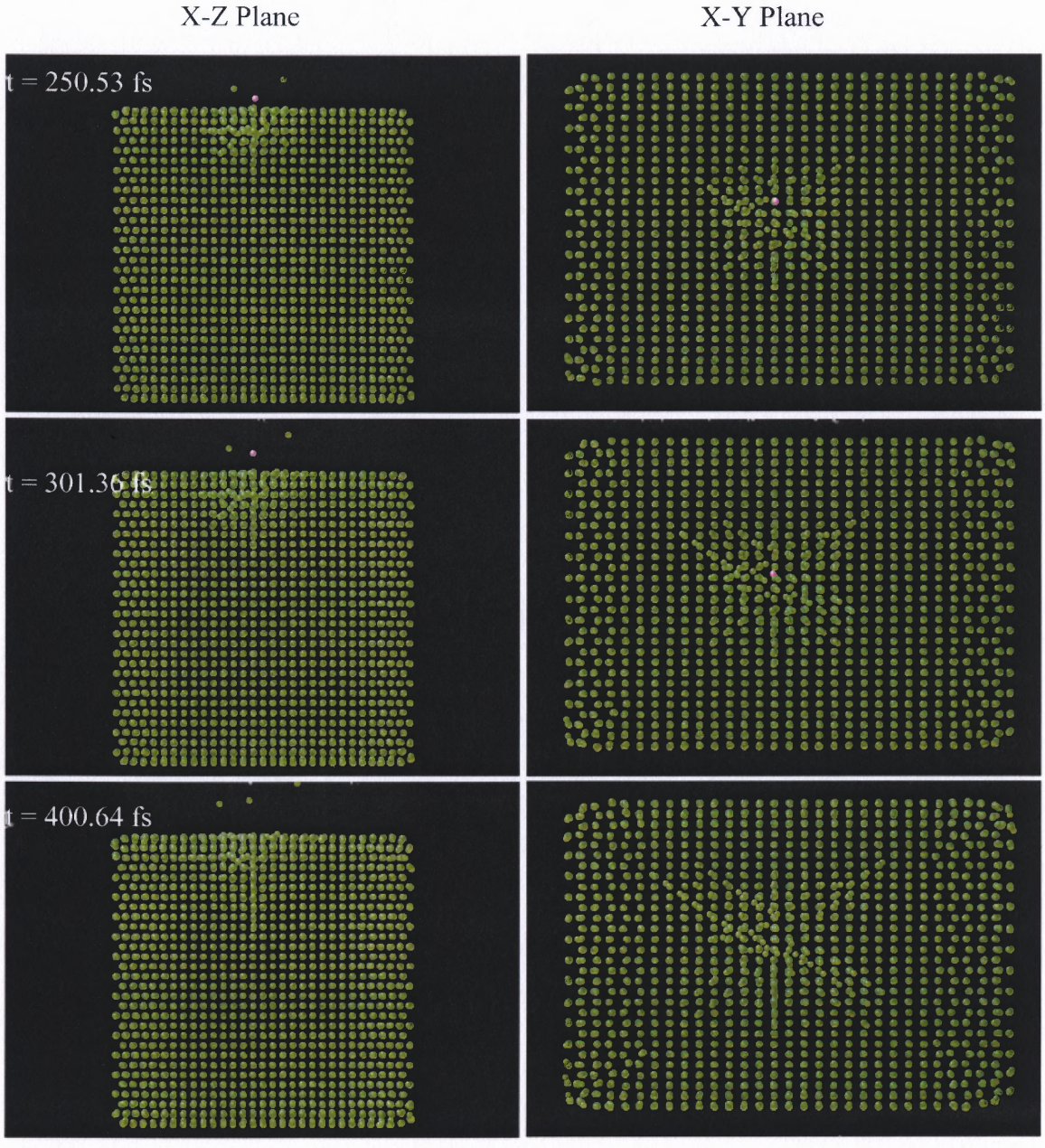

Figure 5.4 Ion impact event development (for the times shown) in cross section (X-Z plane) and on the surface (X-Y plane). Consecutive frames show the system x, y, z at 250~400 fs after the ion collision with the surface. Ion energy is 150 eV, impact point 1 (see Figure 5.1).

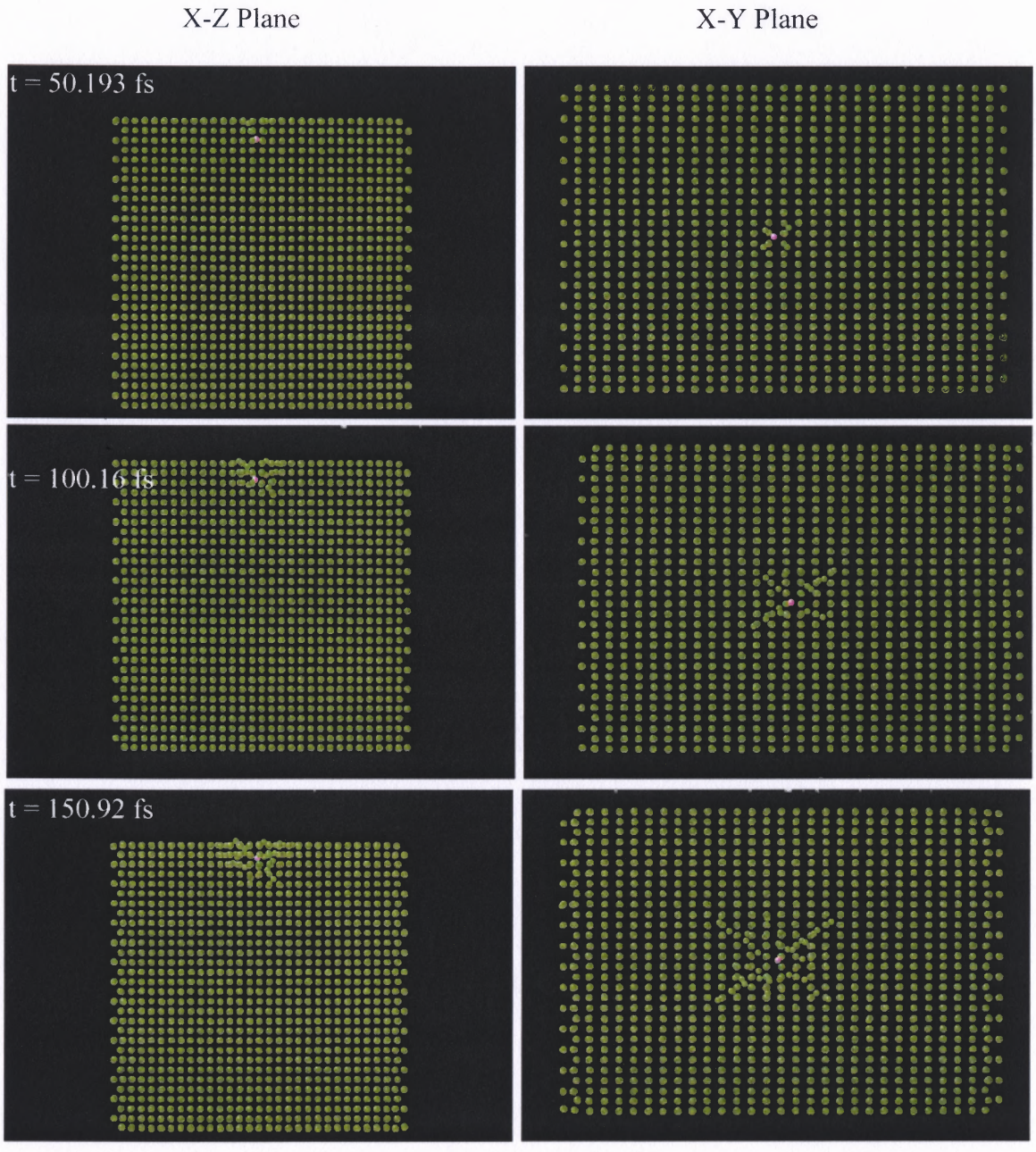

Figure 5.5 Ion impact event development (for the times shown) in cross section (X-Z plane) and on the surface (X-Y plane). Consecutive frames show the system x, y, z at 50~150 fs after the ion collision with the surface. Ion energy is 150 eV, impact point 2 (see Figure 5.1).

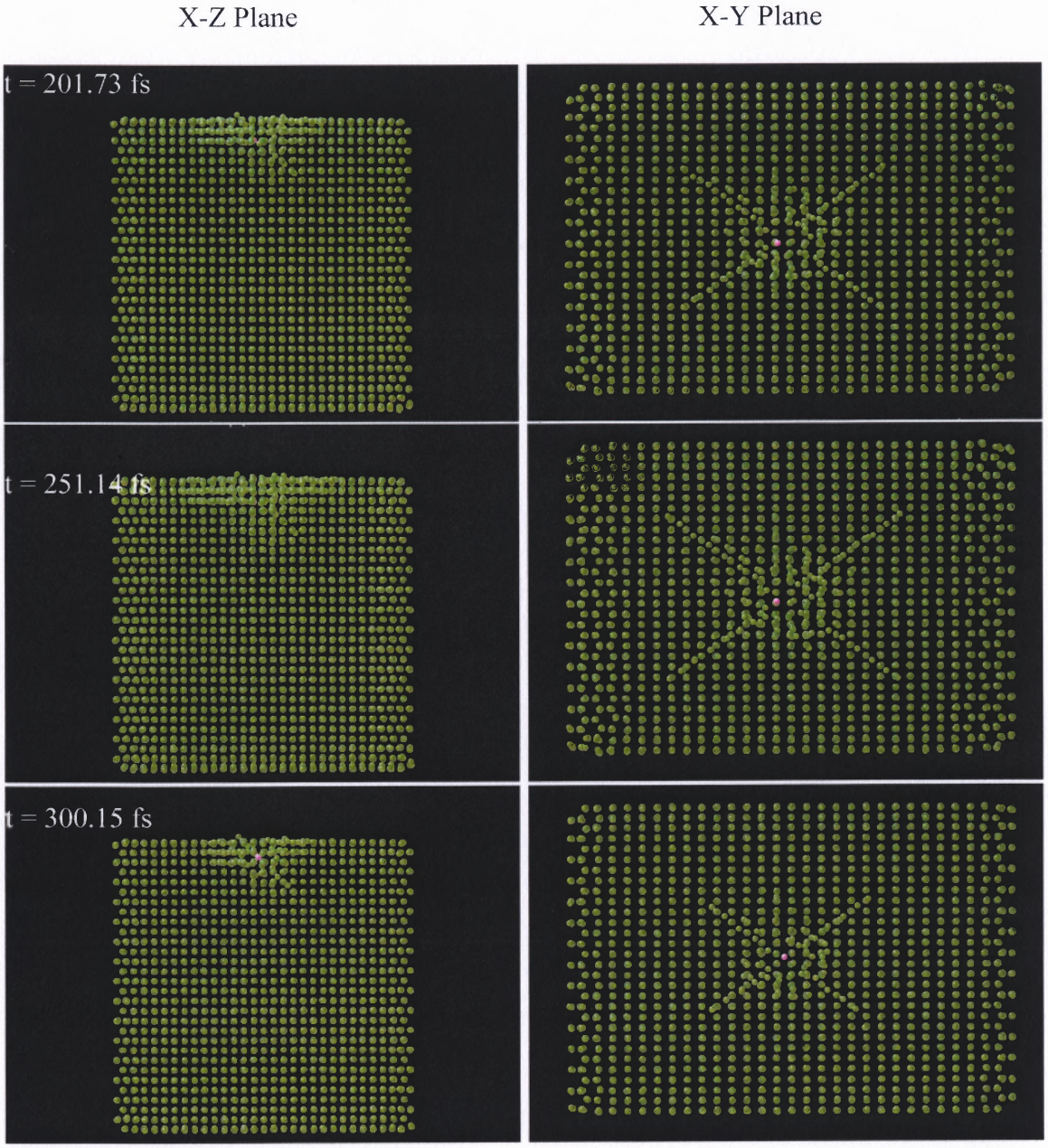

Figure 5.6 Ion impact event development (for the times shown) in cross section (X-Z plane) and on the surface (X-Y plane). Consecutive frames show the system x, y, z at 200~300 fs after the ion collision with the surface. Ion energy is 150 eV, impact point 2 (see Figure 5.1).

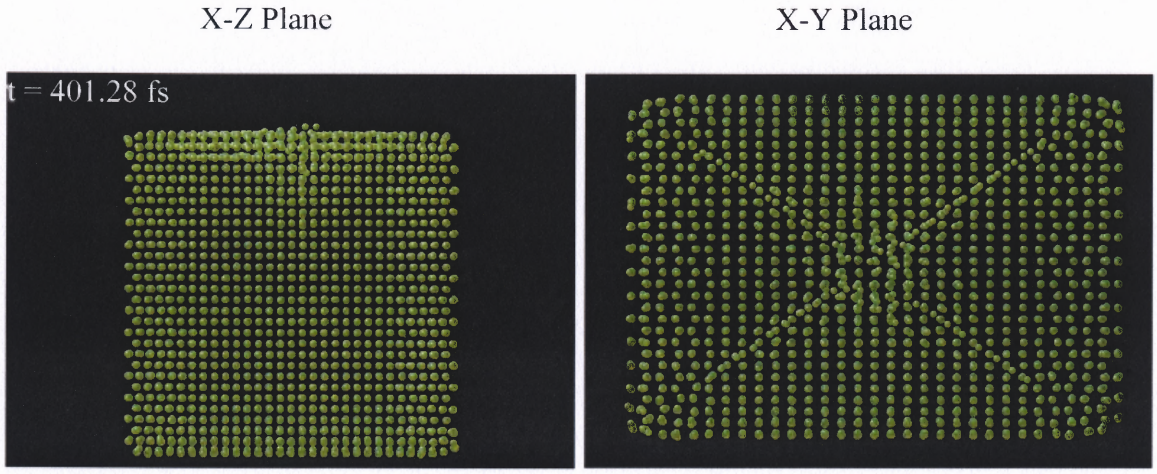

Figure 5.7 Ion impact event development (for the time shown) in cross section (X-Z plane) and on the surface (X-Y plane). Consecutive frames show the system x, y, z at 400 fs after the ion collision with the surface. Ion energy is 150 eV, impact point 2 (see Figure 5.1).

These series of images clearly record the development of collisions with time. During this process, Ta thin film atoms which absorbed enough energy from ion impacts move away from their original position and transfer their energy to other surrounding atoms through secondary collisions. These Ta thin films atoms finally settle down at new crystal lattice positions when their energy is decayed to sufficiently low values. As we can see, there exists an energetic volume in which the Ta atoms are displaced and even rearranged into different positions than their original places in the lattice. This energetic volume develops with time as the ion impact energy is dissipated through multi-collision processes. Several simulations were performed in order to get the information about the energetic volume size and duration time. These may be related to the volume of the film and the time in which an ion impact affects the crystal structure.

Regarding the collision cascade duration time, it was observed from images like those above images that the Ta thin film atoms motion 400 fs after impact was not only induced by ion impact but also by lattice reconstruction which was due to the finite size of the bcc crystal lattice instability. A larger size bcc Ta target (100860 atoms, about 10 times larger than the previous target) was also used to perform the same simulation for 150 eV ion impact. It was also found that the Ta thin film atoms motion would involve lattice reconstruction after 400 fs. It gave us a time limit of about 400 fs within which the displacements of atoms by a collision cascade could be reliably investigated by this method. Fortunately, we found that the energetic collision cascade, caused by the ion impacts in the investigated energy range, subsides in a shorter time than this limit. In addition, the reconstruction does not increase the atoms kinetic energy so that the high velocity of some atoms can be attributed only to the ion impact event.

In order to learn the size of the energetic volume around 400 fs, two different critical conditions were used to define it by analyzing the Ta target after bombardment: the atoms' displacement from their original positions and their kinetic energy. For example, 400 fs after a 150 eV ion impact at location 1 (Figure 5.1) on the target of 13500 atoms, 9 Ta atoms were displaced from their original positions by more than half the lattice constant distance 400 fs after impact. For those atoms $[\mathrm{sqrt}((x_1-x_0)^2+(y_1-y_0)^2+(z_1-z_0)^2)] > 1.5$ Å, where x_0 and x_1 are initial and final x coordinates. Figures 5.8 (a) and (b) show the original lattice positions of the 9 atoms and those 400 fs after the impact, respectively.

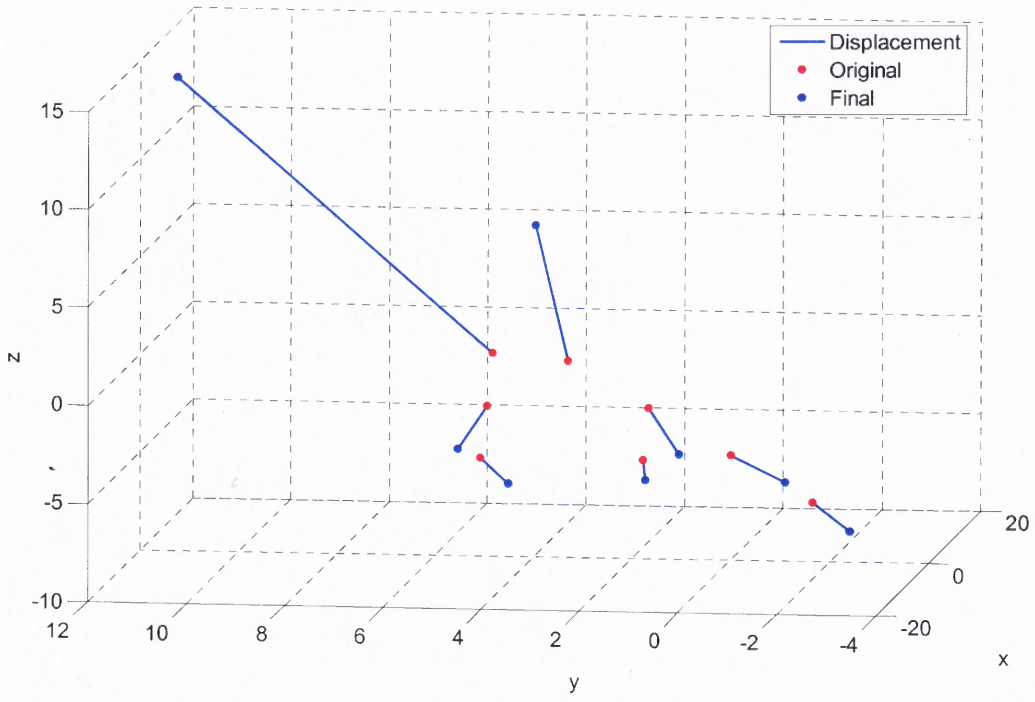

Figure 5.8 Ta target atoms whose lattice displacement [sqrt($(x_1-x_0)^2+(y_1-y_0)^2+(z_1-z_0)^2$)] more than 1.5 Å at 400 fs before and after bombardment by a 150 eV Ar ion.

Before the impact, the atoms were arranged in the well ordered lattice position, within a volume of 5×5×7 $Å^3$, with only very low energy (at 300K), thermal oscillations(<0.004 nm rms). After the impact, atom number 2 and 3 are sputtered away from the surface with energies 8 and 19 eV respectively. The rest of atoms shown are scattered into a volume of 20×15×10 $Å^3$ and have average energies ~ 0.14 eV. The reason for choosing this somewhat arbitrary criteria of atomic displacement by a half lattice constant is that such a movement is likely to lead to a major transformation of the lattice, such as from bcc to tetragonal Ta phase.

As mentioned above, for the reason that bcc targets are only "metastable" when described by a tight-binding potential, they will tend to recrystallize to a fcc structure, starting from the edges of the target and gradually moving in. This was also observed by seeing Kalypso's visualiser window during the simulation. According to the program author's recommendation, this process can be slowed by moving the cut-off distance to a point between coordination shells, but it cannot be avoided completely. Other possible ways to reduce this problem are to work with very wide targets (so that edge effects do not affect the simulation). One has to be very careful that the target reconstruction is not producing artifacts in the simulation results.

In order to prove the reliability of the simulation results, a series simulation on ten times larger size target, 100860 atoms (41×82 rows in x-y plane and 30 layers in depth), were also performed for ion bombardment on a bcc (110) Ta target at different bias voltages. Figure 5.9 shows the image of those Ta target atoms displaced by 1 Å with respect to their original lattice position 250 fs after impact. The bcc (110) target lattice does not change much with the impact processing as compared with smaller size target as observed by "visualiser" window.

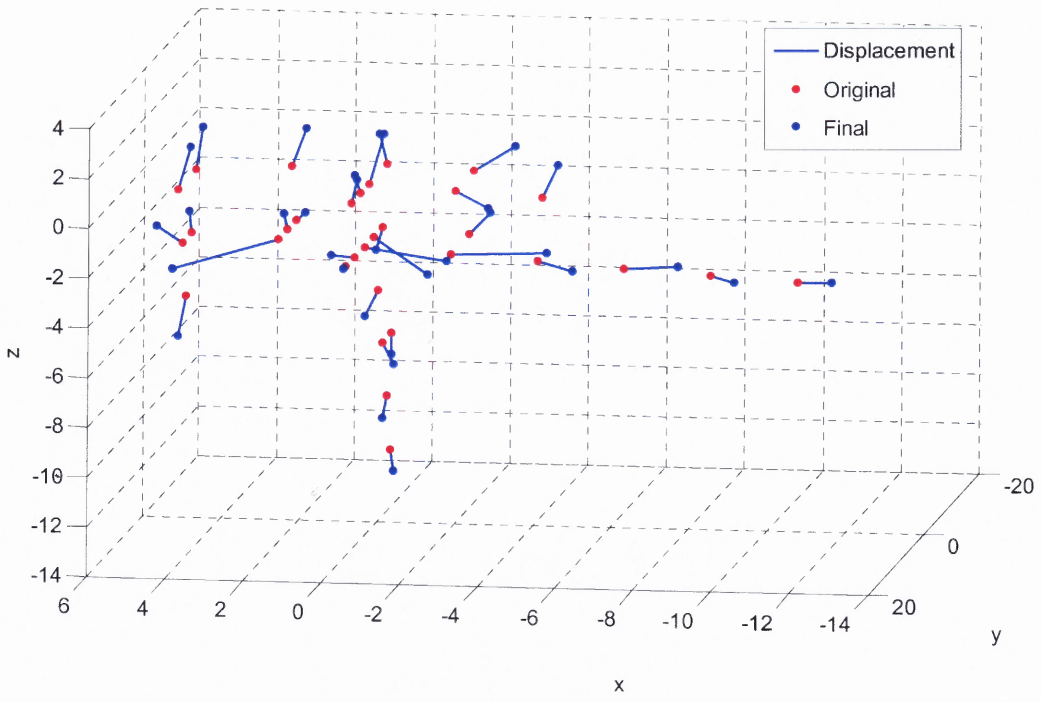

Figure 5.9 Ta target atoms whose lattice displacement [sqrt($(x_1-x_0)^2+(y_1-y_0)^2+(z_1-z_0)^2$)] is more than 1 Å at 250 fs before and after bombardment by a 150 eV Ar ion on a larger target.

As a comparison, the same simulation data on the larger size target was also analyzed by using the Ta atoms kinetic energy as critical conditions to define the energetic volume. Figure 5.10 shows the Ta target atoms kinetic energy to be larger than 0.5 eV which may lead to crystal structure change too. The size of the energetic volume determined by these two methods is approximately the same. Atoms within this energetic volume (i.e., the atoms within this volume were affected by ion impact through series collisions) would possess enough energy to move to new lattice positions, and finally lead to transformation of the film crystallographic structure.

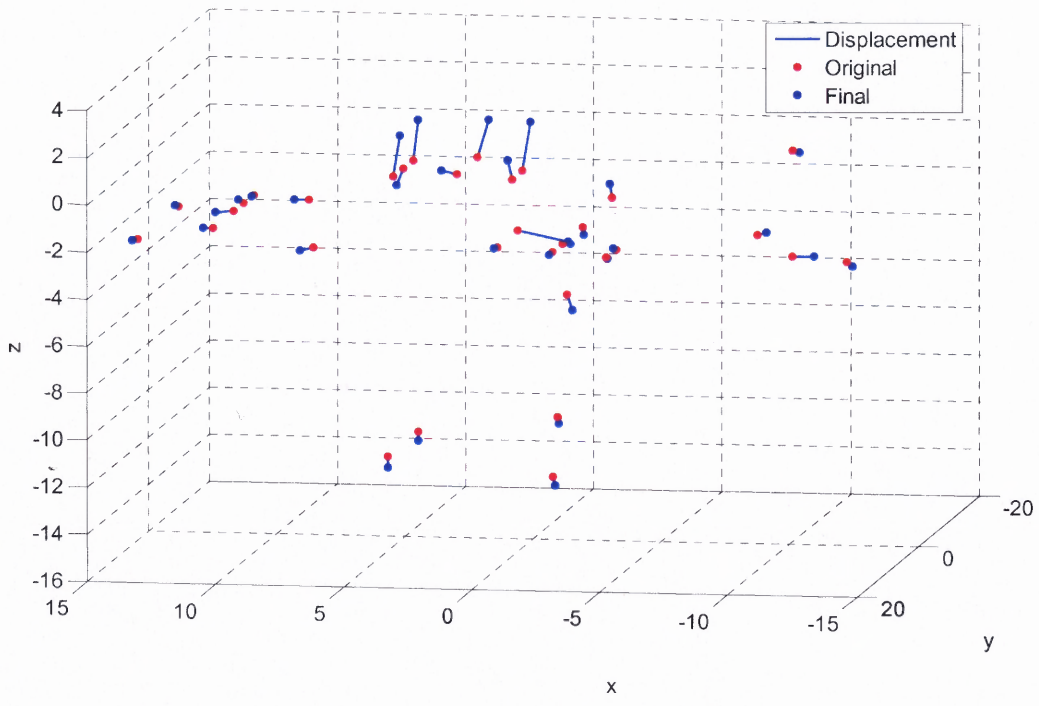

Figure 5.10 Ta target atoms whose kinetic energy is higher than 0.5 eV at 250 fs before and after bombardment by a 150 eV Ar ion on a larger target.

5.3 Energy Transferred by MD Simulation

The MD simulation also gives the energy of the projectile atom after each impact, from which the total energy transferred to a Ta target for different energies of the ion bombardment was derived. The energy transfers averaged over 875 impacts for different ion energies are given in Table 5.1. The energy carried off by sputtered Ta atoms is also given.

Table 5.1 Ar Projectile Energy Transferred to the Film

Ar projectile energy before impact (eV)	10	100	150	300
Averaged Ar projectile energy after impact (eV)	5.98	23.54	28.46	38.97
Ave. energy of sputtered Ta atoms (eV)	0	0.51	5.33	14.29
Ave. energy transferred to the target system during bombardment (eV)	4.02	75.95	116.21	246.74
% Ar ions reflected from surface	100%	100%	99.5%	78.1%

The higher energy ion impacts, the lower the fraction of the projectile energy is transferred but higher the absolute energy is delivered to the Ta target. At 10 eV, only approximately 4 eV (43.2%) of the ion bombardment energy is transferred to the Ta target, while at 300 eV the transferred energy is 246.74 eV (82%).

5.4 Sputtering Yield by Molecular Dynamic Simulation

The sputtering yield is one of the most important parameters of the sputtering process, and it can be derived by using the "Kalypso" MD simulation program. The sputter deposited tantalum thin films generally grow as either (001) oriented tetragonal crystallographic structure β-phase or as a (110) oriented bcc crystallographic α-phase structure. In this case, the target was set up as a (110) oriented bcc crystal with 20 layers for a total of 17640 Ta atoms. The Ar projectile energies ranged from 10 eV to 300 eV. A total of up to 875 impacts with different impact parameters was simulated for each

projectile energy to get good statistics. A desktop personal computer with a Pentium 4, 2.80 GHz processor took about 72 hours for simulation of one energy.

Sputtering yields are derived based on the results of filtering sputtered Ta target atoms from "Dynvar.snk" simulation result files for all the impacts by the "Winnow" program. For example, using the filter condition "$r_z>5*10^{-10}$ m" and "rw>1" (in the "Winnow" program) refers to the Ta atoms positions 5 nm above the target surface, the number of sputtered Ta target atoms is 154 after 875 Ar impacts at 100 eV. This gives a sputtering yield of "154/875≈0.176". Table 5.2 lists the simulated sputtering yields of tantalum, and compares them with the value derived from RBS measurements of thin films deposited under different bias voltages.

Table 5.2 Sputtering Yield of Growing Tantalum Thin Film under Different Energy Ar Ion Bombardments

Bias voltage (V)	Sputtering yield	
	RBS measurement	MD simulation
0	0*	0
-100	0.17	0.176 ± 0.013
-150	0.30	0.378 ± 0.019
-300	0.45	0.877 ± 0.033

*The sputtering yield under 0 V bias is assumed to be 0 for RBS measurement, and is used as a reference for deriving experimental sputtering yields under other bias voltages.

These results are illustrated in the Figure 5.10 together with the results of the semi-empirical formula discussed in the following section. The sputtering yield from MD simulations increases with increasing ion bombardment energy, as expected. The sputtering yields derived from RBS measurements are based on the assumption of zero

sputtering at 0 V bias (Ar projectile energy is 10 eV), and it also shows the trend of increasing with ion bombardment energy increasing. At an Ar energy of 10 eV, the sputtering yield is zero from simulation result, which agrees with the assumption and is reasonable since it is lower than the Ta sputtering threshold energy, 26 eV [117]. Moreover, the sputtering yield derived for 100 eV, 150 eV and 300 eV agrees well with the values reported by Stuart et al. [117] and extrapolates to the previously reported experimental value of 0.57 at 500 eV Ar [104]. The RBS measurement and MD simulation results of sputtering yields at -100 V and -150 V bias are in a reasonably good agreement, but the sputtering yield at -300 V bias calculated by MD simulation is almost double the value of that derived from RBS measurement. This discrepancy is mostly due to the limited size bcc Ta target, and also the single crystal structure of MD simulation Ta target did not represent well the real polycrystalline structure thin film. However, the sputtering yield measured by RBS was quite close to the reference experimental data reported by Stuart etc. [117] as seen from the Figure 5.11 below. The MD simulations much better fit the data at low energy than the values given by the semi empirical formula of Yamamura [118](see next section).

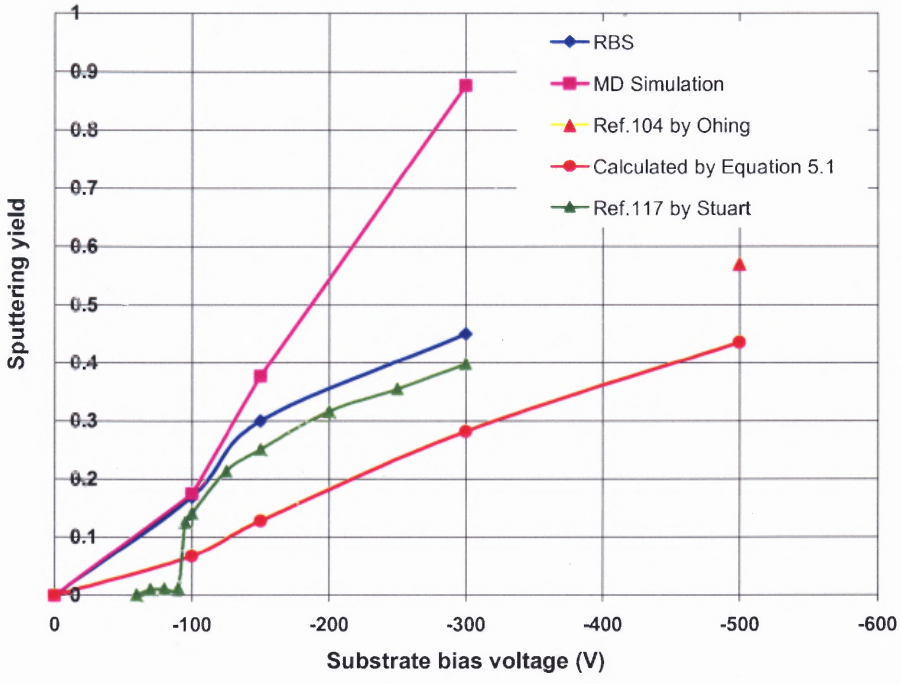

Figure 5.11 Sputtering yield of growing tantalum thin film under different energy ion bombardment derived by RBS measurement and MD simulations along with reference data.

5.5 Sputtering Yield by a Semi-empirical Formula

Since the sputtering yield is the most fundamental parameter for characterizing the sputtering process, much effort has been made to evaluate it by using experimental data and to predict it by theoretical methods, or a combination of both. Among those used are a semi-empirical formula derived by Matsunami et al. in 1984 [119] and an equation shown below by Yamamura and Itoh in 1989 [118] which is based on a combination of Lindhard's theory of nuclear and electronic stopping with experimental sputtering yield data. In the book "Ion-Solid Interactions" written by Nastasi, Mayer and Hirvonen [120] at 1996, this semi-empirical formula was also introduced in detail for calculating the sputtering yield. Here a semi-empirical formula was also used to calculate the sputtering

yield of Ta in the Ar energy of 10 eV to 500 eV and compare them to the re-sputtering data of the growing Ta thin film. The sputtering yield Y_E at the ion energy E, calculated by this empirical formula (5.1) fits both heavy and light ion sputtering and shows below (formula 9.9 from ref.[120]):

$$Y_E(E) = 0.42 \frac{\alpha_S Q_S S_n(E)}{U_0[1 + 0.35 U_0 S_e(\varepsilon)]} [1 - (E_{th}/E)^{0.5}]^{2.8} \quad (5.1)$$

where $Y_E(E)$ is the sputtering yield for ions with energy E bombarding a target at normal incidence. α_S and Q_S are empirical parameters derived from experimental sputtering data. $S_n(E)$ is the nuclear stopping cross-section in units of 10^{-15} eV cm^2 and U_0 is the surface binding energy (estimated from the cohesive energy). $S_e(E)$ is the reduced Lindhard electronic stopping cross-section, and E_{th} is the sputtering threshold energy.

According to the ref. [120],chapter 9, page 224, the empirical parameter α_S is found to be dependent on both the incoming ions and the target, and the empirical formula (5.2) is given by the following expression (formula 9.16 of ref.[120]):

$$\alpha_S = 0.10 + 0.155(M_2/M_1)^{0.73} + 0.001(M_2/M_1)^{1.5} \quad (5.2)$$

The value of empirical parameter Q_S for tantalum is 0.62 from Yamamura and Itoh [118]. The nuclear stopping cross-section, $S_n(E)$, is dependent on the incoming ion energy and can be calculated by the formula (5.3) (formula 9.12 from ref. [120]):

$$S_n(E) = K_n S_n(\varepsilon) \quad (5.3)$$

Where K_n and $S_n(\varepsilon)$ are defined separately by the formula (5.4) and (5.5) (formula 9.13 and 9.14 from ref. [120]):

$$K_n = \frac{8.478 Z_1 Z_2}{(Z_1^{2/3} + Z_2^{2/3})^{1/2}} \frac{M_1}{(M_1 + M_2)} (10^{-15} eVcm^2/atom) \quad (5.4)$$

$$S_n(\varepsilon) = \frac{3.441\varepsilon^{1/2}\ln(\varepsilon + 2.718)}{1 + 6.355\varepsilon^{1/2} + \varepsilon(6.882\varepsilon^{1/2} - 1.708)} \tag{5.5}$$

In which, the reduced energy ε in the Thomas-Fermi form given by formula (5.6) (formula 9.15 from ref. [120]):

$$\varepsilon = \frac{0.03255}{Z_1 Z_2 (Z_1^{2/3} + Z_2^{2/3})^{1/2}} \frac{M_2}{(M_1 + M_2)} E(eV) \tag{5.6}$$

The surface binding energy U_0 for tantalum is 8.10 eV from Kittel [121].

The Lindhard-Scharff electronic stopping cross-section is often expressed in reduced notation as formula (5.7) (formula 5.59 from ref. [120]):

$$S_e(\varepsilon) = \left(\frac{d\varepsilon}{d\rho}\right)_e = k\varepsilon^{1/2} \tag{5.7}$$

where k is defined by the formula (5.8) (formula 5.60 from ref. [120]):

$$k = \frac{Z_1^{2/3} Z_2^{1/2} \left(1 + \frac{M_2}{M_1}\right)^{3/2}}{12.6(Z_1^{2/3} + Z_2^{2/3})^{3/4} M_2^{1/2}} \tag{5.8}$$

The sputtering threshold energy, E_{th}, corresponding to the minimum energy required for sputter away the target atoms, can be calculated by using the method introduced by Yamaura and Bohdansky in 1985 [122], and the formula (5.9) (formula 9.10 from ref. [120] is shown in the following:

$$E_{th} = \left\{ \begin{array}{l} \left(\frac{4}{3}\right)^6 \frac{U_0}{\gamma} \; when M_1 \geq M_2 \\ \left(\frac{2M_1 + 2M_2}{M_1 + 2M_2}\right)^6 \frac{U_0}{\gamma} \; when M_1 < M_2 \end{array} \right\} \tag{5.9}$$

where γ is the energy-transfer factor for elastic collisions, defined in the formula 5.10 (formula 9.11 from ref. [120]):

$$\gamma = \frac{4M_1M_2}{(M_1 + M_2)^2} \tag{5.10}$$

Therefore the sputtering yield of argon ions (atomic number Z_1=18 and mass M_1=39.948) bombarding tantalum (atomic number Z_2=73 and mass M_2=180.95) with an energy from 10 eV to 500 eV is calculated and also plotted in Figure 5.11.

From Figure 5.11, the sputtering yields for Ar bombarding Ta within the energy range 10 eV to 500 eV, calculated by this semi-empirical formula, are lower than both which derived from RBS measurement and MD simulation. It is worth noting, however, that the formula does not fit other experimental data in the energy range used in this study too either. For example, the experimental sputtering yield data for Ar ions on Ta target provided by Stuart and Wehner [117] which is also illustrated in ref. [60] and Figure 250 of ref. [111].

CHAPTER 6

DISCUSSION

Combining the experimental and MD simulation results of ion assisted tantalum thin film deposition, it's clear that the film crystallographic structure and micro-morphology is strongly affected by ion bombardment conditions. Here, the relation between the crystallographic structure of Ta films and the ion bombardment conditions are discussed in more detail. The role of the substrate is also examined. The effect of ion bombardment on the film thickness, lattice strain, and grain size is discussed as well. Finally the statistics of ion impacts and deposition of tantalum atoms, together with the duration of these events is related to the mechanism of the ion bombardment modification of the growing film.

6.1 Ion Bombardment Conditions

In this research, as discussed in Section 3.1, the current of bombarding Ar ions (ion flux) which are attracted by supplying different substrate negative bias voltages in the RF magnetron sputtering process only increases a little because of the fixed system configuration and the power input, so the major ion bombardment parameter which can be manipulated in this ion assisted RF magnetron sputtering process is the ion bombardment energy and it is determined by the substrate bias voltages. From the experiments, it was clearly shown that the energy of ions bombarding the film during deposition had a strong influence on its crystallographic structure. Such an effect had been reported earlier, and the explanations varied from the role of incorporation of impurities to the kinetics of ion-atom collisions. Here the results will be discussed in

comparison with two more recent and extensive studies of ion assisted Ta deposition [60, 75, 76]. Surprisingly, it is found that deposition with the bias voltage around -150 V results in the α-phase Ta films on Si-100, with the β-phase or mixed phase films being deposited at lower or higher voltage, while the data in references[60] and [75, 76] show that the α-phase grows with the substrate bias of approximately 20 V and below, and the β-phase or mixed phase at higher voltages.

In making such comparisons, it is important to account for all significant differences in the apparatus and the deposition parameters, which may affect the results. The two other different systems being compared to are a dual RF magnetron sputtering system in reference [60] and a hollow cathode enhanced magnetron sputtering system in reference [75, 76], while in this work a conventional RF magnetron sputtering system with the provision of substrate DC biasing is used. The target-substrate distance in this experiments (50 mm) lies between those in the two earlier experiments, 30 mm [60] and 100 mm [75, 76], and this difference is not considered to be very significant by itself. A more important parameter is the ratio of the mean free path of the sputtering gas to this distance, which in the paper of Ino et al. [60] is almost the same as in ours (~0.3), but in the very low pressure of the apparatus used by the IBM group [76], the mean free path is more than 2.5 times larger than the target-substrate distance. In the latter case many Ar ions, accelerated by the high voltage of the target, are reflected back as neutral atoms and reach the film without collisions in the gas. Similarly, the Ta atoms, sputtered from the target, impact the film with higher energies as they reach it with fewer gas collisions. Thus the films in this case may be exposed to a higher particle flux and energy than the energy and flux due to the acceleration by the substrate bias voltage. This is confirmed in

their paper by significant incorporation of Ar in the films deposited even at zero bias and the presence of compressive stress in the films. According to the author's own estimate, the total energy brought to the film by particle bombardment, including energetic Ta atoms is about 100 eV per deposited atom at zero bias [76].

In contrast, in this work and that of Ino et al. [60], the bombarding energy E_i is only defined by the ion accelerating substrate voltage V_b, $E_i = q_i V_b + V_p$, where V_p is the plasma potential of only a few volts, and q_i is the ion charge. Another critical parameter in ion assisted deposition is the flux of ions bombarding the substrate, or rather the ratio of ion and atom fluxes. In this work, this ratio is close to one, as well as 0.5 in that of reference [76], while the flux of ions required for deposition the α-phase reported in reference [60] was around 15, and only the β-phase Ta films were obtained when the ratio was 10 and less. The high ion flux increases the total energy brought to the growing film per deposited Ta atom. For example, at E_i = 10 eV and ion to atom flux ratio of 15 (typical values quoted in reference [60]), the total energy brought to the film by the ion bombardment is approximately the same as in this study for V_b = 150 V. It is not so easy to estimate the ion bombardment energy input to the growing film in the work of Catania et al., because of the presence to the flux of energetic Ar and Ta atoms, in addition to the flux of ions accelerated by the substrate bias voltage. It appears that the former flux is sufficient for the growth of the bcc α-phase even at zero bias voltage and increasing the bias above 20 V results in deposition of β-phase films. In the work of Ino et al., the β-phase was deposited at ion energies $\leq$ 10 eV until the ion to atom flux ratio was increased to about 15 and more. The higher ion flux resulted in deposition of pure α-phase films

until the ion energy was increased further resulting in β-phase films, regardless of the ion flux.

By concurring with the conclusions of both papers[60, 76], and also with further work at IBM on different ion assisted deposition methods of Ta [75] that the impact of energetic particles during film deposition promotes the growth of the bcc α-phase of Ta. There is a certain energy, or momentum, range below and above which the deposition of the α-phase is suppressed and a more disordered β-phase grows. The figure of merit appears to be the ion energy per deposited atom. This is somewhat unexpected since the cascade of atomic collisions following an impact of an energetic ion is different than the effect of, say, 10 impacts of ions with one tenth of the energy. Nevertheless, both events can rearrange adatoms on the growing film surface and provide sufficient energy for atomic displacements that may leads to the change in crystal lattice type. In all the cases discussed, the energy input to the growing film is rather large. An impact of a 150 eV ion can rearrange a cluster of atoms on the surface. Our preliminary molecular dynamics simulations indicate that atoms in at least three atomic layers are affected. Moreover, in this case, each site on the surface where an atom is deposited is also subjected to an ion impact, and thus a number of ion impacts, each of them rearrange several atoms, affect every adatoms. While the details of the mechanism of a particular Ta phase growth are still to be better understood when there is sufficient energy available in the ion assisted deposition to rearrange the deposited atoms. This rearrangement is caused by rapid and energetic collision cascades, with energies much higher than kT for substrate heating to temperature of 400 °C, and above, that also leads to deposition of bcc rather than tetragonal phase of Ta [10].

6.2 Film Thickness

It is well known that bulk tantalum usually appears to be bcc α-phase structure, however, thin film tantalum is often β-phase or mixed phase structures. So film thickness accompanied with the crystal lattice strain may be one of the factors which affect the film phase structures. The results of RBS measurements on different film samples deposited for 10 minutes show that their thicknesses depends on the bias voltage applied during deposition. This is explained as the process of re-sputtering of the deposited films by the bombarding ions. There is no re-sputtering of the film at $V_b = 0$ since in this case the ion energy is very low, below the sputtering threshold, estimated at 26 eV [117]. The sputtering yield at the higher ion energies were thus derived by comparing the thickness of the films deposited at different substrate bias voltages with the film deposited at zero bias voltage. The sputtering yield derived for 100 eV, 150 eV and 300 eV is consistent with the values reported by Stuart et al. [117] as seen in Figure 5.11. Moverover, the presence of Ar was only found in the films deposited at V_b = -300 V, and estimate its atomic concentration at 10 %, in agreement with the result reported by Catabia et al. [76].

6.3 Lattice Strain and Grain Size

The small grain size of the α-phase films (≤ 20 nm) may be a reflection of the high density of nucleation sites on the surface bombarded by energetic ions. As discussed below, each ion impact rearranges a cluster of surface atoms creating a potential seed for a new grain growth. Under continuous high intensity energetic ion bombardment (150 eV, ion to atom ratios ~ 1), the α-phase grain size is small (~ 20 nm) and does not change significantly while the film thickness increases fourfold from approximately 100 nm to

400 nm (Figure 4.21). For comparison, the α-phase Ta films deposited at 400 °C by DC sputtering without energetic ion bombardment, had a grain size varying from 25 to 35 nm as the film thickness increased in the same range [10]. The grain size in the films of this research decreases with increasing ion energy, in both α and β-phase.

The positive strain in the normal direction, determined from XRD data, indicates that the films are in compressive stress (in the lateral direction). The stress of the α-phase can be estimated as $\sigma = \frac{\varepsilon}{2\nu} Y$, using the elastic modulus of bcc Ta: $Y = 1.962 \times 10^{11}$ Pa, and the Poisson ratio $\nu = 0.35$. The above expression gives the compressive stress in the range 0.42 to 2.5 GPa for the strain values 0.0015 and 0.009, respectively, corresponding to the data span in Figs. 4.21 and 4.22.

The data show that as the ion energy increases from the low values at zero bias voltage, the film crystallographic phase changes from β, or mixed phase to the α-phase at -150 V bias, independently of the substrate material. This phase change, with disappearance of large β-phase crystals, is accompanied by the significant relief of the compressive internal strain (Figure 4.22). The strain decreases with increasing film thickness (Figure 4.21) to 0.1% at film thickness of 456 nm which is lower than in the film of the same thickness deposited by DC sputtering (0.5%) [10]. Further increase of the bombardment energy, above 150 eV, leads to the increase in compressive strain. The implanting of atoms, self-interstitials as well as impurities, such as Ar, into the film structure is known to cause compressive stress in sputtered films [123, 124], and these effects may explain the observed increasing strain with increasing ion bombardment energy, above 150 V bias. This strain, however, and similar strain at zero bias, are approximately the same as the strain in the α-phase Ta films deposited at 400 °C by DC

sputtering without energetic ion bombardment [10]. The β-phase structure in the film deposited on Si at -300 V bias has even higher strain (0.019) than the α-phase films deposited on Al under the same conditions (0.009).

Overall, for Ta thin film deposited at different bias voltages with different thicknesses, it is found that the α-phase Ta (110) oriented crystal grain size did not change much with a change in the bias voltages as well as the film thickness, however, the lattice strain of α-phase (110) crystals decreased as the magnitude of the bias voltage increases up to -100 V, and also decreased with increasing the film thickness. On the other hand, it is observed that large size β-phase Ta (002) oriented crystals with lower level lattice strain tend to grow with low energy of ion bombardment, at zero substrate bias, especially in the thicker films. High energy ion bombardment (~300 eV) depresses the β-phase crystal grain size and increases the lattice strain, particularly in thinner films. The appearance of β-phase Ta film may be controlled by both crystal grain size (nucleation sites density) and crystal internal stress. For the β-phase Ta crystals, with increasing ion bombardment energy, the grain size decreases since nucleation sites density increases, also the crystal stress will increase. In this study, the β-phase with large grain size crystals and with low internal stress was grown at low ion energy. With increasing ion bombardment energy, β-phase grows in small size crystallite with increasing internal stress. At some point, the β-phase crystal can not sustain the internal stress, and it collapses (ion to atoms flux ratio ~1.0 at -150 eV). As the ion energy increases further, the crystal grain size decreases to the level where it can sustain the internal stress.

6.4 The Substrate Effect

Many of the measured film properties, including strain and grain size, do not depend significantly on the substrate material and can be thus attributed to the effects of ion bombardment. Generally, however, the aluminum substrate appears to promote a more robust growth of the α-phase. This is apparent in XRD patterns of films with different thickness deposited with -100V bias (Figure 4.12 and Figure 4.13) and in films deposited for 10 minutes with -300 V bias (Figure 4.3 and Figure 4.4), which show the presence of strong β-phase peaks in samples on Si but not on Al. It has been known that certain substrates promote the growth of Ta α-phase. Among them is Nb with a bcc crystal structure and a lattice constant very close to that of bcc Ta (0.3 % difference) that facilitates epitaxial Ta growth [39]. Al, with the fcc structure was also found to promote bcc Ta growth with strong (110) texture. The growth of bcc Ta on Al had been interpreted as an approximate epitaxial matching of some atoms on the (110) Ta plane with atoms of the fcc Al on the (111) plane [125]. The matching is only very good only along the <110> axis of the Al (111) plane aligned with the <111> axis of (110) Ta plane, but it is apparently sufficient for nucleation of bcc Ta crystals. This quasi-epitaxial relation between Al and Ta may also contribute to the growth of the α phase in this case.

The role of the substrate is also demonstrated by the necessity to perform the pre-deposition sputter etching step. The sputter etching removes loosely bonded contaminant species from the substrate surface as well as a thin native oxide layer. This effect is especially strong for silicon substrates as there was no α-phase Ta growth on silicon substrates, even under -150 V bias, without performing the pre-deposition sputter etching cleaning step.

The phase of tantalum thin films deposited on silicon substrates with sputter etching performed under 0 V bias is not consistent (in some films strong α-phase structure is detected, in others strong β-phase structure), in contrast to the thin films deposited under other bias conditions. During 0 V bias depositions, the energy of the ions is very low, 10 eV, and their effect is too weak to influence the crystallographic structure of deposited tantalum thin films, while the substrate may play the main role. The crystallographic structure of the tantalum thin films growing under very low energy ion bombardment may thus be very sensitive to the substrate state, and small differences in this after sputter etching may lead the crystallographic phase changing.

It was observed that tantalum thin films deposited under a high bias voltage (~300 V) have a β-phase structure on silicon substrates, but an α-phase structure on aluminum substrates. It is proposed that the reason for this is the modification of the surface structure of silicon substrate by energetic ions in the early stage of the Ta film growth. It is well known that the energetic ion bombardment creates damage in silicon lattice that accumulates and amorphizes the crystals at sufficient ion dose. The amorphizing dose is of the order of 10^{-15} cm^{-2}, which in our case accumulates in time in which a few monolayers of tantalum are deposited. Since the damage of an ion impact may easily reach the depth of several atomic layers, some amorphizing of silicon surface is possible. The effect strongly depends on ion energy and appears to be significant only above 150 eV in this case. It should be noted that tantalum films on Si substrate deposited initially at -150 eV bias, and with continuing deposition at the bias increased to -300 V, also shows α-phase structure (Figure 4.17). Thus the initial stage of the deposition, with -150 V bias,

during which silicon structure was not sufficiently damaged, determined the crystallographic phase of the Ta film, most of which was deposited at -300 V bias.

The metallic aluminum substrate, on the other hand, is not amorphized by such ion bombardment because of the nature of its metallic bond. In metals, the atomic positions are not fixed by rigid covalent bonds and the lattice is not easily destroyed by atomic displacements.

6.5 MD Simulation

The molecular dynamics simulation provided insight into the phenomena occurring in Ta films bombarded by energetic Ar ions. This includes the relative numbers of reflected and implanted Ar ions, their energy and thus the ion energy deposited in the film. The duration and the spatial extent of the collision cascade could be also estimated. In addition, MD simulation provided the values of the sputtering yield of bcc Ta bombarded by Ar ions at energies used in this investigation. In order to get statistically significant results, a total of 875 impacts with different impact positions with respect to the (110) oriented bcc α-phase Ta lattice were simulated.

The simulations show that in the projectile energy range: 10 eV to 150 eV almost all Ar ions are scattered back after colliding with the tantalum target atoms, while at an energy of 300 eV, 192 Ar ions out of 875 remain embedded in the target. This roughly agrees with the approximately 10% Ar concentration measured by RBS in tantalum thin films deposited under -300 V bias conditions.

From MD simulations, the energy deposited into the growing tantalum thin films by Ar ion impacts can be determined. At -150 V bias (Ar ion input energy of 150 eV), approximately 120 eV was transferred on average into the deposited tantalum thin film, while at the bias voltage of -300 V the transferred energy is 250 eV. The fluxes of ions and Ta atoms are approximately equal, however, the input energy was not the energies delivered per single atom of film during the bias sputtering process, instead it was delivered through multi-collision process to more than one atom as well as dissipated through both nuclear and electron collisions. However, for the atoms which received enough energy and this energy was higher than the binding energy of Ta atoms, then they were capable of leaving their original position and rearranging themselves in the new lattice position in the film.

The MD simulation sputtering yield is close to the sputtering yield derived from the RBS measurement for 0 V, -100 V and -150 V bias conditions, however there is a significant difference between the simulated and experimental sputtering yield for 300 eV bias. An obvious difference in the simulation and the experimental systems is that the simulation is for (110) oriented bcc Ta crystallographic structure, while the crystallographic structure of tantalum thin films deposited under -300 V bias conditions is β-phase. The sensitivity of sputtering yield obtained from MD simulations to the crystallographic structure of target was demonstrated by comparing its values for (100) and (110) oriented bcc Ta target which were 0.292 ± 0.017 and 0.378 ± 0.019 for 150 eV Ar, respectively.

One possible reason that the sputtering yield derived from MD simulation is higher than the sputtering yield derived the RBS measurement may be due to the fact that the film consists of polycrystalline material while MD simulation assumes a single crystal target in which atoms bound in perfect lattice. Another reason is due to the surface oxide on the thin films which may lower the observed sputtering yield. Under the condition of base pressure 10^{-8} Torr and thin film deposition rate 0.3 nm/s, the estimated upper limit of oxygen incorporation during our Ta deposition is about 0.002 which would grow a surface oxide at $\sim 7\times10^{-4}$ nm/s if all O_2 reacted with surface during deposition. This is about 400 times less than the arrival rate of Ta atoms during sputtering. If oxide regrows faster than which can be removed, then the lower sputtering yield can be expected since the sputtering yield of Ta_2O_5 is lower than pure Ta (at bombarding argon ion energy in 600 eV, the sputtering yield for Ta is 0.62 and for Ta_2O_5 0.15 is [126]). So it means that at least 38% Ta_2O_5 is required for lowering the sputtering yield getting from MD simulation (0.877) to mach the result from RBS measurement (0.45). As mentioned before, this is not the only reason for the measured low value of sputtering yield. Also, even this MD simulation author suggested that the sputtering yield getting from this simulation can be used as a comparison but not good enough for the purpose of predicting the absolute value.

6.6 Statistics of Deposited Atoms and Ion Impacts and its Role in the Mechanism of Ion Assisted Deposition

For the purpose of understanding how ion impacts may affect the film structure, mathematical calculations of the time and space relation of the atom deposition and ion impacts are presented below.

The ion assisted deposition process can be looked as consisting of two basic physical events: (1) deposition of an atom (also called adatom) which can move (diffuse) on the surface before being trapped (attached) to a lattice site, and (2) impact of an ion on the film surface which creates a collision cascade affecting a finite film surface and volume for a certain time. The key question is under the conditions of these analyzed experiments do these two events occur simultaneously in a given film volume or are separated in time and space.

Consider now two impacts of ions with the flux f_i. Assuming these events happen randomly and uniformly on the thin film surface, there are τf_i ions that land on a unit area after time τ, or the average area that includes one ion is $1/(\tau f_i)$. Taking τ as the time duration of the impact event, consider only "active" impact" sites, i.e., those that are affected by the energetic ions. The average distance between these active sites is calculated by considering a circular area around each, with a circle radius r that can be expressed as $(\pi\tau f_i)^{-1/2}$. The mean distance between the centers of two consecutive events is then 2r. The relationship between the event distance, 2r, and time τ is presented in Figure 6.1. In this study, $f_i \approx 10^{15}$ cm^{-2} s^{-1}, and τ estimated from MD simulation is 400 fs, which gives 2r = 560 μm. Since the area affected by each impact is much smaller, it is concluded that the impact events do not overlap and occur independently of each other in

time and space. Since the atom and ion fluxes are approximately equal, the same conclusion applies to deposition events of adatoms.

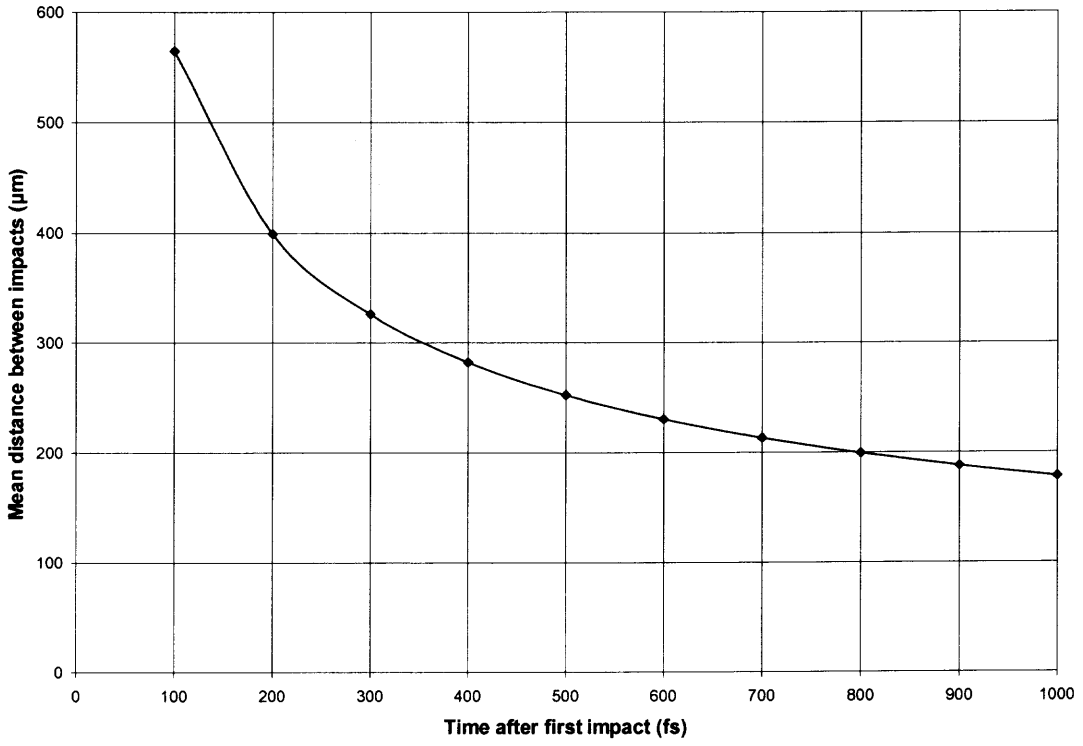

Figure 6.1 The development of the mean distance between deposited atom and ion impact with time.

Considering now two random events: the deposited Ta atoms arrive with atomic flux, f_a, and diffuse through the average area, A_a, in time τ_a before attaching to the thin film crystal lattice position, and the ions come with flux f_i and affect the thin film atoms in an average surface regime A_i by collision cascade in time τ_i before their energy are dissipated.

From the statistical point of view, the probability of two areas A_1 and A_2 partially overlapping in a unit surface area is approximately $n_1A_1+n_2A_2$ where n_1 and n_2 are the numbers of areas A_1 and A_2 in a unit surface area respectively under the condition of $n_1A_1 \ll 1$ and $n_2A_2 \ll 1$. Based on the MD simulation, A_a is close to zero and A_i is about

$20\times15*10^{-16}$ cm^2 when τ_i is 400 fs which satisfies $f_i\tau_iA_i \approx 1.2*10^{-11}\ll1$ ($f_i\tau_iA_i = 10^{15}\times400*10^{-15}\times300*10^{-16}$). So using this in the consideration of time and space coincidence of atom diffusion and ion impact, the probability of these two events coincidence is approximately $f_a\tau_aA_a+f_i\tau_iA_i \approx 10^{-11}$. This means that the chance for these two events coincidence in the time and space is very small, almost zero. In another words, there will be $f_af_i\tau_iA_i = 12000$ atoms affected by ions per second but they will be distributed over a "large" area of 1 cm^2 on which there will be 10^{15} impacts per second, so again the probability that an adatom is affected by ion impacts is very small (~12000/ $3\times10^{15} = 4\times10^{-11}$).

Therefore, the atoms condense on the surface forming thin film before an ion impact occurs nearby, and also the consecutive ion and atom impacts are too far apart to affect each other. Thus, an atom attaches to the film before it can be affected by an ion impact and the collision cascade created by the ion dies out before an atom lands on the surface near the ion impact. Moreover, each ion impacts affect about 20 atoms which are already condensed, i.e., in the real thin film deposition process as in this work, each condensed Ta atoms will be moved and rearranged several times before finally settled down, and this will contribute to the thin film crystal structure transformation.

From the above analysis, it's clear that film deposited by biased RF magnetron sputtering process is a combination of two physical processes: deposition of Ta atoms with relatively low energy ($\leq$ 10 eV) and bombardment of the substrate (initially) and the growing film surface by ions with relatively high energy (depending on the biasing voltage), and these two processes in space and time analysis shows that they are independent. The arriving Ta atoms (adatoms) with relatively low energy diffuse on the

growing thin film surface and lose their kinetic energy to the surface atoms until binding to a stable position first, then the incoming Ar ion with relatively high energy will quickly transfer its energy to the surrounding film atoms in a collision cascade which extends over certain surface area and depth. Thus it was concluded that the role of ion bombardment in the biased sputtering process is modification of the already formed Ta thin film structure. MD simulations further suggest that the volume of Ta film that can be modified by an Ar ion impact is several atomic layers deep and covers the area of several nm^2 on the film surface. The impacts are widely separated in space and time, so that modification by ion bombardment proceeds over small volume at a given time.

CHAPTER 7

SUMMARY AND CONCLUSIONS

The purpose of this research was to investigate the tantalum thin film deposition by the biased sputtering process at ambient temperature. The effect of ion bombardment on the crystallographic phase of tantalum (Ta) thin films as well as the thin film surface morphology was studied. The Ta thin films were deposited on two types of substrates, (100) oriented silicon and on polycrystalline aluminum. A negative bias voltage, 0 – 300 V, was applied to the substrate to control the energy of the ions bombarding the growing film. The films were characterized by X-ray diffraction (XRD), for identification of Ta crystallographic phases, and by Rutherford backscattering spectroscopy (RBS), for measuring the film thickness and foreign atoms incorporation. The film surface morphology was investigated by scanning electron microscopy and the roughness by atomic force microscopy. It was found that the presence of two crystallographic phases of Ta (body centered cubic and tetragonal) in thin films can be controlled by the substrate bias voltage.

The experiments confirmed that energetic ion bombardment during deposition by magnetron sputtering affects the crystallographic phase of Ta thin films. New conditions for the growth of, the usually desired, bcc Ta films were found. In contrast to earlier reports this phase can grow under Ar^+ ion bombardment close to 150 eV with the ion flux comparable with the flux of deposited Ta atoms. While this energy is much higher than the ion energy used previously to grow bcc Ta films, it was found that the total energy delivered by ions per deposited atom in this and in previous work is approximately the same.

In addition to the experiments, molecular dynamics simulations were performed to further understand this ion assisted deposition process. The average area of the film surface and the volume affected by an ion impact, as well as the duration of the energetic collision cascade were estimated from the simulations. A statistical analysis of ion impacts and atom impingements showed that the two events occur independently and do not coincide in time and space. Therefore the thin film crystal structure is transformed by rearrangement of deposited atom clusters by ion impact induced by collision cascades and not by imparting energy to adatoms before their attachment to the growing film.

From the point of view of applications, the new conditions for deposition of bcc Ta films can be achieved in a relatively simple system comprised of a magnetron sputtering source supplied with RF power and DC substrate biasing. Such a deposition system is easier to scale up to industrial operation than those described earlier, which require complex apparatus.

REFERENCES

1. M. H. Read and C. Altman, "A new structure in tantalum thin films," Applied Physics Letters 7 (3), 51-52 (1965).

2. V. P. Belevskiy, M. V. Belous, V. G. Permyakov and V. M. Yashnik, "Electrophysical properties and phase composition of thin cathode-sputtered tantalum films," Physics of Metals and Metallography 33 (3), 105-110 (1972).

3. R. B. Marcus and S. Quiglay, "Formation of f.c.c., b.c.c. and β-tantalum films by evaporation," Thin Solid Films 2 (5-6), 467-477 (1968).

4. A. Arakcheeva, G. Chapuis and V. Grinevitch, "The self-hosting structure of β-Ta," Acta Crystallographic B 58 (1), 1-7 (2002).

5. R. D. Burbank, "An X-ray study of β-tantalum," Journal of Applied Crystallography 6 (3), 217-224 (1973).

6. L. M. Hsiung and D. H. Lassila, "Shock-induced omega phase in tantalum," Scripta Materiala 38 (9), 1371-1376 (1998).

7. G. Das, "A new structure of sputtered tantalum," Thin Solid Films 12 (2), 305-311 (1972).

8. D. Millis, "The structure of sputtered tantalum," Journal of Canadian Ceramic Society, 35, 48-52 (1966).

9. "Tantalum," [Document posted on Web site of Mineral Information Institute]. Retrieved March 20, 2006 from the World Wide Web: http://www.mii.org/Minerals/phototant.html

10. L. Gladczuk, A. Patel, C. Singh Paur and M. Sosnowski, "Tantalum films for protective coatings of steel," Thin Solid Films 467 (1-2), 150-157 (2004).

11. W. Ensinger, "Low energy ion assist during deposition—an effective tool for controlling thin film microstructure," Nuclear Instruments and Methods in Physics Research B 127/128, 796-808 (1997).

12. M. Poksinski, "Fundamentals of glow discharge processes," [Document posted on Web site of Linköpings universitet]. Retrieved March 20, 2006 from the World Wide Web: http://cms.ifm.liu.se/materialphysics/thinfilm/research/fundamentals_of glow_disc/

13. "Tantalum," [Document posted on Web site of Los Alamos National Laboratory]. Retrieved March 24, 2006 from the World Wide Web: http://periodic.lanl.gov/elements/73.html

14. "Tantalum," [Document posted on Web site of Jefferson Lab]. Retrieved March 24, 2006 from the World Wide Web: http://education.jlab.org/itselemental/ele073.html

15. S. Maeng, L. Axe, T. A. Tyson and P. Cote, "Corrosion behaviour of electrodeposited and sputtered Cr coatings and sputtered Ta coatings with α and β phases," Surface and Coatings Technology 200 (20-21), 5767-5777 (2006).

16. D. W. Matson, E. D. McClanahan, S. Lee and D. Windover, "Properties of thick sputtered Ta used for protective gun tube coatings," Surface and Coatings Technology 146/147, 344-350 (2001).

17. S. L. Lee, D. Windover, M. Doxbeck, M. Nielsen, A. Kumar and T. M. Lu, "Image plane X-ray diffraction and X-ray reflectivity characterization of protective coatings and thin films," Thin Solid Films 377/378, 447-454 (2000).

18. A. Rubinshtein, R. Shneck, A. Danon, J. Hayon, S. Nathan and A. Raveh, "Surface treatment of tantalum to improve its corrosion resistance," Materials Science and Engineering A 302 (1), 128-134 (2001).

19. S. L. Lee, D. Windover, M. Audino, D. W. Matson and E. D. McClanahan, "High-rate sputter deposited tantalum coating on steel for wear and erosion mitigation," Surface and Coatings Technology 149 (1), 62-69 (2002).

20. "What are refractory metals," [Document posted on Web site of Metal Powder Industries Federation]. Retrieved March 26, 2006 from the World Wide Web: http://www.mpif.org/DesignCenter/refractory.pdf

21. F. Cardarelli, P. Taxil and A. Savall, "Tantalum protective thin coating techniques for the chemical process industry: molten salts electrocoating as a new alternative," International Journal of Refractory Metals and Hard Materials 14, 365-381 (1996).

22. F. Brossa, G. Piatti and M. Bardy, "Tantalum protective coatings for fusion reactor applications," Journal of Nuclear Materials 103, 261-265 (1981).

23. C. H. Liu, S. J. Chang, J. F. Chen, S. C. Chen, J. S. Lee and U. H. Liaw, "High-quality ultrathin chemical-vapor-deposited Ta_2O_5 capacitors prepared by high-density plasma annealing," Materials Science and Engineering B 106 (3), 234-241 (2004).

24. D. Gerstenberg and C. J. Calbick, "Effects of nitrogen, and oxygen on structure and electrical properties of thin tantalum films," Journal of Applied Physics 35 (2), 402-407 (1964).

25. M. Stavrev, C. Wenzel, A. Moller and K. Drescher, "Sputtering of tantalum-based diffusion barriers in Si/Cu metallization: effects of gas pressure and composition," Applied Surface Science 91 (1-4), 257-262 (1995).

26. M. Stavrev, D. Fischer, C. Wenzel and T. Heiser, "Study of Ta(N,O) diffusion barrier stability: analytical and electrical characterization of low level Cu contamination in Si," Microelectronic Engineering 37/38, 245-251 (1997).

27. M. S. Angyal, Y. Shacham-Diamand, J. S. Reid and M. A. Nicolet, "Performance of tantalum-silicon-nitride diffusion barriers between copper and silicon dioxide," Applied Physics Letters 67 (15), 2152-2154 (1995).

28. K. Holloway and P. M. Fryer, "Tantalum as a diffusion barrier between copper and silicon," Applied Physics Letters 57 (17), 1736-1738 (1990).

29. G. S. Chen, P. Y. Lee and S. T. Chen, "Phase formation behavior and diffusion barrier property of reactively sputtered tantalum-based thin films used in semiconductor metallization," Thin Solid Films 353 (1-2), 264-173 (1999).

30. Z. L. Yuan, D. H. Zhang, C. Y. Li, K. Prasad, C. M. Tan and L. J. Tang, "A new method for deposition of cubic Ta diffusion barrier for Cu metallization," Thin Solid Films 434 (1-2) 126-129 (2003).

31. R. Hoogeveen, M. Moske, H. Geisler and K. Samwer, "Texture and phase transformation of sputter-deposited metastable Ta films and Ta/Cu multilayers," Thin Solid Films 275 (1-2), 203-206 (1996).

32. R. J. Gutmann, J. M. Steigerwald, L. You, D. T. Price, J. Neirynck, D. J. Duquette and S. P. Murarka, "Chemical-mechanical polishing of copper with oxide and polymer interlevel dielectrics," Thin Solid Films 270 (1-2), 596-600 (1995).

33. A. F. Jankowski, R. M. Bionta and P. C. Gabriele, "Internal stress minimization in the fabrication of transmissive multilayer x-ray optics," Journal of Vacuum Science and Technology A 7 (2), 210-213 (1989).

34. Y. X. Leng, H. Sun, P. Yang, J. Y. Chen, J. Wang, G. J. Wan, N. Huang, X. B. Tian, L. P. Wang and P. K. Chu, "Biomedical properties of tantalum nitride films synthesized by reactive magnetron sputtering," Thin Solid Films 398/399, 471-475 (2001).

35. A. Schauer, "Method of producing thin tantalum films," U. S. Patent No. 3, 878, 079 (April 15, 1975).

36. S. L. Lee, M. Cipollo, D. Windover and C. Rickard, "Analysis of magnetron-sputtered tantalum coatings versus electrochemically deposited tantalum from molten salt," Surface and Coatings Technology 120/121, 44-52 (1999).

37. D. W. Matson, M. D. Merz and E. D. McClanahan, "High rate sputter deposition of wear resistant tantalum coatings," Journal of Vacuum Science and Technology A 10 (4), 1791-1796 (1992).

38. S. L. Lee and D. Windover, "Phase, residual stress, and texture in triode-sputtered tantalum coatings on steel," Surface and Coatings Technology 108/109 (1-3), 65-72 (1998).

39. D. W. Face and D. E. Prober, "Nucleation of body-centered-cubic tantalum films with a thin niobium underlayer," Journal of Vacuum Science and Technology A 5 (6), 3408-3411 (1987).

40. L. Liu, H. Gong, Y. Wang, J. Wang, A. T. S. Wee and R. Liu, "Annealing effects of tantalum thin films sputtered on [001] silicon substrate," Materials Science and Engineering C 16 (1-2), 85-89 (2001).

41. S. L. Lee, M. Doxbeck, J. Mueller, M. Cipollo and P. Cote, "Texture, structure and phase transformation in sputter beta tantalum coating," Surface and Coatings Technology 177/178, 44-51 (2004).

42. D. W. Matson, E. D. McClanahan, J. P. Rice, S. L. Lee and D. Windover, "Effect of sputtering parameters on Ta coatings for gun bore applications," Surface and Coatings Technology 133/134, 411-416 (2000).

43. P. Shivaramkrishnan, "Characterization of tantalum coatings on steel substrates," M.S. thesis, New Jersey Institute of Technology, 1999.

44. K. Hieber and N. M. Mayer, "Structural changes of evaporated tantalum during film growth," Thin Solid Films 90 (1), 43-50 (1982).

45. J. E. Nestell Jr, K. J. Scoles and R. W. Christy, "Optical conductivity of amorphous Ta and beta-Ta films," Journal of Applied Physics 53 (12), 8993-8998 (1982).

46. M. H. Read and D. H. Hensler, "A-ray analysis of sputtered films of beta-tantalum and body-centered cubic tantalum," Thin Solid Films 10 (1), 123-135 (1972).

47. A. P. Mammana, I. L. Torriani, M. A. Silveira and L. A. C. de Almeida, "Characterization of Ta thin films obtained by dc sputtering," Vacuum 41 (4-6), 1403-1404 (1990).

48. H. F. Rizzo, A. W. Echeverria, W. L. Wien and T. B. Massalski, "Formation of metastable structure and amorphous phases in plutonium-based systems using the triode sputtering technique," Materials Science and Engineering 98, 57-60 (1988).

49. F. Sajovec, P.M. Meuffels and T. Schober, "Structural and electrical properties of ion beam sputter deposited tantalum films," Thin Solid Films 219 (1-2), 206-209 (1992).

50. S. Sato, "Nucleation properties of magnetron-sputtered tantalum," Thin Solid Films 94 (4), 321-329 (1982).

51. S. L. Lee, D. Windover, T. M. Lu and M. Audino, "In situ phase evolution study on magnetron sputtered tantalum thin films," Thin Solid Films 420/421, 287-294 (2002).

52. K. Hieber, "Structural and electrical properties of Ta and Ta nitrides deposited by chemical vapour deposition," Thin Solid Films 24 (1), 157-164 (1974).

53. L. G. Feinstein and R. D. Huttemann, "Factors controlling the structure of sputtered Ta films," Thin Solid Films 16 (2), 129-145 (1973).

54. A. Schauer, W. Peters and W. Juergens, "A very pure thin film tantalum phase," Thin Solid Films 8 (3), R9-R12 (1971).

55. A. Schauer and W. Peters, "The influence of film thickness on the formation of β-Ta and b.c.c.-Ta," Thin Solid Films 27 (1), 95-99 (1975).

56. E. Krikorian and R. J. Sneed, "Deposition of tantalum, tantalum oxide, and tantalum nitride with controlled electrical characteristics," Journal of Applied Physics 37 (10), 3674-3681 (1966).

57. P. N. Baker, "R.f. sputtered tantalum films deposited in an oxygen doped atmosphere," Thin Solid Films 6 (5), R57-R60 (1970).

58. W. D. Westwood and F. C. Livermore, "Phase composition and conductivity of sputtered tantalum," Thin Solid Films 5 (5-6), 407-420 (1970).

59. P. N. Baker, "Preparation and properties of tantalum thin films," Thin Solid Films, 14 (1), 3-25 (1972).

60. K. Ino, T. Shinohara, T. Ushiki and T. Ohmi, "Ion energy, ion flux, and ion species effects on crystallographic and electrical properties of sputter-deposited Ta thin films," Journal of Vacuum Science and Technology A 15 (5), 2627-2635 (1997).

61. D. Fischer, O. Meissner, B. Bendjus, J. Schreiber, M. Stavrev and C. Wenzel, "AFM characterization of Ta-based diffusion barriers for use in future semiconductor metallization," Surface and Interface Analysis 25 (7-8), 522-528 (1997).

62. N. Schwartz and E. D. Feit, "Impurity effects in the nucleation of alpha (bcc)-tantalum or beta-tantalum films," Journal of the Electrochemical Society 124 (1), 123-131 (1977).

63. D. M. Mattox and G. J. Kominiak, "Structure modification by ion bombardment during deposition," Journal of Vacuum Science and Technology 9 (1), 528-532 (1972).

64. A. Schauer and M. Roschy, "R.F. sputtered β-tantalum and b.c.c. tantalum films," Thin Solid Films 12 (2), 313-317 (1972).

65. K. Hieber and E. Lautenbacher, "Stabilization of sputtered β-tantalum by a tantalum silicide interlayer," Thin Solid Films 66 (2), 191-196 (1980).

66. W. D. Westwood, "The influence of conducting underlayers on the properties sputtered tantalum films," Thin Solid Films 6 (5), 307-320 (1970).

67. G. S. Chen, S. T. Chen, S. C. Huang and H. Y. Lee, "Growth mechanism of sputter deposited Ta and Ta-N thin films induced by an underlying titanium layer and varying nitrogen flow rates," Applied Surface Science 169/170, 353-357 (2001).

68. E. G. Colgan and P. M. Fryer, "Method of making alpha-Ta thin films," U. S. Patent No. 5, 221, 449 (June 22, 1993).

69. L. Gladczuk, A. Patel, J. D. Demaree and M. Sosnowski, "Sputter deposition of bcc tantalum films with TaN underlayers for protection of steel," Thin Solid Films 476 (2), 295-302 (2005).

70. H. Shimada, I. Ohshima, T. Ushiki, S. Sugawa and T. Ohmi, "Tantalum nitride metal gate FD-SOI CMOS FETs using low resistivity self-grown bcc-tantalum layer," IEEE Transactions on Electron Devices 48 (8), 1619-1926 (2001).

71. T. Tanaka and K. Kawabata, "Preparation of Ta/Mo structure by using RF-DC coupled magnetron sputtering," Thin Solid Films 312 (1-2), 135-138 (1998).

72. P. J. Kelly and R. D. Arnell, "Magnetron sputtering: a review of recent developments and applications," Vacuum 56 (3), 159-172 (2000).

73. P. F. Knewstubb and A. W. Tickner, "Mass spectrometry of ions in glow discharges. III. Nitrogen and its mixtures with hydrogen and oxygen," The Journal of Chemical Physics 37 (12), 2941-2949 (1962).

74. L. I. Maissel and P. M. Schaible, "Thin films deposited by bias sputtering," Journal of Applied Physics 36 (1), 237-242 (1965).

75. R. A. Roy, P. Catania, K. L. Saenger, J. J. Cuomo and R. L. Lossy, "Role of energetic atoms and ions in Ta films grown by different physical vapor deposition methods," Journal of Vacuum Science and Technology B 11 (5), 1921-1927 (1993).

76. P. Catania, R. A. Roy and J. J. Cuomo, "Phase formation and microstructure changes in tantalum thin films induced by bias sputtering," Journal of Applied Physics 74 (2), 1008-1014 (1993).

77. P. Catania, J. P. Doyle and J. J. Cuomo, "Low resistivity body-centered cubic tantalum thin films as diffusion barriers between copper and silicon," Journal of Vacuum Science and Technology A 10 (5), 3318-3321 (1992).

78. H. C. Cook, "Investigation od sputtered beta-tantalum thin films," Journal of Vacuum Science and Technology 4 (2), 80-86 (1967).

79. L. A. Clevenger, A. Mutscheller, J. M. E. Harper, Jr C. Cabral and K. Brmak, "The relationship between deposition conditions, the beta to alpha phase transformation, and stress relaxation in tantalum thin films," Journal of Applied Physics 72 (10), 4918-4924 (1992).

80. S. K. Kim and B. C. Cha, "Deposition of tantalum nitride thin films by D.C. magnetron sputtering," Thin Solid Films 475 (1-2), 202-207 (2005).

81. A. E. Kaloyeros and E. Eisenbraun, "Ultrathin diffusion barriers/liners for gigascale copper metallization," Annual Review of Materials Science 30 (1), 363-385 (2000).

82. T. Oku, E. Kawakami, M. Uekubo, K. Takahiro, S. Yamaguchi and M. Murakami, "Diffusion barrier property of TaN between Si and Cu," Applied Surface Science 99 (4), 265-272 (1996).

83. K.-H. Min,K.-C. Chun and K.-B. Kim, "Comparative study of tantalum and tantalum nitrides (Ta_2N and TaN) as a diffusion barrier for Cu metallization," Journal of Vacuum Science and Technology B 14 (5), 3263-3269 (1996).

84. M. L. Lovejoy, G. A. Patrizi, D. J. Roger and J. C. Barbour, "Thin-film tantalum-nitride resistor technology for phosphide-based optoelectronics," Thin Solid Films 290/291, 513-517 (1996).

85. E. O. Ezugwu and J. Wallbank, "Manufacture and properties of ceramic cutting tools: a review," Materials Science and Technology 3 (11), 881-887 (1987).

86. Y. M. Lu, R. J. Weng, W. S. Hwang and Y. S. Yang, "Study of phase transition and electrical resistivity of tantalum nitride films prepared by DC magnetron sputtering with OEC detection system," Thin Solid Films 398/399, 356-360 (2001).

87. Y. M. Lu, R. J. Weng, W. S. Hwang and Y. S. Yang, "Electrical properties of Ta_xN_y films by implementing OES in the sputtering system," Materials Chemistry and Physics 72 (2), 278-280 (2001).

88. H. B. Nie, S. Y. Xu, S. J. Wang, L. P. You, Z. Yang, C. K. Ong, J. Li and T. Y. F. Liew, "Structural and electrical properties of tantalum nitride thin films fabricated by using reactive radio-frequency magnetron sputtering," Applied Physics A 73 (2), 229-236 (2001).

89. K. Radhakrishnan, Ng Geok Ing and R. Gopalakrishnan, "Reactive sputter deposition and characterization of tantalum nitride thin films," Materials Science and Engineering B 57 (3), 224-227 (1999).

90. K. Holloway, P. M. Fryer, Jr C. Cabral, J. M. E. Harper, P. J. Bailay and K. H. Kelleher, "Tantalum as a diffusion barrier between copper and silicon: failure mechanism and effect of nitrogen additions," Journal of Applied Physics 71 (11), 5433-5444 (1992).

91. M. Stavrev, D. Fischer, C. Wenzel, K. Drescher and N. Mattern, "Crystallographic and morphological characterization of reactively sputtered Ta, TaN and TaNO thin films," Thin Solid Films 307 (1-2), 79-88 (1997).

92. R. Westergard, M. Bromark, M. Larsson, P. Hedenqvist and S. Hogmark, 'Mechanical and tribological characterization DC magnetron sputtered tantalum nitride thin films," Surface and Coatings Technology 97 (1-3), 779-784 (1997).

93. P. Saha and J. A. Barnard, "Effect of structure on the mechanical properties of Ta and Ta(N) thin films prepared by reactive DC magnetron sputtering," Journal of Crystal Growth 174 (1-4), 495-500 (1997).

94. X. Sun, E. Kolawa, J.-S. Chen, J.S. Reid and M.-A. Nicolet, "Properties of reactively sputter-deposited Ta—N thin films," Thin Solid Films 236 (1-2), 347-351 (1993).

95. J.-C. Chuang and M.-C. Chen, "Properties of thin Ta-N films reactively sputtered on $Cu/SiO_2/Si$ substrates," Thin Solid Films 322 (1-2), 213-217 (1998).

96. M. H. Tsai, S. C. Sun, H. T. Chiu, C. E. Tsai and S. H. Chuang, "Metalorganic chemical vapor deposition of tantalum nitride by terbutylimidotris(diethylamido)tantalum for advanced metallization," Applied Physics Letters 67 (8), 1128-1130 (1995).

97. K. Bba, R. Hatada, K. Udoh and K. Yasuda, "Structure and properties of NbN and TaN prepared by ion beam assisted deposition," Nuclear Instruments and Methods in Physics Research B 127/128, 841-845 (1997).

98. Q. Y. Zhang, X. X. Mei, D. Z. Yang, F. X. Chen, T. C. Ma, Y. M. Wang and F. N. Teng, "Preparation, structure and properties of TaN and TaC films obtained by ion beam assisted deposition," Nuclear Instruments and Methods in Physics Research B 127/128, 664-668 (1997).

99. W. Ensinger, M. Kiuchi and M. Satou, "Low-temperature formation of metastable cubic tantalum nitride by metal condensation under ion irradiation," Journal of Applied Physics 77 (12), 6630-6635 (1995).

100. L. A. Clevenger, N. A. Bojarczuk, l. Holloway, J. M. E. Harper, Jr C. Cabral, R. G. Schad, F. Cardone and L. Stolt, "Comparison of high vacuum and ultra-high-vacuum tantalum diffusion barrier performance against copper penetration," Journal of Applied Physics 73 (1), 300-308 (1993).

101. M. Takeyama, A. Noya, T.Sase, A. Ohta and K. Sasaki, "Properties of TaN_x films as diffusion barriers in the thermally stable Cu/Si contact systems," Journal of Vacuum Science and Technology B 14 (2), 674-678 (1996).

102. S. C. Brown, Basic Data of Plasma Physics: The Fundamental Data on Electrical Discharges in Gases, 1st ed. (American Institute of Physics, 1997).

103. S. Raina, "Deposition of tantalum thin films by RF sputtering with substrate bias," M.S. thesis, New Jersey Institute of Technology, 2005.

104. M. Ohing, The Materials Science of Thin Films, (Academic Press, 1992).

105. JCPDS-ICDD File Card No. 00-002-1104

106. JCPDS-ICDD File Card No. 01-089-1545

107. P. Šutta, "Internal stresses in plastically deformed gold films investigated by X-ray diffraction," Materials Structure 8 (2), 68-70 (2001).

108. M. Meier, "Crystallite size measurement using X-ray diffraction," [Document posted on Web site of University of California]. Retrieved May 9, 2006 from the World Wide Web: http://www.matsci.ucdavis.edu/MatSciLT/EMS-162L/Files/XRD-CSize1.pdf

109. "Scanning Electron Microscope (SEM)," [Document posted on Web site of University of Nebraska-Lincoln]. Retrieved October 20, 2006 from the World Wide Web: http://www.unl.edu/CMRAcfem/

110. P. T. Moseley and C. J. Seabrook, "The crystal structure of β-tantalum," Acta Crystallographica B B29 (5), 1170-1171 (1973).

111. Y. Yamamura and H. Tawara, "Energy dependence of ion-induced sputtering yields from monatomic solids at normal incidence," Atomic Data and Nuclear Data Tables 62 (2), 149-253 (1996).

112. S. Roland, D. Annick, K. Dmitry and F. Laurent, "Molecular Dynamics Simulations," [Document posted on the Web site of Swiss node of EMBnet]. Retrieved July 7, 2006 from the World Wide Web: http://www.ch.embnet.org/MD_tutorial/index.html

113. M. A. Karolewski, "Classical Dynamics Simulation of Projectile-surface interactions," Surface and Interface Analysis 27 (2), 114-122 (1999).

114. M. A. Karolewski, "Tight-binding potentials for sputtering simulations with FCC and BCC metals," Radiation Effects and Defects in Solids 153 (3), 239-255 (2001).

115. M. A. Karolewski, "Kalypso: a software package for molecular dynamics simulation of atomic collisions at surface," Nuclear Instruments and Methods in Physics Research B 230 (1-4), 402-405 (2005).

116. M. A. Karolewski, "Kalypso: software for simulation of atomic collisions at surfaces, version 2.1 User Guide," [Document posted on the Web site of Dr. Karolewski]. Retrieved July 15, 2006 from the World Wide Web: http://www.geocities.com/karolewski/

117. R. V. Stuart and G. K. Wehner, "Sputtering yields at very low bombarding ion energies," Journal of Applied Physics 33 (7), 2345-2352 (1962).

118. T. Itoh, Ion beam assisted film growth, (Elsevier Science Ltd., 1989).

119. N. Matsunami, Y. Yamamura, Y. Itikawa, N. Itoh, Y. Kazumata, S. Miyagawa, K. Morita, R. Shimizu and H. Tawara, "Energy dependence of the ion-induced sputtering yields of monatomic solids," Atomic Data and Nuclear Data Tables 31, 1-80 (1984).

120. M. Nastasi, J. W. Mayer and J. K. Hirvonen, Ion-Solid Interactions: Fundamentals and Applications, (Cambridge University Press, 1996).

121. C. Kittel, A. Zettle and P. McEuen, Introduction to Solid State Physics, (John Wiley & Sons Inc, 2004).

122. Y. Yamamura and J. Bohdansky, "Few collisions approach for threshold sputtering," Vacuum 35 (12), 561-571 (1985).

123. B. Window and G. L. Harding, "Gas incorporation during ion-assisted deposition in bias sputtering," Journal of Vacuum Science and Technology A 11 (4), 1447-1450 (1993).

124. A. Misra and M. Nasrasi, "Limits of residual stress in Cr films sputter deposited on biased substrates," Applied Physics Letters 75 (20), 3123-3125 (1999).

125. S. Morohashi, K. Gotoh and S. Komiya, "Fabrication of josephson junctions using an Al/Ta/Nb structure for x-ray detection," Applied Physics Letters 64 (6), 785-787 (1994).

126. P. D. Stephen, G. J. Leslie and C. Alferd, "Method for using a hard mask for critical dimension growth containment," U. `S. Patent No. 6, 951, 820 (October 4, 2005).